On The Effects of Sub-GeV Dark Matter Particles to White Dwarfs and Thermonuclear Supernovae
探討次千兆電子伏特質量之暗物質對白矮星以及熱核超星新爆炸之影響

CHAN, Ho Sang

A Thesis Submitted in Partial Fulfilment
of the Requirements for the Degree of
Master of Philosophy
in
Physics

The Chinese University of Hong Kong
Jan 2022

Thesis Assessment Committee

Professor LAW, Chi Kwong (Chair)
Professor CHU, Ming Chung (Thesis Supervisor)
Professor LI, Hua Bai (Committee Member)

Abstract

This project investigate the effects of admixing sub-GeV, Fermionic dark matter particles to white dwarfs and thermonuclear supernovae.

The research begins with computing a series of equilibrium models for non-rotating, spherically symmetric Dark Matter-Admixed White Dwarfs. In contrast to some previous studies, our results showed that admixing Fermionic dark matter with a sub-GeV particle mass to a white dwarf does not necessarily reduce the total mass of both components. Instead, we found a new class of massive Dark Matter-Admixed White Dwarfs that have a dark matter component comparable in mass and radii to that of the normal matter. We extended our studies to include rotational effects on the normal matter component. We calculated a series of equilibrium models for axial symmetric, Dark Matter-Admixed Rotating White Dwarfs. Due to the extra gravitational attractions from the dark matter component, the normal matter component is more compact and faster rotating, but the total angular momentum would be reduced due to a reduction in the sizes and masses of the normal matter. Although the dark matter is assumed to be non-rotating, it will react to the flattened structure of the normal matter, in which it deformed to an ellipsoidal shape that gives rise to a non-trivial multi-pole moment for itself. We found that even though such objects follow universal relations among the I (moment of inertia), Love (tidal Love number), and Q (quadrupole moment) that are robust for different normal matter equations of state, these relations differ from and span bands above those without dark matter admixture. They may be used to probe astronomical dark matter.

This project continue as we simulated the spherically symmetric thermonuclear explosion of Dark Matter-Admixed White Dwarfs, which is also termed as the Dark Matter-Admixed Type Ia supernovae. We assumed the deflagration model with the deflagration-detonation transition. In all the models we have considered, the dark matter is left behind after the explosion as a compact dark star. The presence of dark matter lengthens the deflagration phase to produce a comparable amount of iron-group elements and more thermoneutrinos. Dark matter-admixed Type Ia supernovae also give dimmer but slowly declining light curves, consistent with some observed peculiar supernovae. Throughout our studies, we had predicted the effects of dark matter admixtures on white dwarfs and Type Ia supernovae. We anticipate our results could help facilitate the searches for astronomical dark matter.

摘要

本次研究旨在探討混合具費米子特性，次千兆電子伏特質量之暗物質對白矮星以及熱核超星新爆炸之影響．
於首部份，作者建構一系列非旋轉及球面對稱之混合了上述暗物質的白矮星模型。研究發現有異於昔日前人所作。結果顯示混合此類暗物質未必能減低白矮星與暗物質的整體質量，而且身處裡頭之暗物質部份具能與白矮星部份可比擬之半徑長度及質量。此系列乃前人未所發現之嶄新奇異星體。其次，作者延伸研究方向到加入旋轉效應。作者亦建構一系列軸向對稱之混合了上述暗物質的白矮星模型。研究結果表示因應暗物質之額外重力影響，此類旋轉奇異星體比起一般正常旋轉白矮星更密致及具更快旋轉速度。然則因為白矮星部份之質量和尺寸有所下跌，而導致整體角動量下降。此系列模型並毋考慮暗物質之旋轉效應。然而因為白矮星部份的快速旋轉會令之有所變形，暗物質部份亦因受此影響而變成橢圓球體。故此，此系列模型之暗物質部份將具有非平凡的質量多極矩。除此以外，研究結果顯示混合了上述暗物質的旋轉白矮星雖則依然遵守星體自身之I (轉動慣量), Love (潮汐洛夫數) 與Q (質量四極子) 的萬有關係，然而其萬有關係與一般正常白矮星之$I-\mathrm{Love}-Q$ 萬有關係有所偏差。作者因而提出此等偏差可作為探索星際暗物質之可行方案。
再者，本文深入探討混合了上述暗物質的白矮星之熱核爆炸，亦則Ia型超新星。作者透過電腦計算，模擬球面對稱之混合了上述暗物質的Ia型超新星。電算模型假定了爆炸過程是由緩燃向爆轟轉捩。研究結果顯示無論混合暗物質之模型有何等差異，所有暗物質依然不具足夠能量逃逸其自身之重力深井。因應暗物質之額外重力影響，爆炸的緩燃過程有延長，導致此等Ia型超新星比起一般正常Ia型超新星製造了可比擬數目之重鐵元素以及更多熱微中子。作者計算爆炸過後之光變曲線並發現此類Ia型超新星比一般為之暗，而且光度變化較慢。此類特質與某類觀察發現之奇特超新星特性吻合，可視作為此類奇特超新星的可行解釋。
總結而言，本文透過探討混合具費米子特質，次千兆電子伏特質量之暗物質對白矮星以及熱核超星新爆炸之影響，總結出一系列可以作為非直接探索星際暗物質的方法。作者期望本論文之研究結果，有助日後天文學家尋找星際暗物質以及探討暗物質的本性。

Acknowledgement

I would like to thank my supervisors Prof. Chu, Ming-Chung, and Dr. Lin, Lap-Ming. They have continuously provided guidance and encouragement for me to complete the graduation thesis. I am grateful that Prof. Chu, Ming-Chung had always come up with exciting and innovative ideas to inspire me to search for a good direction for my postgraduate projects. His insights on using simple physical ideas to simplify complicated pictures will always benefit me in my future research career; I am also thankful that Dr. Lin, Lap-Ming had always provided useful comments. He posses a solid background in computer simulations and gravitational physics that could help me figuring out errors in my research works. I am grateful for their patience in guiding and teaching me throughout the past two years, especially there was a period of time that I have almost no research output. They lead an inexperienced undergraduate to complete a master thesis. I could not have complete this work without their advice and encouragement.

I would also like to thank my mentor Dr. Leung, Shing-Chi for his guidance and teaching. I have learned almost everything about supernovae from him. I would like to thank him for his patience in answering me whenever I am confused about some concepts and physics on supernovae. He had participated and work hard on our collaborative publication. Without his participation, we could not have finished the research work. He had also provided opportunities and a helping hand for me to pursue further studies in physics. I am grateful that he had been a member of our group.

Finally, I would like to thank my family for supporting me in pursuing the Master studies. They did not urge me to look for industrial job but they have given me high degree of freedom to complete what I wanted. I would also like to thank my fellow classmates and friends, who always come up with visionary insights that helped me a lot.

Contents

Chapter 1

Introduction

1.1 Dark Matter and Astronomy

The discovery of an asymptotically flat galaxy rotation curve [289] challenges our knowledge of gravitational physics on the galactic scale. The existence of a hypothetical, unseen dark matter (DM) was proposed to explain the extra gravitational pull to account for the observed rotation curve [288] for the visible normal matter (NM). Later on, observational evidence of the DM have been discovered in spiral galaxies [168, 169, 170], dwarf galaxies [50, 274], and star clusters [223, 73]. DM is believed to be the dominant component of galaxy clusters [72], large-scale structures of the Universe [79], as well as a host of other astrophysical objects [244]. Theoretical studies show that DM is responsible for the formation of the cosmological large-scale structures [33, 171, 172], and the ΛCDM model has become the standard model of cosmology [79, 126, 339]. Many extensions of the Standard Model of Particle Physics proposed DM candidates such as Axions, Neutralinos, Gravitinos, and Axinos, Kaluza-Klein dark matter (see, for example, [320, 98] for a survey of DM

particle candidates). However, there is still no direct evidence from collider or direct detection experiments to confirm the existence of DM. Experiments are carried out to search for specific models of DM particles at facilities such as the LHC [161, 4], IceCUBE [1, 19], Super-Kamiokande [104, 8], and XENON [9, 10]. Nonetheless, astrophysical searches for the DM will remain an important channel to complement terrestrial experiments.

1.2 Dark Matter-Admixed Stellar Objects

DM constitutes more than 95% of the mass in a typical galaxy [106] and 23% of the mass-energy budget of the Universe [257]. Hence, it is natural to hypothesize that stellar objects comprising NM and DM may form. Indeed, DM could be captured by NM in a region where there is a high concentration of DM particles [56, 325, 12]. Therefore, stars may contain a DM component. It was shown that the effect of DM on stellar evolution could be significant depending on the stellar evolution models [298, 371, 325, 107, 212, 326, 270]. Therefore, anomalous stars could be used as probes for astrophysical DM.

Besides, on-going studies have been focusing on different aspects of compact. Such examples include the structures of white dwarfs (WD) [180, 195, 124], neutron stars [25, 179, 80, 180, 69, 191, 192, 358, 250, 281, 151, 162], and quark stars [231, 251, 253, 211, 252]. Recently, studies have been made on Bosonic DM-admixed compact objects [204, 40, 22, 91], Bosonic dark stars [308, 90, 222, 27, 26], formation of neutron stars through the accretion-induced collapse of DM-admixed white dwarfs [200, 372], thermalization of the white dwarf (WD) core to produce a thermonuclear

runaway [39, 5, 154, 321], and thermonuclear supernovae with point-mass DM cores [193]. Other than compact and exotic objects, effects of DM admixture on stellar formation [13] and evolution [299, 108, 213] are actively investigated. In particular, the evolution of AGB stars is used to constrain the properties of axion-like particles [86]. DM-admixed astrophysical objects have become a new channel to search for astrophysical DM.

1.3 White Dwarf Rotation

Stellar rotation is a natural phenomenon. The observation of the westward movements of sunspots suggests rotational motions of the Sun. Doppler shifts of the stellar spectral lines indicate that most stars exhibit a certain degree of rotations [331], which induce additional mixing of stellar materials to explain the isotope distribution near the stellar surface that deviates from those with the non-rotating model [224, 134]. Due to the large reduction in the size of a molecular cloud during its collapse phase, a small initial angular momentum could result in a rapidly rotating proto-star [136, 127]. However, most of the angular momentum of a proto-star would be carried away through wind-magnetic field interactions, leading to a slowly rotating newborn star [275, 341, 38]. In addition, diffusion of material from the core to the surface of a WD lowers its final spin [140, 113]. Therefore, the primordial angular momentum of a low-mass star that eventually ends up as a WD contributes to only a small portion of the final total angular momentum. Indeed, dimensional analysis suggests that extra angular momentum transported to WDs is necessary to explain the observed WD rotation rates [318, 167]. Possible scenarios include accretion from a companion star [186, 364] and mergers between two or more WDs

[366, 21, 129, 269]. Rotating WDs have been proposed to be progenitors of neutron stars formed by core contractions [138, 139, 365, 111, 132], as well as super-luminous thermonuclear supernovae, due to the fact that rotating WDs could support more mass than their traditional Chandrasekhar limit [322, 259, 258, 346, 100]. Recently, studies have been made on finite-temperature corrections to modeling of rotating WDs [35, 367], as well as effects of the strong magnetic field on the equilibrium structures of WDs [216, 105, 24, 63], for which the WD rotation takes a critical role.

1.4 Thermonuclear Explosion of White Dwarfs

WDs are believed to be the progenitors for thermonuclear supernovae [141, 217, 209]. However, it is not clear which kind of WDs and explosion mechanisms are responsible for such energetic events [290]. It is believed that most of the progenitor WDs consist of carbon and oxygen [209]. A mixture of carbon, oxygen, and neon seems to be also possible [81, 82, 218, 45, 349, 49, 290, 16]. The progenitor models for thermonuclear supernovae are classified as either the Single-Degenerate scenario or the Double-Degenerate scenario [217, 210, 290].

The Single-Degenerate scenario has been studied for several decades. Early simulations investigated thermonuclear supernovae that are driven by a pure detonation [11] and a pure deflagration [238] initiated near the center of the WD. While there were over-productions of iron-group elements in the former, the latter was too slow to generate a healthy explosion. Results from either pure detonation or pure laminar deflagration do not fully reproduce the observed features in a typical thermonuclear supernova. Moreover, it was argued that a pure detonation would be quenched at high density, casting doubts on the possibilities of a prompt detonation [181].

A deflagration wave is subject to several hydrodynamical instabilities [141, 283]. Turbulence would induce convolutions on the deflagration surface, which would allow the deflagration to propagate at an effective speed greater than the laminar value [239, 292]. Early studies of the pure turbulent deflagration model used the mixing-length theory described in [238] and [239] (The W7 model). A fast deflagration wave with a propagating speed around 20 – 30 % of the local speed of sound was assumed. These models could produce healthy explosions. However. they produced too much ^{58}Ni when compared with the constraints from the galactic chemical evolution [153][1]. Multi-dimensional studies on the pure turbulent deflagration model also under-produced the amount of ^{56}Ni and explosion energy [277, 52, 101, 283], with most of the unburned material left behind at the center of the WD. This is inconsistent with spectroscopic observations [214]. The carbon-oxygen fuel should only exist at the outer ejecta [114]. Although later studies showed that some good agreements with observations in terms of the nickel mass and the ejecta velocity could be obtained [279, 293], another major shortcoming of the pure turbulent deflagration model is the underproduction of the silicon-group elements at the outer layers of the ejecta [294], which are strongly mixed with the iron-group elements [214].

1.4.1 The Deflagration-Detonation Transition Model

A transition to detonation from a deflagration is observed in several terrestrial experiments with closed boundaries [267, 47]. It is therefore natural to hypothesize that

[1]However, we cannot rule out the possibility for the fast deflagration model, given the prevailing view that the Single-Degenerate scenario probably only constitutes a small population of the thermonuclear supernovae. We thank the referee for pointing this out.

a transition to detonation could also happen in open boundaries such as the interior of a WD. [173] proposed the deflagration-detonation transition (DDT) model, which gives a comparable amount of iron-group and silicon-group elements to the observed thermonuclear supernovae. The DDT model was also shown to fit the observed supernova light curves in V and R band reasonably well [144]. To trigger the DDT, the Zel'dovich gradient mechanism [370] is used. Besides, there are also other proposed mechanisms [62]. In the Zel'dovich mechanism, the local eddy motions near the flame front would help flatten the temperature gradient to trigger the DDT. [233, 41, 267, 47]. Whether the turbulence could robustly help to attain the required criteria for a DDT is surely a concern [233, 206, 352]. In principle, turbulent motions could mix the cold fuel and hot ash to obtain the required pre-conditioned field [249, 141]. However, numerical simulations had shown that the required turbulent strength [249] would be too large so that the implied velocity fluctuations [282] is only marginally sufficient for triggering the DDT. Yet some semi-analytical studies [312] and hydrodynamical simulations using a sub-grid scale turbulent model have confirmed that a WD can meet the criteria for a DDT [68]. The required strength of the turbulence was later found to be less than that previously believed [267], and a DDT is possible in an environment with weak turbulence [46]. Furthermore, the DDT model was shown to produce spectra that match well with some of the observed supernovae [32, 30, 317].

1.4.2 Explosion Models Other than DDT

Accompanied with the diversities of the observational data, variations of the DDT model had also been proposed, such as the gravitationally confined detonation model [264, 336, 158, 303], where the gravitational contraction increases the density and

temperature of the collision region towards the conditions for detonations, and the pulsating reverse detonation models [42, 43, 44], where a weak deflagration leads to the pulsation of a Chandrasekhar WD. An accretion shock is formed and confines the carbon-oxygen core and transforms the kinetic energy from the collapsing material into thermal energy of the core until an inward moving detonation is formed. On the other hand, a failure in initiating a detonation after a weak deflagration may produce a failed explosion, leaving behind a bound carbon-oxygen white dwarf mixed with some intermediate-mass elements. This is called the failed-detonation scenario and is used to explain some of the peculiar Type Iax supernovae [159, 182].

Other than the Single-Degenerate scenario, the Double-Degenerate scenario has emerged as one of the most promising models in recent years [311]. In the Double-Degenerate scenario, a WD would accrete material from its companion star [316]. A detonation could be generated before the WDs are merged to form a single compact star [272], and this detonation is initiated at the outer envelop that contains a thin and modest amount of helium [338]. The converging detonation waves trigger a second detonation at the carbon-oxygen core, hence producing a prompt eruption [227, 272, 330, 125]. While some observational results seem to favor the Double-Degenerate scenario [353, 217, 121], suggesting that they might constitute the majority population of thermonuclear supernovae [103, 66, 203], some recent studies found that they could be in a tight tension with the γ-ray ejected time against Nickel mass relation [184].

1.4.3 Dark Matter-Admixed Thermonuclear Supernovae

[5], [39] and [321] pointed out that accreting DM to a WD could lead to a kinetic energy transfer from the DM to the NM through particle scattering, which helps to heat up the carbon-oxygen core towards the temperature necessary for triggering a thermonuclear runaway. On the other hand, [195] showed that the admixture of non-self-interacting DM could reduce the Chandrashekhar mass of a WD so that a thermonuclear flame is generated when the mass of the WD is below the traditional Chandrashekhar limit.

[193] have demonstrated that DM-admixed thermonuclear supernovae could produce sub-luminous light curves. If the heavy Fermionic DM consists of particles with a mass of around 1 GeV, the DM component is small enough to be approximated as a stationary point gravitational source located at the center of the WD. Recent constraints on the DM particle mass derived from lab experiments [71] and observed neutron star masses [152] have not ruled not the parameter space for sub-GeV DM particles. Some extensions of the Standard Model of Particles Physics have also suggested the existence of sub-GeV DM particles [89]. Therefore, we are motivated to study the effects of admixing sub-GeV DM to a thermonuclear supernova. As we shall see, admixing sub-GeV DM would create an extended DM component that we could not treat as a point mass, and so we need to describe the explosive hydrodynamics using a two-fluid formalism.

1.5 Motivation

The equilibrium structures of non-rotating, DM-admixed WD (DMWD) were studied in [195]. They assumed a heavy DM particle mass over 1 GeV. In addition, DM-admixed rotating WD (DMRWD) have been computed and used as a progenitor for the accretion-induced collapse in the work by [201] and [373], but they assumed the DM component to be spherically symmetric. A two-fluid study of the equilibrium structure of a DMRWD that takes into account the gravitational interactions between the NM and DM self-consistently has not been carried out. Therefore, as a first step, we study both spherically symmetric non-rotating and axial symmetric rotating admixed with sub-GeV DM particles under Newtonian gravity. Besides, in [193], the DM-admixed thermonuclear supernova is studied by considering the pure turbulent deflagration model without a DDT. In this work, we extend the study of [193] by (1) focusing on the robust DDT model and (2) adding the dynamics of the DM component in the picture by using the fully non-linear two-fluid simulations.

A number of new telescopes such as the LISA and LSST are expected to begin construction or operation in the upcoming decade. It is estimated that over 150 million WDs could be detected in the final phase of the 10-year LSST survey [96] and that over 25,000 WD binaries could be observed through the LISA telescope [177]. Furthermore, it was shown that over 10,000 super-luminous Type Ia supernovae per year may be captured by the LSST [343], and even more is expected for the total population of Type Ia supernovae. Our goal is to provide predictions to facilitate searches for DM through astrophysical observations.

1.6 Thesis Structure

We summarize the structure of this research thesis below. In Chapter 2, we introduce the methods of obtaining the equilibrium structures for time-independent 1. spherically symmetric DMWD, and 2. axial-symmetric DMRWD models. We then present our results and discuss the implications of our findings in the same chapter. In Chapter 3, we enumerate the tools necessary for simulating the one-dimensional thermonuclear explosion of DMWD. We also present and discuss their results in the same chapter. We point out the limitations of our current study in Chapter 4, and we conclude our study in Chapter 5. We provide additional information in the Appendix Section.

□ End of chapter.

Chapter 2

Time-Independent Equilibrium Structures

In this chapter, we describe the methods of constructing the equilibrium structure for DM-admixed non-rotating and rotating WDs. We show the effects of admixing DM to these WDs and discuss the physical implications of our findings. This chapter is based on part of the published article in The Astrophysical Journal, 914(2), 138., and is based on a submitted article to Physical Review D.

2.1 Methods

2.1.1 Dark Matter-Admixed White Dwarfs

We construct a series of DMWD by solving the Newtonian hydrostatic equilibrium equations [296, 70, 200]:[1]

$$\frac{dp_i}{dr} = -\frac{G(m_1 + m_2)\rho_i}{r^2}, \tag{2.1}$$

$$\frac{dm_i}{dr} = 4\pi r^2 \rho_i. \tag{2.2}$$

Here, the subscript $i = 1(2)$ denotes the DM (NM) quantities, and ρ, p, m and r are the density, pressure, enclosed mass, and radial coordinate respectively. We vary the DM particle mass from 0.1 GeV to 0.3 GeV in 0.05 GeV steps. For each value of the DM particle mass, we vary the DM central density from 10^8 g cm^{-3} to 10^{10} g cm^{-3}. We will show the effects of admixing sub-GeV DM particles to static WDs by analyzing this series of models.

2.1.2 Dark Matter-Admixed Rotating White Dwarfs

We also compute a series of DM-admixed rotating WDs (DMRWDs) by solving the Newtonian hydrostatic equations, including the centripetal force:

$$\vec{\nabla} P_i = -\rho_i \vec{\nabla}\Phi + \rho_i \omega(s)_i^2 s \delta_{i2} \hat{s}. \tag{2.3}$$

Here, the subscript $i = 1(2)$ denotes the DM (NM) quantities, and ρ, p, and ω are the density, pressure, and angular speed for the fluid element. s is the perpendicular distance from the rotation axis, and $\hat{s}$ is the unit vector orthogonal to and pointing

[1] Though the first two works are based on the relativistic formulation, Equation 2.1 and 2.2 can be obtained by taking the non-relativistic limit.

away from that axis. The angular speed is assumed to be a function of s only. δ_{i2} is the Kronecker-Delta function, indicating that only the NM is rotating. Φ is the gravitational potential governed by the two-fluid Poisson equation:

$$\nabla^2\Phi = 4\pi G(\rho_1 + \rho_2). \tag{2.4}$$

Following [93], [130] and [7], we can integrate the equation of equilibrium:

$$\int \frac{dP_i}{\rho_i} = -\Phi + \delta_{i2}\int \omega(s)_i^2 s ds + C_i, \tag{2.5}$$

where C_i is an integration constant. In particular, following [130], we define:

$$\int \frac{dP_i}{\rho_i} = H_i, \tag{2.6}$$

$$\int \omega(s)_i^2 s ds = -h_i^2\psi_i, \tag{2.7}$$

where H is the enthalpy, ψ is the rotational potential, and h^2 is a constant to be determined. So, the equation of equilibrium can be written in the integral form as:

$$H_i + \Phi + \delta_{i2}h_i^2\psi_i = C_i. \tag{2.8}$$

The equations of equilibrium for the DM and NM will be solved together iteratively to obtain the equilibrium configurations.

Rotational Rule

In this work, we assume only the NM is rotating. We have considered multiple rotation profiles from [130] and [367] including (1) the rigid rotation:

$$\omega(s)_2^2 = \Omega_i^2, \tag{2.9}$$

and (2) the Keplerian-flow-like rotation profile:

$$\omega(s)_2^2 = k_i/(d^{3/2} + s^{3/2}). \tag{2.10}$$

For the last two rules, the parameter d governs the degree of differential rotation. We choose $d = 0.1$ for this work. We integrate the angular velocity to obtain the effective potential for the rigid rotation:

$$\psi_2 = -s^2/2, \tag{2.11}$$

The effective potential for the Kepler rule is:

$$\begin{aligned}\psi_2 = -\frac{1}{9}\Bigg[-\frac{6\sqrt{s}}{s^{\frac{3}{2}} + d^{\frac{3}{2}}} + \frac{1}{d}\ln\left(\frac{(\sqrt{d}+\sqrt{s})^2}{d+s-\sqrt{sd}}\right) \\ -\frac{2\sqrt{3}}{d}\tan^{-1}\left(\frac{1-2\sqrt{s/d}}{\sqrt{3}}\right)\Bigg].\end{aligned} \tag{2.12}$$

The Self-Consistent Method

We follow [130] to adopt an axial symmetric spherical grid. We adopt dimensionless units so that we set the gravitational constant G, maximum NM density $\rho_{\rm Max2}$ and NM equatorial radius $r_{\rm eq2}$ to be one. The computational domain is described by the

radial coordinate r and $\mu = \cos\theta$, where θ is the polar angle. We divide μ and r into KDIV and NDIV equal portions, respectively. Therefore,

$$\begin{cases} r_j = r_0 \frac{j-1}{\mathrm{NDIV}-1}, & (1 \leq j \leq \mathrm{NDIV}), \\ \mu_k = \frac{k-1}{\mathrm{KDIV}-1}, & (1 \leq k \leq \mathrm{KDIV}). \end{cases} \tag{2.13}$$

Here, r_0 is the size of the computational domain. In this work, when there is no DM component, we choose KDIV = 257, $r_0 = \frac{16}{15}$, and NDIV = 257. When there is a DM admixture, r_0 and NDIV are enlarged to accommodate the DM fluid. We compute the gravitational potential in spherical coordinate using the multipole expansion method:

$$\begin{aligned} \Phi(\mu, r) = -4\pi G \int_0^\infty dr' \int_0^1 d\mu' \times \\ \sum_{n=0}^{\mathrm{LMAX}} f_{2n}(r', r) P_{2n}(\mu) P_{2n}(\mu') \rho(\mu', r'), \end{aligned} \tag{2.14}$$

where $P_{2n}(\mu)$ is the Legendre polynomial, and LMAX is the maximum number of moments. We choose LMAX= 16, and

$$f_{2n}(r', r) = \begin{cases} \frac{r'^{2n+2}}{r^{2n+1}}, & r' < r, \\ \frac{r^{2n}}{r'^{2n-1}}, & r' > r. \end{cases} \tag{2.15}$$

To compute the equilibrium structure of a pure NM rotating WD, we need to specify the boundary condition for which $\rho_2 = 0$. The equatorial boundary is set at $r_{a2} = 1, \theta = \frac{\pi}{2}$, while the axis boundary is set at $0 \leq r_{b2} \leq 1$, $\theta = 0$. The axis-ratio of the NM is defined as $\kappa_2 = r_{b2}/r_{a2}$. We need one more parameter to completely specify the system. We choose it to be the radial position of the DM equatorial boundary r_{a1}. Now we describe the procedure for obtaining the equilibrium structures:

1. Specify $\rho_{\rm Max2}$, r_{b2} and r_{a1};

2. Solve the two-fluid equations (2.8) iteratively.

In general, the DM mass changes during iterations. Therefore, we use the bisection method to vary $r_{\rm b1}$ to obtain the targeted DM mass. In solving Eq. (2.8), we choose to terminate the iterations once h_i, C_i and the maximum of H_i for both fluids converge, i.e., their relative changes are less than 10^{-10}.

2.1.3 The Equation of States

We adopt the ideal degenerate Fermi gas equation of state (EOS), assuming spin $\frac{1}{2}$ for the DM component [307, 54]. For the sake of consistency, we use the Helmholtz EOS [335] for the NM when we are computing the spherically symmetric DMWDs and simulating their subsequent supernova explosions. We choose to adopt several different EOS for the NM when we are computing the axial symmetric DMRWDs, they include the ideal degenerate Fermi gas EOS and Harrison-Wheeler (HW) EOSs [135]. There are also several parameterized deleptonization formulae to describe the electron capture at high density. In particular, we choose the formulae given in [14] (ASC), in [205] (G15, N13), [51] (S15), and [84, 3] (VUL).

2.2 Calculation Results

2.2.1 Dark Matter-Admixed White Dwarfs

To implement the Helmholtz EOS, we need to specify the isotope and temperature profiles. We assume an equal mixture of ^{12}C and ^{16}O initially. We assume an initial constant temperature of $T = 10^8$ K. We adopt the central density for the NM to

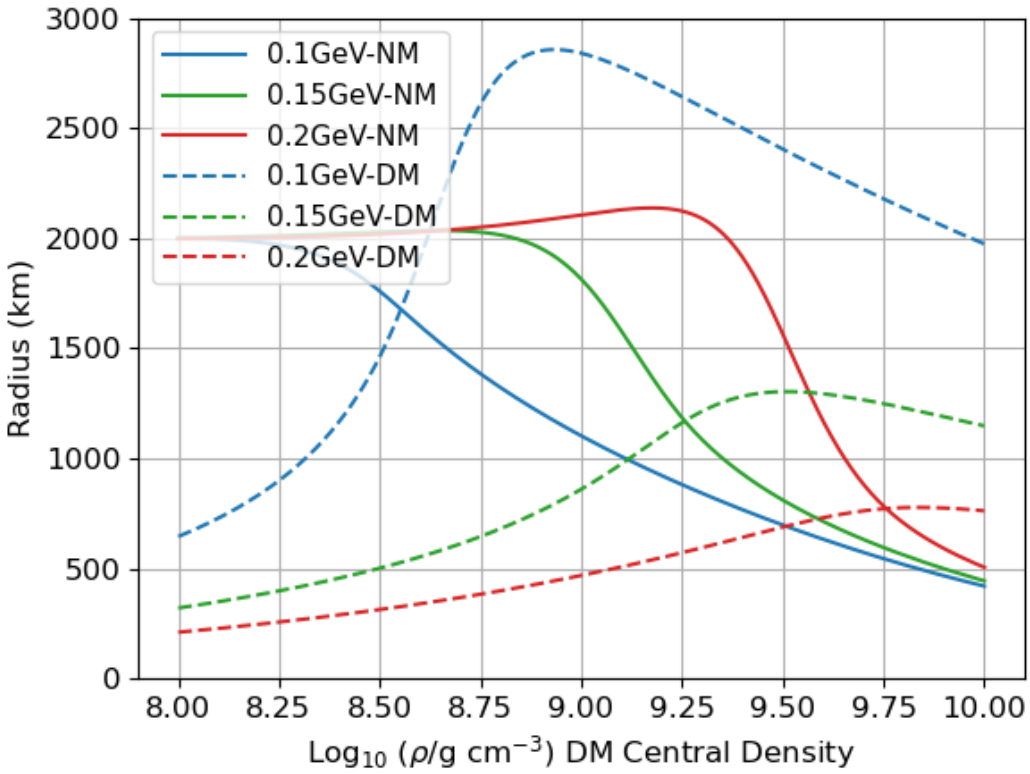

Figure 2.1: The radii of different components against the DM central density, for the DM particle mass of 0.1 (blue), 0.15 (green), and 0.2 GeV (red). The solid (dashed) lines are for the NM (DM) component. The NM central density is kept at 3×10^9 g cm^{-3}.

be 3×10^9 g cm^{-3}. This value gives rise to a thermonuclear explosion that is close to the average thermonuclear supernova. Similar values have also been adopted by a number of previous studies [215, 300, 301, 237, 176]. We vary the DM central density from 10^8 g cm^{-3} to 10^{10} g cm^{-3} to obtain the masses and radii for the NM and the DM components. We find that a higher DM admixture decreases the NM mass, which is consistent with the results in the previous study on DMWD using the BPS EOS [195]. Figures 2.1 and 2.2 show that for a smaller DM particle mass, the DM radii are more extended, and there could exist configurations where the DM

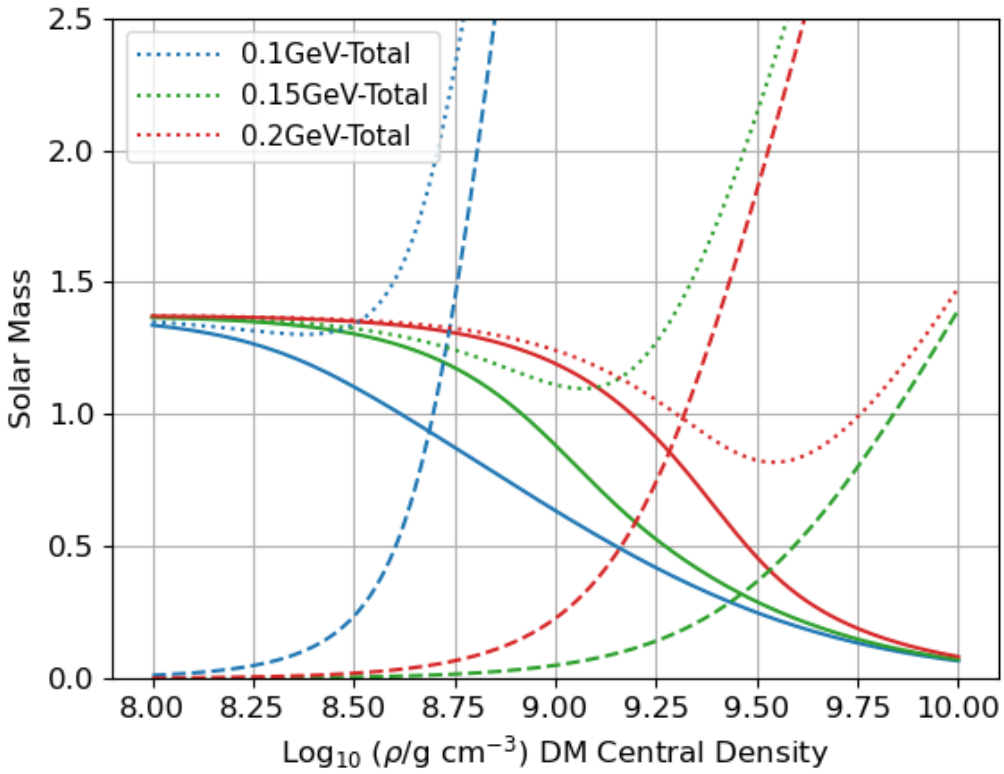

Figure 2.2: Same as Figure 2.1, but for the masses. The dotted lines are the sum of the NM and the DM masses.

and the NM components are comparable in radii and masses. These results are also in contrast with the results presented in [195], for which heavy DM particles would reside near the center of the WD with a extremely small size. Therefore, these exotic DMWDs may represent a new class of exotic object. Figure 2.2 shows that for a given NM mass, a vertical line that crosses the corresponding DM mass curve gives the minimum amount of DM to be admixed so that the WD could attain the conditions necessary for generating a thermonuclear runaway. For the DM particle mass of 0.1 GeV, there is a sharp transition of the DM mass such that it increases drastically near the DM central density of $\sim 8.75 \times 10^8$ g cm^{-3}, while the changes in NM mass

are relatively small. In that case, there exist configurations with $\sim 1\ M_\odot$ of the NM mass and $\sim 0.5\ M_\odot$ of the DM mass. The explosion dynamics of these DMWD will be further investigated in Chapter 3.

2.2.2 Dark Matter-Admixed Rotating White Dwarfs

Table 2.1: Parameters for different DMRWD models.

Model	NM	DM-0.01	DM-0.05	DM-0.1	DM-0.2
DM Mass ($M_\odot$)	0.00	0.01	0.05	0.1	0.2

In this section, we extend our studies of DMWD by incorporating rotational effects to the NM component. The DM component is assumed to be non-rotating, and the legitimacy of our assumption will be discussed in Chapter 4. The DM particle mass is fixed to be 0.1 GeV. We shall focus on the ideal degenerate Fermi gas EOS for the NM in studying DRMWD. For each rotation rule, We construct a few sequences of DMRWD models by varying the maximum NM density $\rho_{\rm Max2}$ from 10^6 g cm^{-3} to $10^{10.5}$ g cm^{-3} with fixed DM admixture from 0 to 0.2 $M_\odot$ in each series. We list them according to the amount of DM mass in Table 2.1 for reference.

Rigid Rotation

We have computed a series of configurations for rigidly rotating DMRWDs. We obtain each sequence of models by fixing $\rho_{\rm Max2}$ while varying the radial position of the NM axis boundary. We terminate the computation once the NM has reached its Keplerian limit. In other words, the outermost layer of the star becomes unbounded.

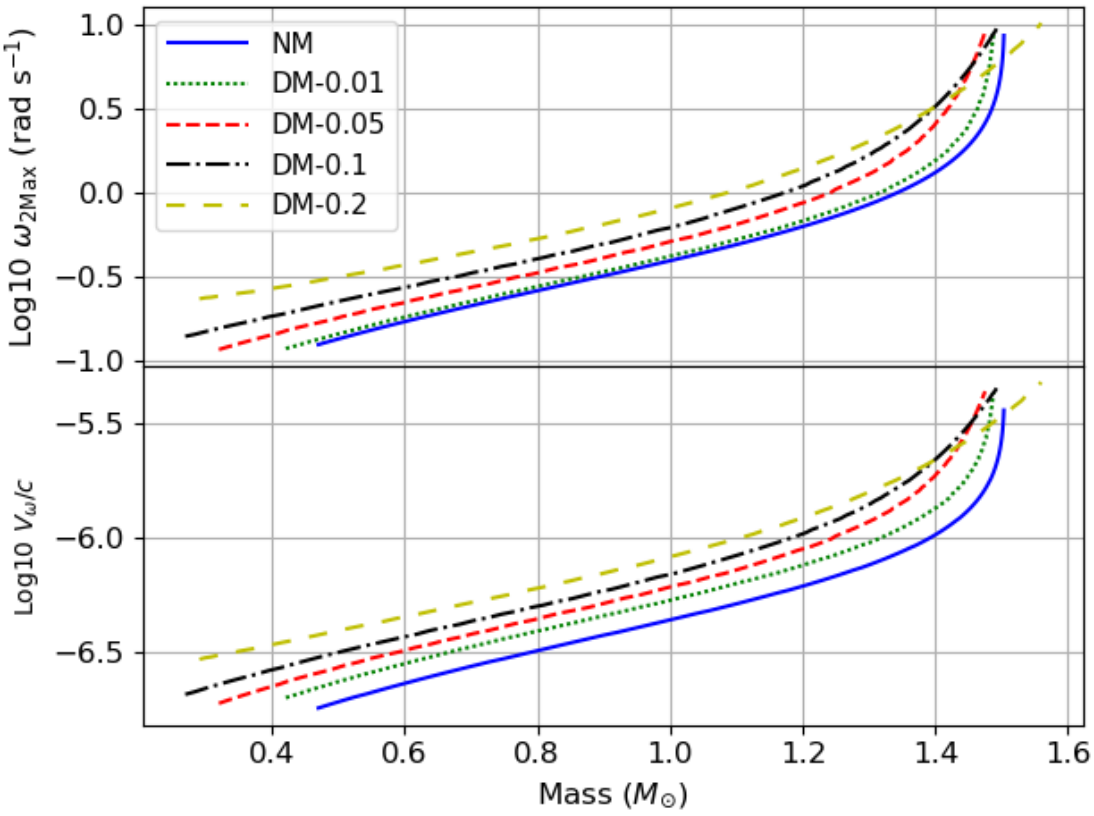

Figure 2.3: Maximum angular speed (upper panel) and maximum rotational speed (in fraction of the speed of light, lower panel), both in the log scale against the total mass, for different models of rigidly rotating DMRWD at the Keplerian limit.

Rotational Speed. We show the maximum angular and rotational speeds for different rigidly rotating DMRWD models at their Keplerian limit in Figure 2.3. We find that these DMRWDs tend to rotate faster than the pure NM WD with the same total mass. In the non-relativistic limit, the radius R_2 of a pure non-rotating NM WD scales with its mass M_2 as $R_2 \sim M_2^{-1/3}$ [344]. A DMRWD having the same total mass as a pure NM WD would have less NM. (This is consistent with several previous studies on DMWDs. See, for instance, [195].). Hence, the scaling relation predicts a larger NM size for the DMRWD. However, Figure 2.5 shows that

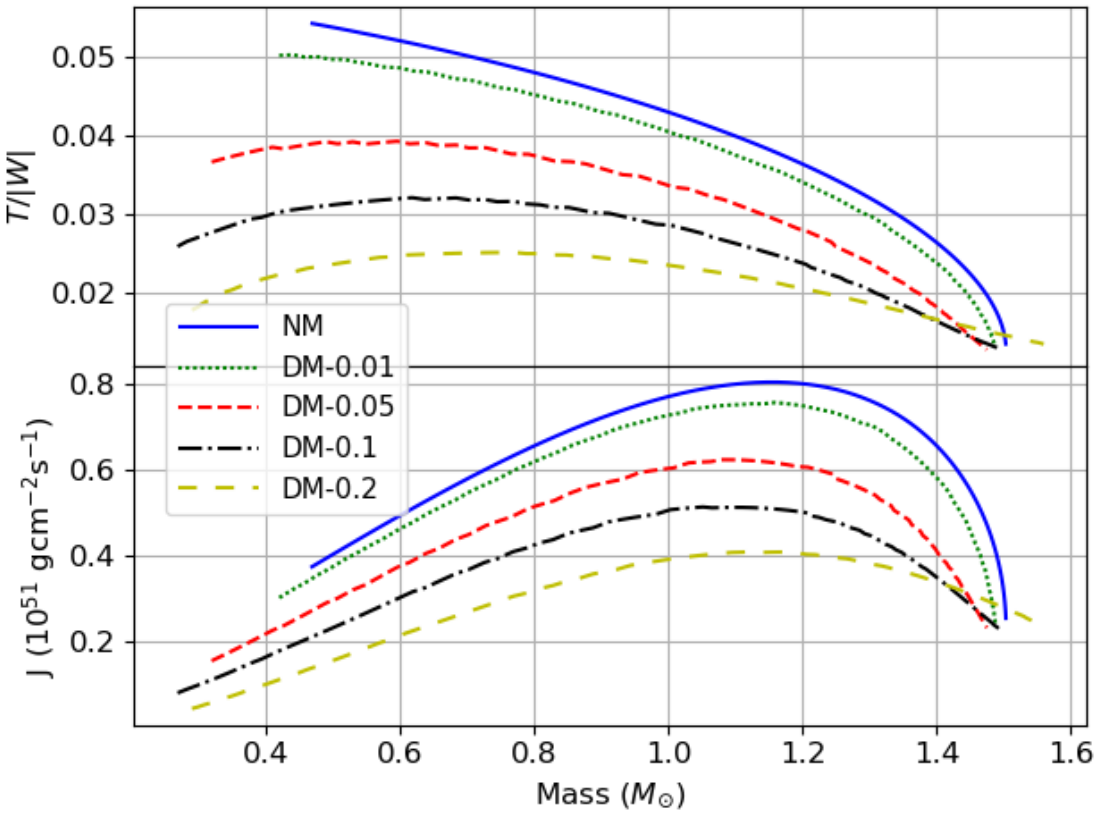

Figure 2.4: Same as Figure 2.3, but for the stability parameter (upper panel) and total angular momentum (lower panel).

admixing DM would decrease the NM equatorial radius. Therefore, the DM provides a significant magnitude of gravitational force to contract the NM to make it more compact. Furthermore, the equation of hydrostatic equilibrium predicts that the angular speed ω_2 of the rotating NM particles scales with the total gravitating mass $M(r_2)$ and its orbital radius r_2 as $\omega_2 \sim (M(r_2)/r_2^3)^{1/2}$. For the same M, a reduction in r_2 would increase ω_2. Hence, the NM component rotates with a larger angular speed.

The Stability Parameter. We show the stability parameters of different rigidly rotating DMRWD models at their Keplerian limit in the upper panel of Figure 2.4.

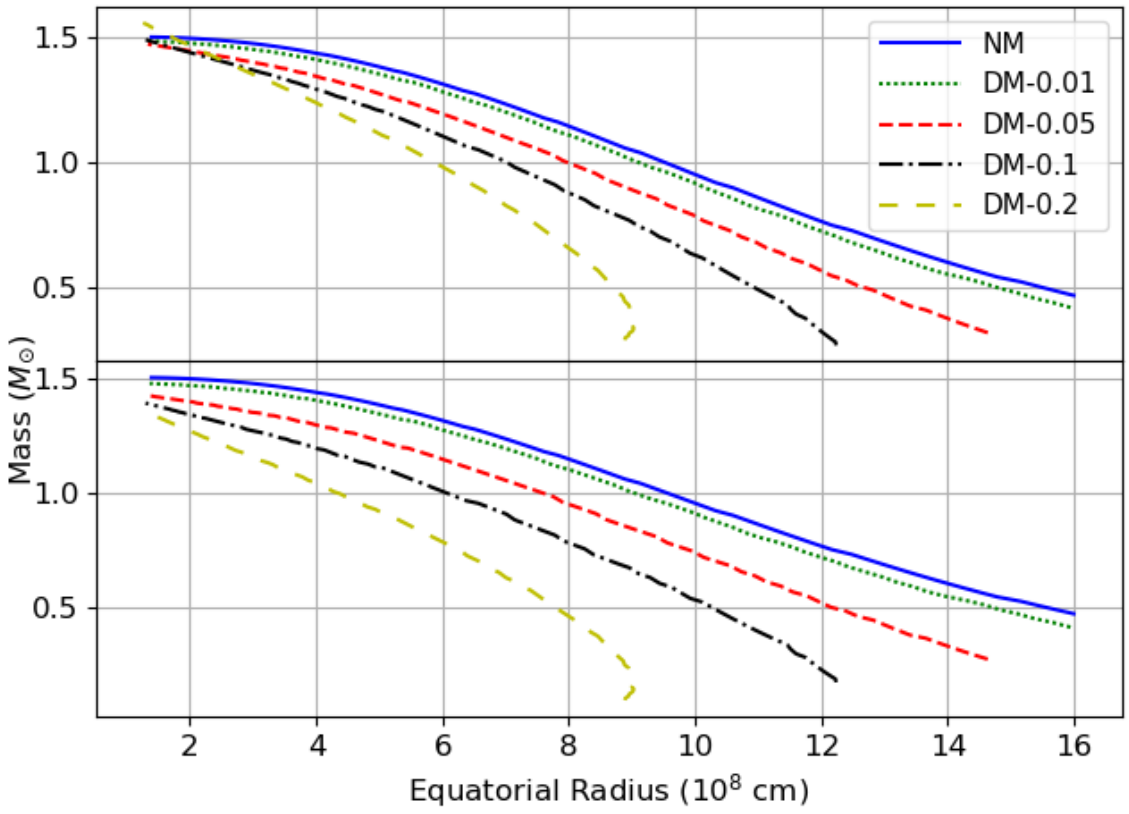

Figure 2.5: Total (upper panel) and NM (lower panel) masses as functions of the NM equatorial radius for different rigidly rotating DMRWD models at the Keplerian limit.

The stability parameter $\sigma \equiv T/|W|$, the ratio of the total kinetic energy T and the magnitude of the total gravitational energy $|W|$, measures how stable the rotating configurations would be against secular and dynamical instabilities. We find that admixing DM while keeping the total mass constant, would reduce the stability parameter so that it stabilizes the rotating configuration. This can be understood in two steps. Firstly, by considering hydrostatic equations, one can show that $T \sim M_2 M/R_2$. Secondly, $|W| \sim M^2/R$. Here, R is the maximum between the NM and DM radii. Therefore, $\sigma \sim (M_2/M)(R/R_2)$. For a given M, more DM implies

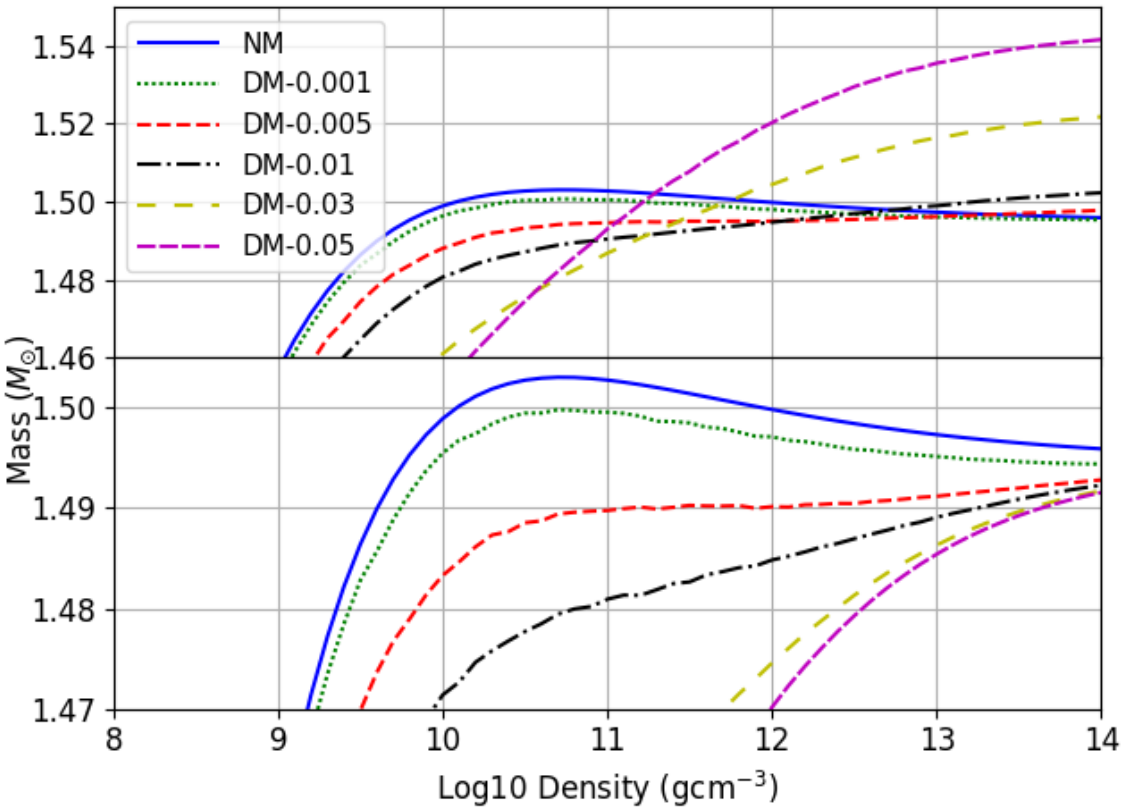

Figure 2.6: Same as Figure 2.5, but for the masses against $\rho_{\rm Max2}$ in the log scale.

less NM (smaller M_2). In addition, in most cases, $R \approx R_2$, and so σ is reduced when more DM is admixed. There is an upper bound of σ for those rigidly rotating DMRWDs that have a heavy DM admixture.

Total Angular Momentum. We show the total angular momenta $J \sim M_2(\omega_2 R_2)^2$ of different rigidly rotating DMRWD models at their Keplerian limit in the lower panel of Figure 2.4. We find that DMRWDs having the same total mass as a pure NM rotating WD would have smaller J. We can apply arguments similar to that we have presented in section 2.2.2. Even though rigidly rotating DMRWDs rotate faster at their Keplerian limit than the pure NM WD with the same total mass, both

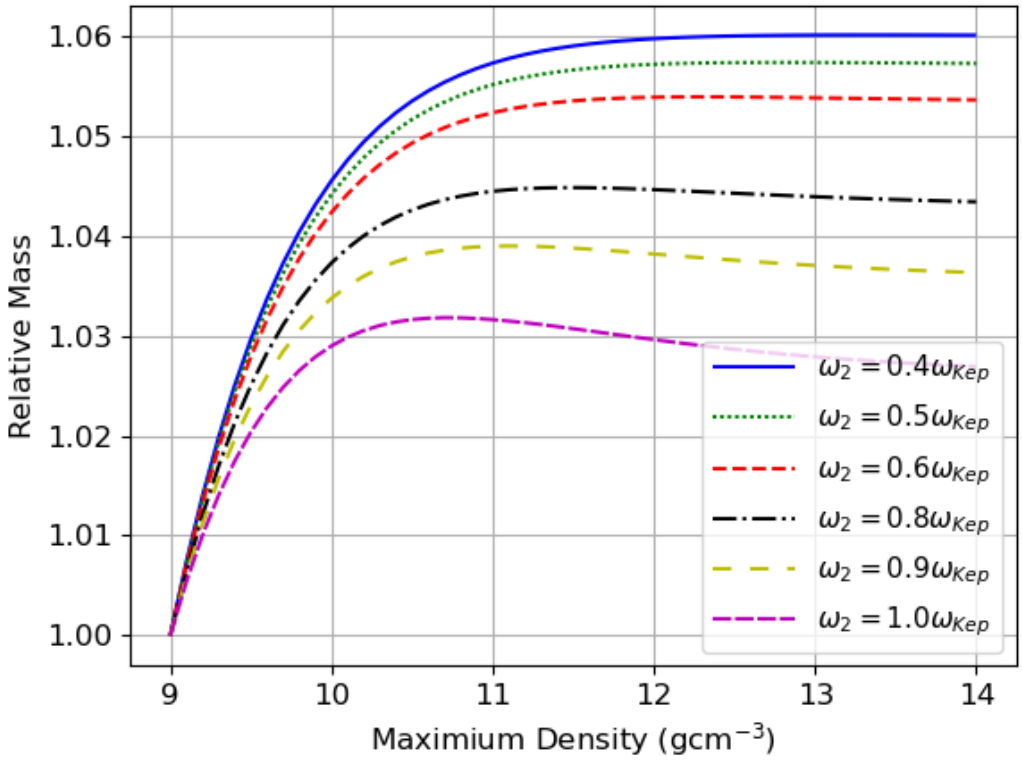

Figure 2.7: Ratios of the NM masses to that computed at $\rho_{\rm Max2} = 10^9$ g cm^{-3} of the pure NM model, rotating at different fractions (listed after each label in the legends) of the Keplerian velocity $\omega_{\rm Kep}$.

M_2 and R_2 are reduced faster than the increase in ω_2 when more DM is admixed, resulting in a reduction in J.

Some Exceptional Cases. The above discussions are no longer valid when the total mass of the models that we considered is $\gtrsim 1.3\ M_\odot$. In this case, the pure NM model has a total mass (which is also the NM mass) that is approaching its traditional Chandrasekhar limit. Such a pure NM WD rotates faster, has less angular momentum, and is less stable than the DMRWD with the same total mass. A more

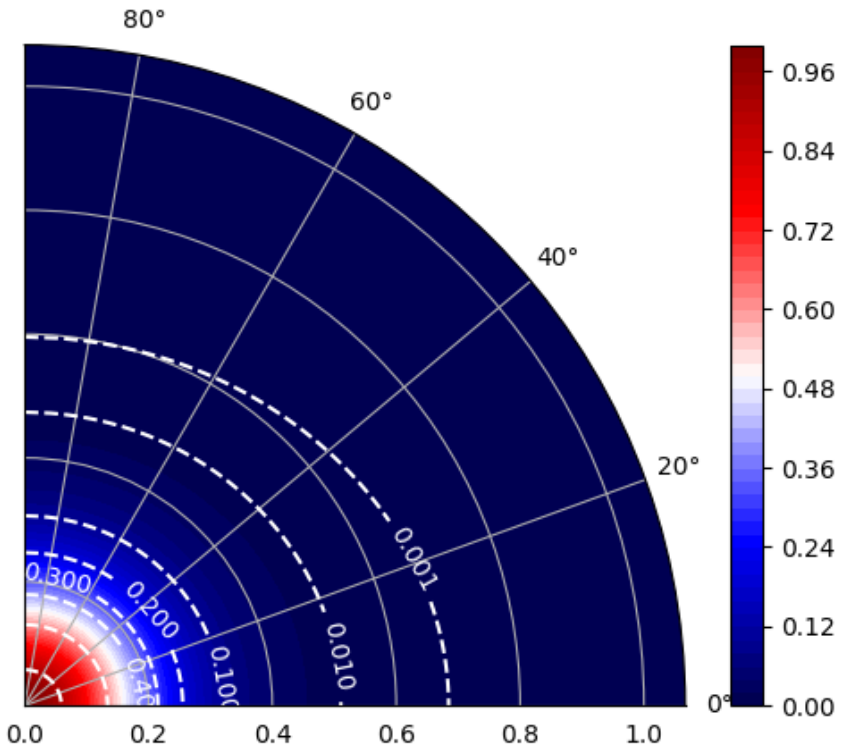

Figure 2.8: NM density contour for a rigidly rotating WD admixed with 0.1 $M_\odot$ of DM, $\rho_{\rm Max2} = 10^{10.5}$ g cm^{-3}, and $\kappa_2 = 0.7$. The density is normalized to $\rho_{\rm Max2}$. The radial distance is in unit of 1.23×10^8 cm.

general WD mass-radius scaling relation reads [175, 344]:

$$R_2 \sim M_2^{((1-n)/(3-n))}. \tag{2.16}$$

Here, $n = 1/(\gamma - 1)$ and γ is the adiabatic index. When the NM mass is approaching its traditional Chandrasekhar limit, the NM average density $\bar{\rho}_2 \sim M_2/R_2^3$ becomes very large. The NM is so compact that the effective adiabatic index $\gamma \to 4/3$ ($n \to 3$). Hence, $R_2 \sim M_2^{-\infty}$ [175, 344], and the NM shrinks significantly. This can be seen in Figure 2.5, in which the model DM-0.2 has a larger NM radius than the pure NM

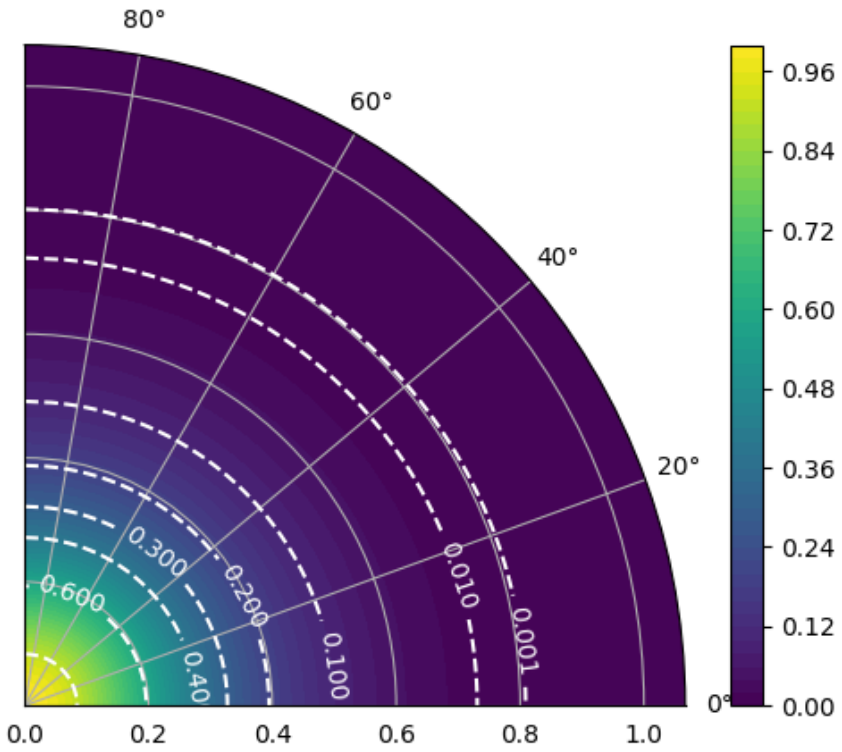

Figure 2.9: Same as Figure 2.8, but for the DM density normalized to $\rho_{\rm Max1} = 10^{9.042}$ g cm^{-3}.

model for $M \approx 1.5\ M_\odot$. Besides, the gravitational energy $|W|$ is now dominated by the compact NM, and it increases faster than T, resulting in a substantial reduction of σ. Furthermore, the decrease in R_2 also reduces J, even if the NM is rotating faster. Therefore, admixing DM to a WD with NM mass near its Chandrasekhar limit reduces $\bar{\rho}_2$, increases γ, and makes the NM less compact when compared to the pure NM WD.

Maximum Total Mass. [191] and [195] have shown respectively that admixing DM to a WD and a neutron star would result in a decrease in its maximum total

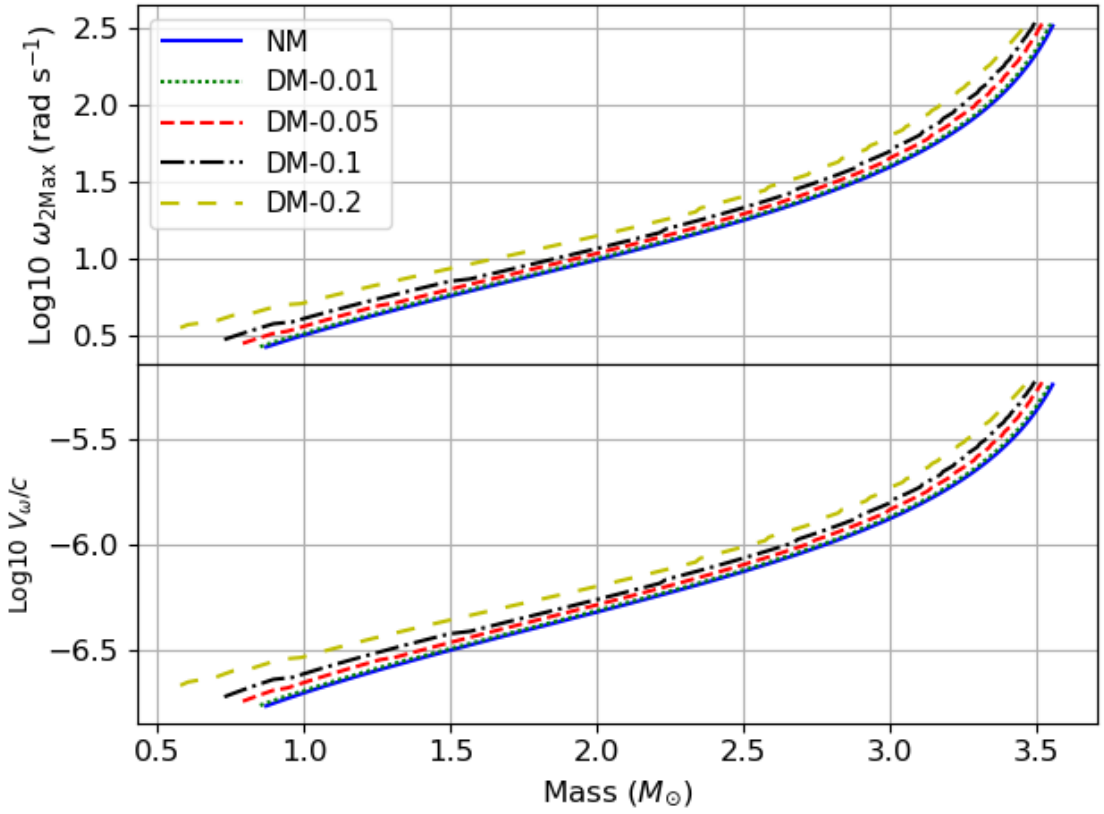

Figure 2.10: Same as Figure 2.4, but for DMRWDs rotating in the Kepler rule and at the secular limit $\sigma = 0.14$.

mass. We show the total and NM masses vs. $\rho_{\rm Max2}$ from 10^9 g cm^{-3} to 10^{14} g cm^{-3} in Figure 2.6. In this plot, we added two more models: DM-0.001 and DM-0.005, indicating DMRWDs with DM masses of 0.001 and 0.005 $M_\odot$, respectively. We find that the effect of admixing DM is to flatten out the intrinsic turning point for the rigidly rotating NM model, so that the maximum total mass could be reached in the traditional $\rho \to \infty$ limit. The maximum total mass would first decrease to a minimum value and then increase with more DM admixtures. We note that the intrinsic turning point for the rigidly rotating NM model at its Keplerian limit has not been discussed in any previous literature. Such a turning point is caused by

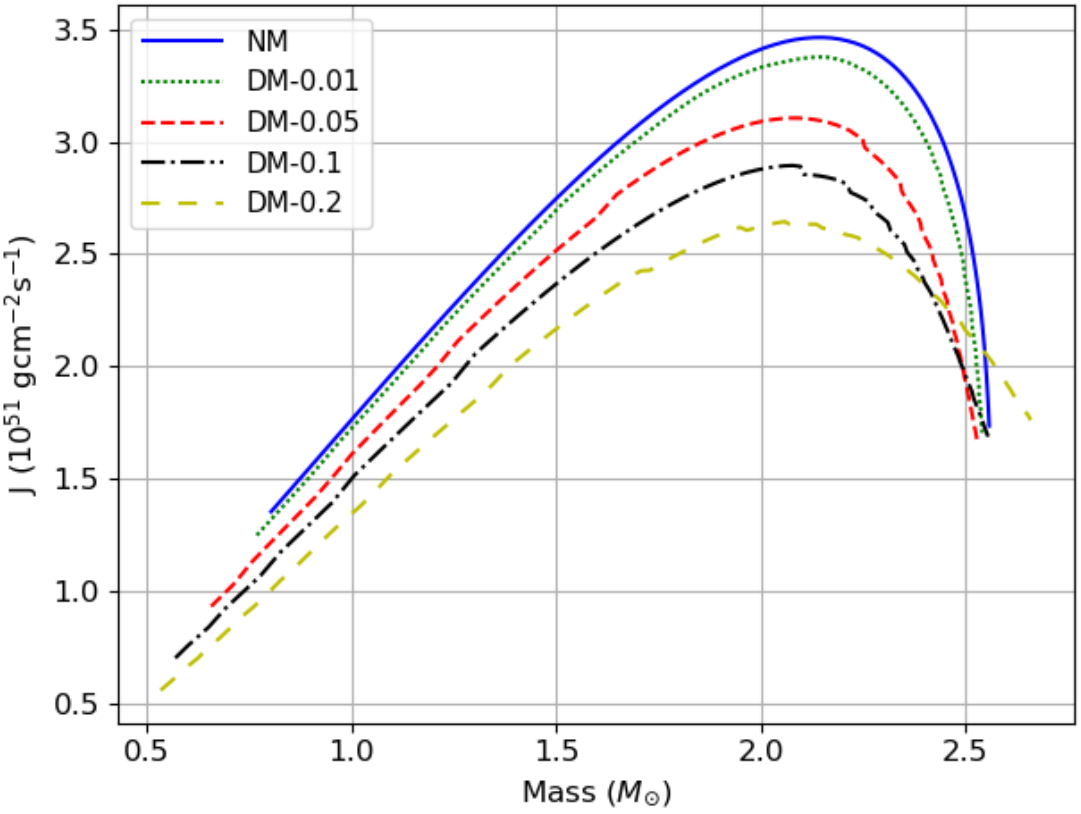

Figure 2.11: Same as Figure 2.10, but for the total angular momentum.

neither the gravitational effects nor the equation of state we employed but is solely related to the fact that the WD is rotating rigidly. We investigate the dependency of such a turning point in Figure 2.7. We find that the turning point does not exist if the NM is rotating at a lower rate (e.g., $\omega = 0.4\ \omega_{\rm Kep}$). The turning point emerges when the NM is rotating close to the Keplerian limit (e.g. $\omega = 0.8\ \omega_{\rm Kep}$).

Kepler Rotation

In contrast to the rigid rotation, a differentially rotating WD can have a much smaller κ_2, but the star is still below the Keplerian limit [245, 92, 117, 118]. These flattened configurations often resemble the shape of that of a 'hamburger' or 'dough-

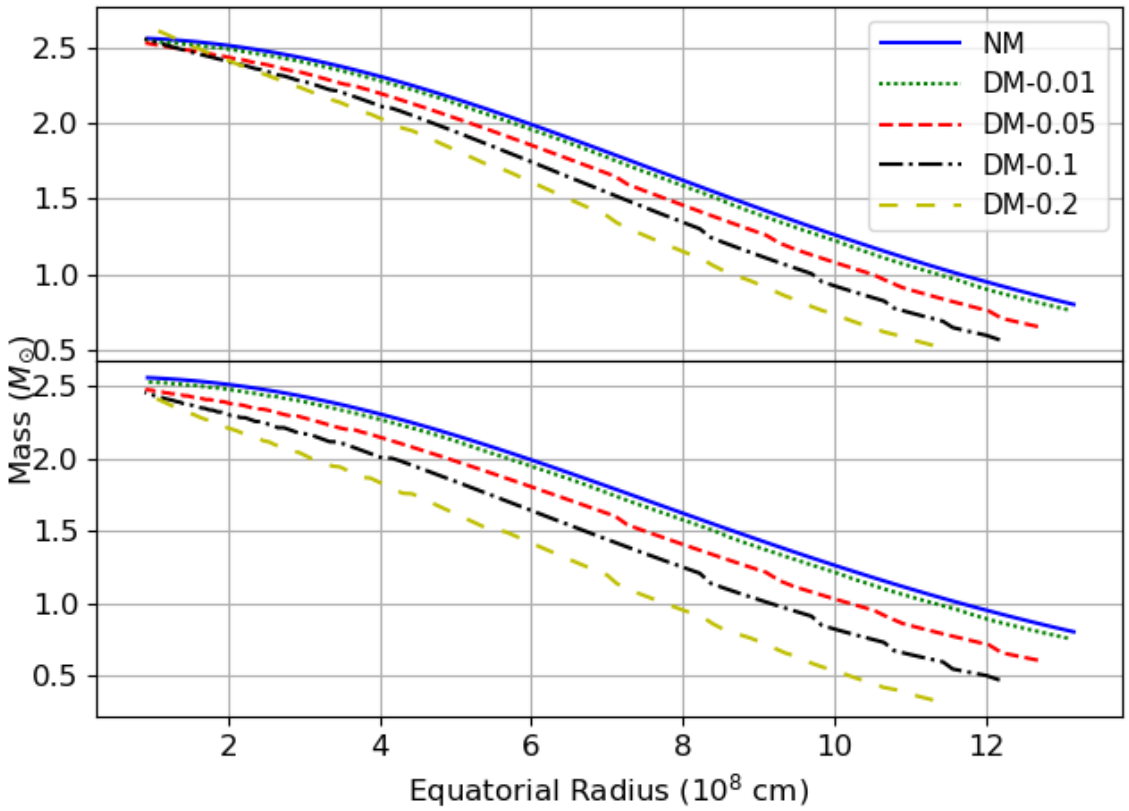

Figure 2.12: Same as Figure 2.5, but for DMRWDs rotating in the Kepler rule and at the secular limit $\sigma = 0.14$.

nut' [112, 131]. In some cases, a WD can theoretically have both boundaries lying on the equatorial axis. Such toroidal configurations were discussed in some previous theoretical calculations [130, 94]. However, we will obtain the sequence of equilibrium configurations by fixing $\rho_{\rm Max2}$ while reducing κ_2 to 0. We do not consider toroidal configurations for DMRWD in this work.

A differentially rotating white dwarf can also support a massive component that is way beyond the traditional Chandrasekhar limit [323, 65, 147, 119, 21, 367] up to 4 $M_\odot$ [245]. However, such a massive configuration could not last long, as the

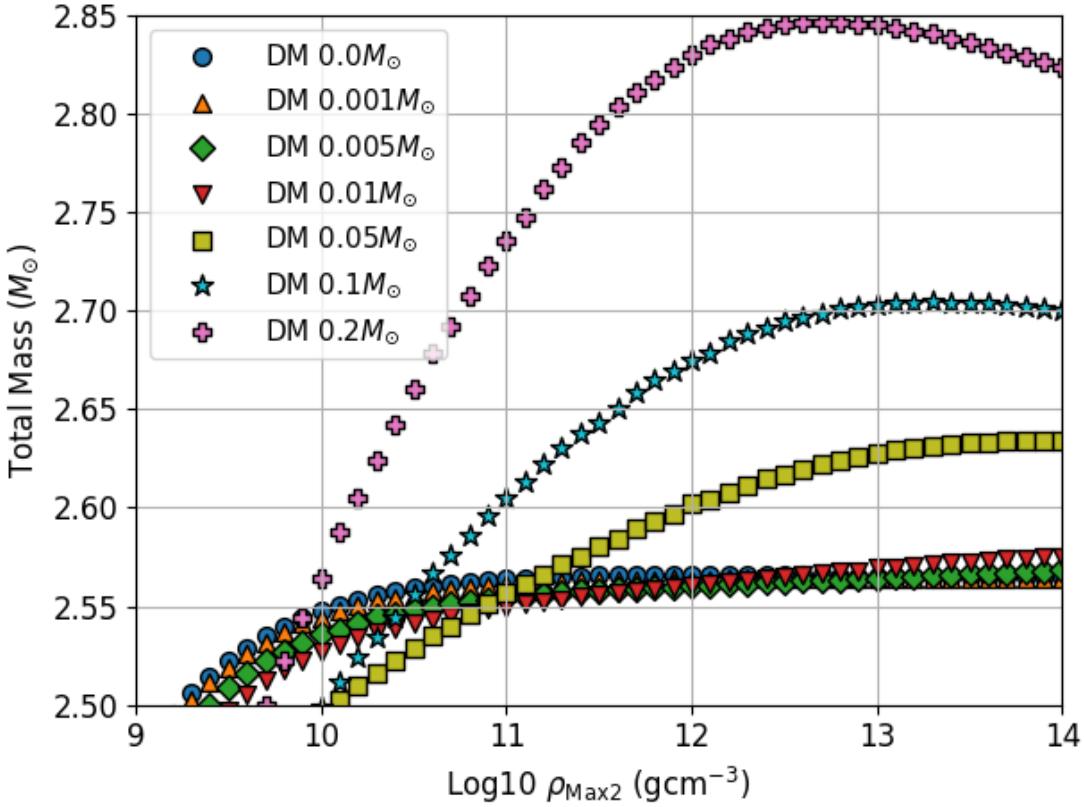

Figure 2.13: Total mass of DMRWDs rotating in the Kepler rule and at the secular limit $\sigma = 0.14$ vs. ρ_{Max2} in the log scale.

secular instability sets in for $\sigma > 0.14$ [28, 88, 110, 364, 133]. This instability is believed to be driven by the gravitational wave emission as the dissipation mechanism [109, 58, 232, 165, 273]. We find that DMRWDs rotating in the Kepler rule could achieve a $\sigma > 0.14$ if κ_2 is small enough. Therefore, we would obtain the configurations for different DMRWDs rotating in the Kepler rule by tuning κ_2 down until reaching the secular limit $\sigma = 0.14$.

Similarities with the Rigid-Rotational Rule. We show the maximum angular and rotational speeds (total angular momentum for $\sigma = 0.14$) for DMRWDs rotating in

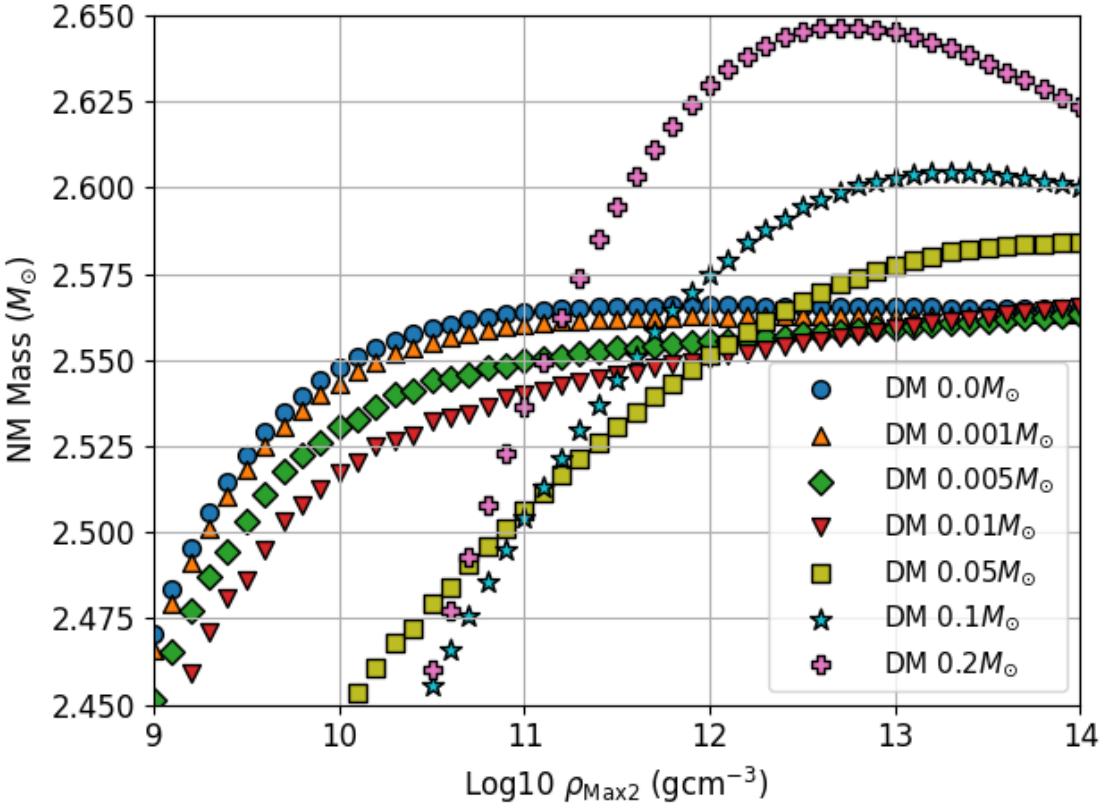

Figure 2.14: Same as Figure 2.13, but for the NM mass.

the Kepler rule in Figure 2.10 (2.11). Similar to what we have found for the case of rigid rotation, admixing DM allows the NM to rotate faster, but with less total angular momentum, than the pure NM model with the same total mass. We have also plotted the total and NM masses against the NM equatorial radius in Figure 2.12. Admixing DM leads to a decrease in the NM mass when compared to the pure NM model (with the same total mass), provided that $\rho_{\rm Max2}$ is not too large ($\lesssim 10^{10}$ g cm^{-3}).

Maximum Total Mass. An apparent effect of admixing DM to compact objects would be the alteration of its limiting mass. [195] showed that admixing DM with

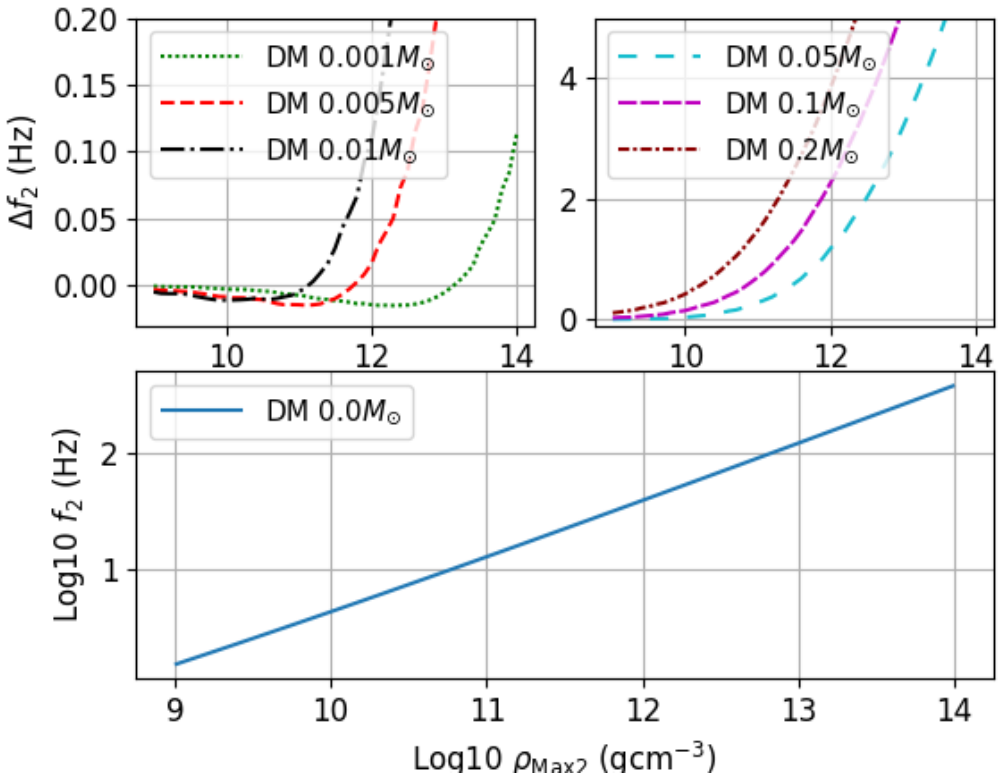

Figure 2.15: Equatorial angular frequency f_2 against $\rho_{\rm Max2}$ for different DM-Admixed models. In the lower panel, the $\log_{10} f_2$ was shown against $\rho_{\rm Max2}$ for the pure NM model. In the upper panel, the differences between f_2 of the DM-admixed models and that of the pure NM model, Δf_2 was shown. As more DM is being admixed, Δf_2 increased and hence the NM is rotating faster.

particle mass of 1 GeV would significantly reduce the Chandrasekhar mass, whereas admixing Fermionic DM with particle mass of around 0.1 GeV would increase the Chandrasekhar mass if one includes more than certain fractions of DM [60]. Here, we study how the limiting mass of differentially rotating WDs would change in the presence of DM. In particular, we compute the total and NM masses against the maximum NM density from 10^9 g cm^{-3} to 10^{14} g cm^{-3} for DMRWDs rotating in the Kepler rule, with a fixed DM mass ranging from 0.001 $M_\odot$ to 0.2 $M_\odot$. We show

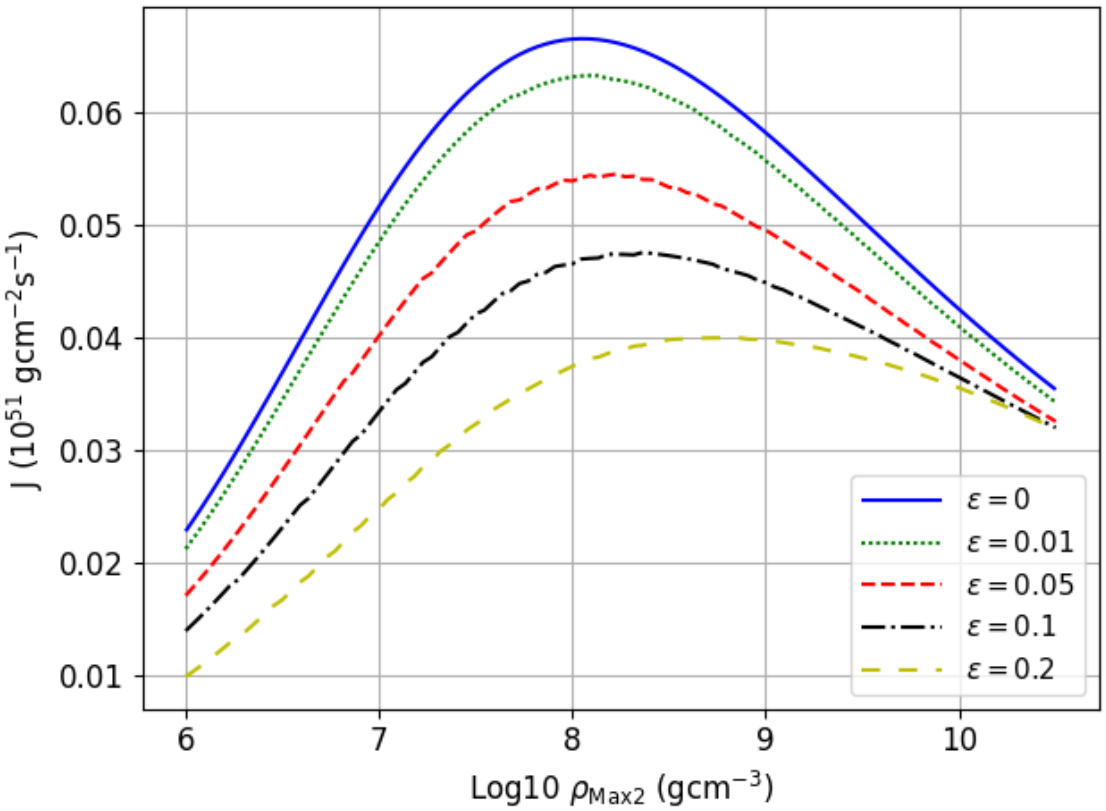

Figure 2.16: Total angular momentum J versus the Log10 NM maximum density $\rho_{\rm Max2}$ for slowly rotating DMRWD of different DM fractions ϵ. This is for DMRWDs rotating in the Kepler rule. The plot for rigidly rotating DMRWDs is similar to this plot and hence omitted.

their results in Figure 2.13 and 2.14 respectively. The ideal degenerate Fermi gas EOS is assumed. The apparent maximum total and NM masses at finite $\rho_{\rm Max2}$ are due to the upper limit of $\sigma = 0.14$ we have set. To better understand the turning point, we can consider a fixed $\rho_{\rm Max2}$. When $\rho_{\rm Max2}$ is large, the central part of the NM becomes more compact. Although this would increase $|W|$, a larger fraction of NM rotates faster so that T also increases. If the NM mass increases indefinitely, T will eventually increase faster than $|W|$, surpassing the limit $\sigma = 0.14$. The upper limiting mass of NM in the high $\rho_{\rm Max2}$ region that do no surpass $\sigma = 0.14$ would be

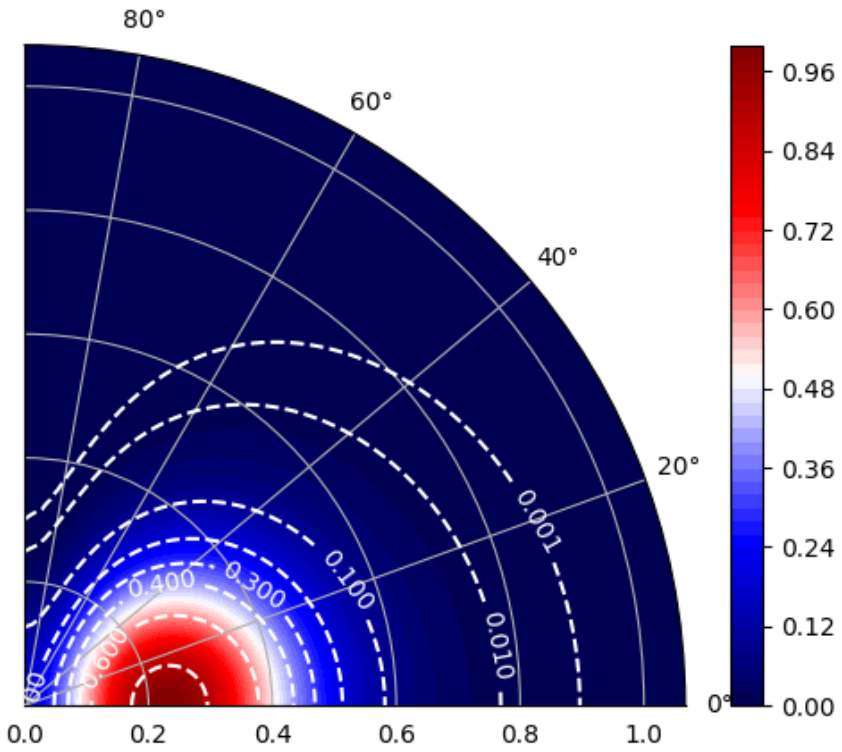

Figure 2.17: Same as Figure 2.8, but for DMRWDs rotating in the Kepler rule, with $\kappa_2 = \frac{1}{3}$. Here, the radial distance is in unit of 0.874×10^8 cm.

reduced, creating the turning point.

We also find that the mass-radius relations for the DMRWD behave differently in the large density limit. Admixing DM into a Kepler-rotating WD does not necessarily reduce the NM mass when compared to the pure NM model (with the same $\rho_{\rm Max2}$ and $\sigma = 0.14$). For instance, model with 0.2 $M_\odot$ of DM could support more NM than the pure NM model for $\rho_{\rm Max2} > 10^{11}$ g cm^{-3}. The maximum NM and total masses occur at a finite $\rho_{\rm Max2}$. We observe that their values first decrease to a minimum, then increase as more DM is admixed. In addition, the corresponding value of $\rho_{\rm Max2}$

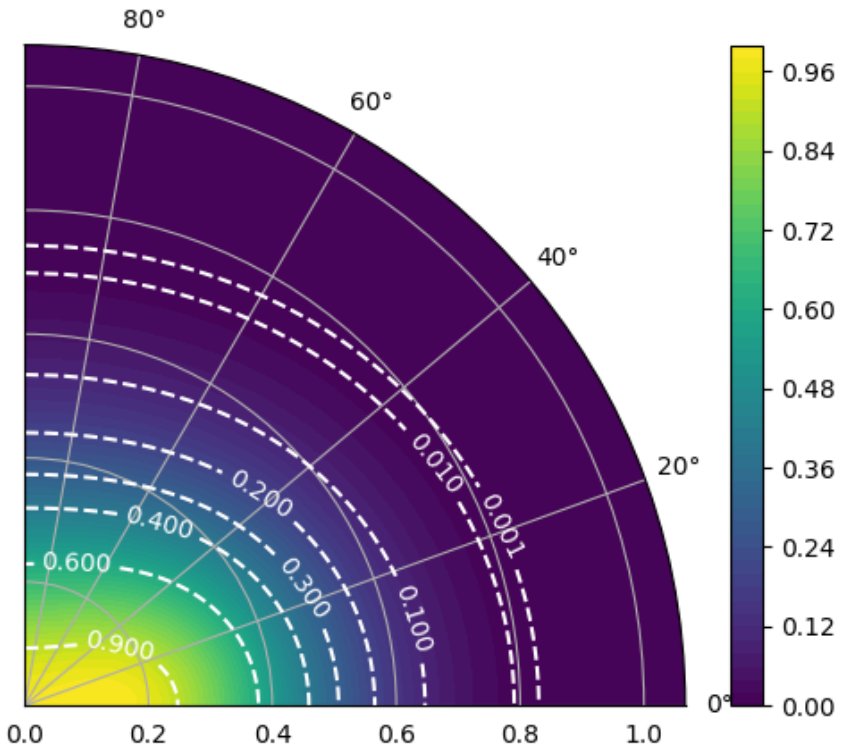

Figure 2.18: Same as Figure 2.17, but for the DM. Here, 0.2 $M_\odot$ of DM is admixed, and $\rho_{\rm Max1} = 10^{9.204}$ g cm^{-3}.

becomes smaller. The increase of the maximum mass, and the shifting of the turning point could be qualitatively understood as the following: when the DM admixture is small, the NM content is reduced to accommodate the DM. The maximum total mass is therefore lowered. The reduction in the NM content reduces its contribution to T. On the other hand, the DM contributes to $|W|$. The turning point for $\rho_{\rm Max2}$ is thus shifted to higher density, where the WD finds itself more compact and thus rotating significantly faster until it surpasses the $\sigma = 0.14$ limit.

However, the situation is different when more DM is admixed. We show in Figure

2.15 the equatorial rotational frequency f_2 against $\rho_{\rm Max2}$. The strong gravitational force from the massive DM contracts the NM to make it more compact and thus faster rotating. The increase in the centrifugal force supports more NM mass, thus increasing the maximum NM and total mass. Although the NM is faster rotating, the contributions to $|W|$ from the NM and DM overcome that in $|T|$. Hence, the limit $\sigma = 0.14$ has not been surpassed even though there are more masses. However, to compensate the increase in the compactness due an increase in the NM and DM mass, the turning point for $\rho_{\rm Max2}$ should move to the less dense region, or else the WD would be even more compact and thus faster rotating, that the requirement $\sigma \leq 0.14$ would be violated.

2.3 Discussion

2.3.1 Dark Matter-Admixed White Dwarfs

We see from Figure 2.2 that, admixing sub-GeV DM would first reduce and then increase the total mass of the DMWD as more DM is being admixed. This change in the total mass is a result of the competition between the NM and DM. The NM mass is reduced to accommodate more DM. However, the reduction of the NM mass could not catch up with the increase in the DM mass if the mass of DM being admixed is large enough, leading to an increment of the total mass. A more quantitative argument (in the Newtonian framework) can be made by considering the following:

$$M_{\rm total} = M_{\rm NM}(M_{\rm DM}) + M_{\rm DM}. \tag{2.17}$$

Here, $M_{\rm total}$ is the total mass of the system. $M_{\rm NM}$ is a decreasing function of $M_{\rm DM}$ and is bound from below by 0. When $M_{\rm DM} \ggg M_{\rm NM}$, we have:

$$M_{\rm total} \approx M_{\rm DM}. \tag{2.18}$$

So $M_{\rm total}$ scales linearly with $M_{\rm DM}$ for large $M_{\rm DM}$ in the Newtonian limit with no maximum $M_{\rm DM}$. This argument could also be applied to the case of admixing DM that has a particle mass over 1 GeV. However, the amount of DM mass required to be admixed in order to increase the total mass will be large, and the DMWD will become a DM-dominant star. Finally, we show in Appendix B that our conclusion holds also in the general relativistic framework.

2.3.2 Dark Matter-Admixed Rotating White Dwarfs

Table 2.2: Stellar parameters of a 2.6 $M_\odot$ DMRWD rotating in the Kepler rule. The density contours of both the DM and NM of this DMRWD are shown in Figures 2.17 and 2.18.

Total Mass ($M_\odot$)	DM Mass ($M_\odot$)		NM Mass ($M_\odot$)
2.61	0.20		2.41
$r_{\rm eq1}$ (10^8 cm)	$r_{\rm eq2}$ (10^8 cm)	$\rm Log_{10}\rho_{Max1}$	$\rm Log_{10}\rho_{Max2}$
0.736	0.874	9.204	10.5

The $I-$Love$-Q$ Relation

[360] discovered universal relations for neutron stars that are independent of the EOS among the (all rotationally-induced) moment of inertia I, mass quadrupole moment Q, and tidal Love number λ_T. These so-called $I-$Love$-Q$ relations are believed to emerge from the strong dependence of I, Q, and λ_T on the structure

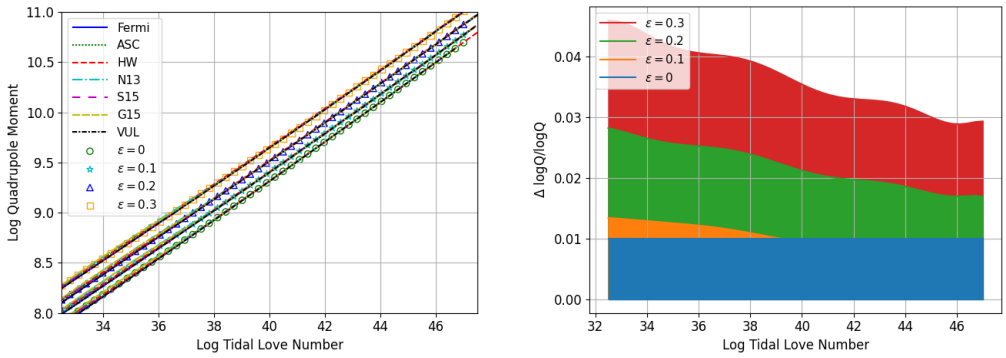

(a) (b)

Figure 2.19: (a) $\log_{10}Q$ vs. $\log_{10}\lambda$ relations for slowly, rigidly rotating DMRWDs having different amounts of ϵ. Models without DM are indicated as $\epsilon = 0$. The scatter plot is best-fit lines generated for each amount of ϵ, and it is obtained using a high-order polynomial fitting. (b) The relative deviation $\Delta\log_{10}Q/\log_{10}Q$ = ($\log_{10}Q_{\rm DM}$ - $\log_{10}Q_{\rm NM}$)/($\log_{10}Q_{\rm NM}$) for different amount of ϵ. $\Delta\log_{10}Q$ is computed by taking differences between the best-fit lines of DM-admixed models with the pure NM model, except for the $\epsilon = 0$ line, which is taken as the MAXIMUM uncertainties of 1% of the $Q-$Love relations for the pure NM model. The coloured bands of parameter spaces are spanned by universal relations of the DM-admixed models and could indicate how much DM is being admixed into the WD. For instance, WDs lying in the green strip are having DM fraction of $0.1 < \epsilon < 0.2$.

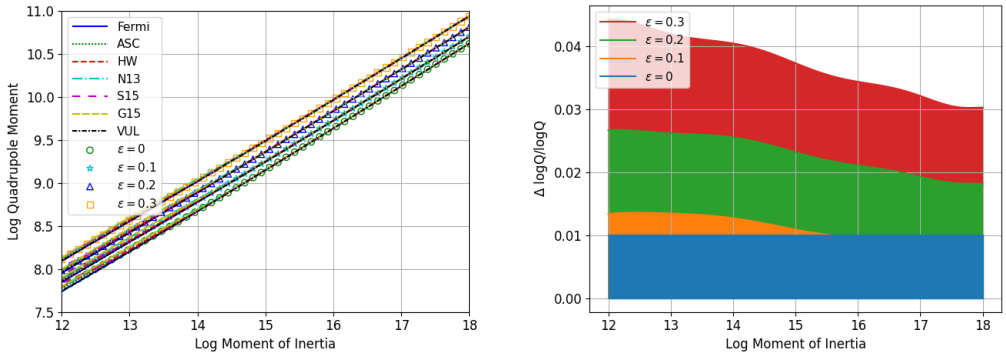

(a) (b)

Figure 2.20: Same as Figure 2.19, but for the $\log_{10}Q$ vs $\log_{10}I$ relation.

of the outer envelope of the neutron star, which is insensitive to the details of the neutron star EOS. A later study revealed that most modern neutron star EOSs are

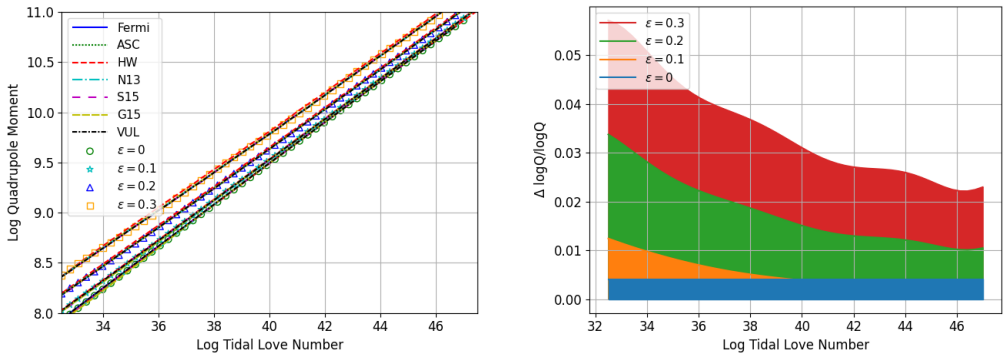

(a) (b)

Figure 2.21: Same as Figure 2.19, but for DMRWD rotating in the Kepler rule. Here, the blue shaded region represents MAXIMUM uncertainties of 0.4%.

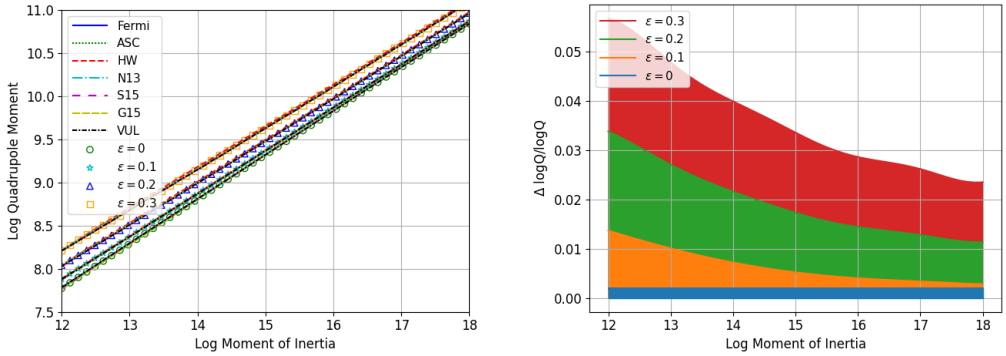

(a) (b)

Figure 2.22: Same as Figure 2.21, but for but for the $\log_{10}Q$ vs $\log_{10}I$ relation, with MAXIMUM uncertainties of 0.2%.

stiff enough to be modeled as an incompressible EOS, which leads to the universality [305]. However, it was pointed out that the similarity of different neutron star EOSs at the outer-most part of a compact object cannot account for such universality, because they can differ from each other by as much as $\sim$ 17% [359]. The reason behind the $I-$Love$-Q$ relations could be an approximate symmetry - isodensity self-similarity, which emerges as one considers stellar objects that are compact [362]. Ever since the discovery of the $I-$Love$-Q$ relations for neutron stars, similar

theoretical studies have been made and confirmed the existence of the universal relations for polytropic stars [363, 23], WDs [37, 36, 286, 333], quark and strange stars [361, 276, 255, 18], and neutron stars with other kinds of realistic EOSs and extreme conditions [137, 219, 61, 314, 254, 157, 6].

The $I-\text{Love}-Q$ information of a compact star is imprinted in its gravitational-wave signature [265, 102, 188, 143]. Even though the sensitivity of current gravitational-wave detectors does not allow direct measurement of the $I-\text{Love}-Q$ numbers, methods for obtaining and testing the universal relations have been proposed [360, 295]. In addition, the $I-\text{Love}-Q$ relations have also been applied to constrain gravitational parity violation [313], extra dimensions [59], gravitational theories [87], neutron star equation of states [271, 64, 255, 183] and moment of inertia [185]. Gravitational-wave measurements of the $I-\text{Love}-Q$ relations could provide an excellent laboratory for testing and understanding fundamental physics.

Although, there are studies of the $I-\text{Love}-Q$ universality for exotic objects such as dark stars [220] and neutron stars admixed with quark matter [20], but none have been made on DM-admixed (rotating) WDs. Here, we extend their studies to DMRWD having a extended component of DM. Since we have computed the equilibrium structures for DMRWDs in a self-consistent way, we can determine I, λ_T and Q by post-processing the density profiles[2]. The moment of inertia of a self-gravitating fluid is given as:

$$I = \int (\rho_1 + \rho_2) s^2 d\tau, \tag{2.19}$$

[2]We expect that the relativistic effect of DMRWDs are small, provided that the WD is not rapidly rotating and ρ_{Max2} is below the nuclear matter density.

while the mass quadrupole moment is:

$$Q = \int (\rho_1 + \rho_2) r^2 P_2(\cos\theta) d\tau, \tag{2.20}$$

where $P_2(x)$ is the $l = 2$ Legendre polynominal. Following [37], we scale I, and Q by:

$$\begin{aligned} I &\to \left(\frac{c^2}{G}\right)^2 \frac{I}{M^3}, \\ Q &\to \left(\frac{Mc^2 Q}{J^2}\right). \end{aligned} \tag{2.21}$$

Here, M is the total mass, and J is the total angular momentum of the DMRWD. On the other hand, λ_T is related to the tidal deformability k_2 as [37]:

$$\begin{aligned} \lambda_T &= \frac{2R^5}{3G} k_2, \\ k_2 &= \frac{3 - \eta_2(R)}{2(2 + \eta_2(R))}. \end{aligned} \tag{2.22}$$

Here, R is the stellar radius, which we take to be the maximum between the NM and DM radii. η_2 is obtained by solving Radau's equation for the unperturbed spherically symmetric configuration [266]:

$$\frac{d}{dr}(r\eta_2) = 6(1 - D(r)(\eta_2 + 1)) - \eta_2(\eta_2 - 2). \tag{2.23}$$

Here, $D(r) = \frac{4\pi r^3 \rho(r)}{3m(r)}$ is the average density of the enclosed mass at a radial distance r. The boundary condition is $\eta_2(0) = 0$. We then scale λ_T as [37]:

$$\lambda_T \to \frac{c^{10} \lambda_T}{G^4 M^5}. \tag{2.24}$$

Previous studies on the $I - \text{Love} - Q$ relations assumed slowly rotating WDs, in

which the equilibrium structures are computed based on the Hartle formalism. In this work, we would mimic small perturbations from the hydrostatic equilibrium by post-processing density profiles that are computed at $\kappa_2 = \frac{239}{240}$.

Deviation of the $I - Love - Q$ Universal relations. We have computed the $I - \text{Love} - Q$ relations for DMRWDs using several EOSs mentioned in section 2.1.3. We construct a few sequences of DMRWD models by varying the maximum NM density ρ_{Max2} from 10^6 g cm^{-3} to $10^{10.5}$ g cm^{-3}. Here, we consider DMRWD with fixed DM fractions $\epsilon = M_1/(M_1 + M_2)$, and we computed DMRWD models with ϵ ranging from 0 to 0.3 in each series.

When there is no DM admixture, the $I - \text{Love} - Q$ relations for WDs computed by using different EOSs lie approximately on the same line for all rotation rules. In particular, the maximum deviations from the best-fit line are within $\sim 1\%$ for the rigid-rotation rules, and $\sim 0.2 - 0.4\%$ for the Kepler-rotation rule. Our results also agree with previous studies on the $I - \text{Love} - Q$ relations of slowly rotating WDs, particularly for the universality lines and the corresponding maximum deviations. For rigidly rotating DMRWDs, we find that admixing a small fraction (e.g. $\sim 5\%$) of DM makes no change to the $I - \text{Love} - Q$ universality. Most of the deviations due to the DM admixture are within the uncertainties of the pure NM model. However, when the dark matter fraction is larger than (e.g. $\sim 10\%$) the $I - \text{Love} - Q$ relations for different EOS are all shifted upwards to higher Q values relative to those without DM admixtures as shown in Figure 2.19 (a) and Figure 2.20 (a). The relative deviation between the universal lines for DMRWDs and those for pure NM models can be larger than $\sim 1\%$ in the log scale, and the deviation is larger with higher DM

fraction. The results for DMRWDs rotating in the Kepler rule are also similar, as shown in Figures 2.21 (a) and 2.22 (a).

In reality, each WD may acquire a different amount of DM. Therefore, WDs would scatter within a band of $I-\text{Love}-Q$ relations spanned by different ϵ. We show these bands together with the uncertainties of the pure NM models in Figures 2.19 (b) and 2.20 (b) for rigidly rotating, and in Figures 2.22 (b) and 2.21 (b) for Kepler rotating DMRWDs, respectively. They are computed by taking differences between the best-fit lines for DM-admixed models with those of the pure NM models. In particular, since the uncertainties (shown as the blue band) of the pure NM model are small, any significant deviation that lies above the pure NM version of the $I-\text{Love}-Q$ relations is possibly a signature of a sub-solar mass scale of DM admixture.

The changes of the universality of the $I-\text{Love}-Q$ relations when DM is admixed could be understood through Equation 2.21. Since $J \sim \bar{\omega} M R^2$, and $Q \sim M R^2$, the scaled Q will be proportional to $1/R^2$. When DM is admixed, the strong gravitational force from the DM would contract the NM to make R smaller, the scaled Q would be increased, which causes the upward shifting of the universal lines. We show the total angular momentum of a slowly rotating DMRWD in Figure 2.16 for a better illustration, where the reduction of J due to an increasing DM Mass (and hence, the fraction ϵ) could be seen.

[333] demonstrated that the $I-\text{Love}-Q$ relations for white dwarfs depend on the degree of differential rotation (the parameter d). However, we find that the

upward shifting of the DM-admixed $I-\text{Love}-Q$ relations from that of the pure NM model is independent of whether the WD is rotating rigidly or differentially. We have computed two entirely different rotational profiles[3] for which the rigid rotation resembles the $d \to \infty$ limit, and we observe the same upward shifting of the $I-\text{Love}-Q$ relations due to DM admixtures. Therefore, we expect similar behavior of the $I-\text{Love}-Q$ relations for different values of d. We note that the universality of the $I-\text{Love}-Q$ relations is violated for hot WDs [**?**]. However, our DMRWD models produce deviations from the NM version of the universal line that are rather different from those of hot WDs. Nonetheless, given the high Fermi energy of degenerate electrons, cold EOS for WDs will remain a good approximation.

Gravitational waves would be emitted in a binary WD merger event [187, 120, 221, 368]. Although the signal is too weak to be detected in the current gravitational-wave detectors, it was estimated that a binary WD merger event could be resolvable for the next generation of detectors [178, 369]. In fact, a method for estimating WD masses by extracting the tidal information from the gravitational-wave signatures has been proposed [350]. Hence, we anticipate that measurements and testing of the $I-\text{Love}-Q$ relations for white dwarfs via gravitational-wave measurement, could help reveal the existence of DM inside rotating WDs, providing in-direct searches for astrophysical dark matter.

[3]Although not shown in this thesis, we have also computed the $I-\text{Love}-Q$ relations for DMRWDs rotating in the j-const rule [130]. The upward shifting of the $I-\text{Love}-Q$ relations due to DM admixtures are also observed.

Ultra-Massive White Dwarf Models

The maximum possible mass of a pure NM, stably rotating WD could be $\sim 2\ M_\odot$ [130, 365, 367]. It was pointed out that ultra-massive WD models with mass up to 3 $M_\odot$ could be accounted for by rotating WDs having strong magnetic fields [76, 78, 77, 324, 24]. However, the limiting value of σ has not been considered. Moreover, it was later pointed out that the ultra-massive magnetic WD models are far from equilibrium because the Lorentz force has been neglected [234]. In addition, the stability of such WDs is limited by pycnonuclear reactions and electron captures [63]. More recent studies give a maximum mass of $\sim 2\ M_\odot$ [105, 246]. Here, and in [367], the maximum mass of a Kepler rotating, pure NM WD is shown to be around 2.58 $M_\odot$.

We show that DMRWDs rotating in the Kepler rule can support a total mass larger than that without DM admixture while being free from secular instability. For example, a DMRWD with a total mass of 2.7 $M_\odot$ can be obtained with 0.2 $M_\odot$ of DM admixtures. Here, we propose DMRWD as an alternative model to construct ultra-massive WDs. For example, we show in Figure 2.17 the NM and 2.18 the DM density contours of a DMRWD model that is rotating in the Kepler rule (see Table 2.2 for its stellar parameters). It has a total mass of 2.61 $M_\odot$ and $\rho_{\rm Max2} \approx 10^{10.5}$ g cm^{-3}, with around 0.2 $M_\odot$ of DM admixture (which is less than 8% of the total mass). Admixing more DM would create stable DMRWDs with an even larger mass. We note that the shifting of the turning points may indicate other kinds of instabilities. However, some of the models that we have constructed are far from the turning points, and so they should be free from these potential instabilities. The investigation of such instabilities will be an interesting future work. A final remark is that the increase

of total mass at a finite $\rho_{2\mathrm{Max}}$ with DM admixed is rotational rule dependent. For instance, we could not find the same phenomenon for j-const rotating DMRWD. The angular velocity profile could be parameterized as follow:

$$\omega(s)_2^2 \propto \frac{1}{(d^a + s^a)^b} \tag{2.25}$$

A systematic study on the criteria of a and b such that total mass could be increased when DM is admixed, will also be an interesting future work.

The recent detection of gravitational waves from a merger event (GW190814) between a 23 $M_\odot$ black hole and a 2.6 $M_\odot$ compact object [2] is puzzling since the mass of the latter falls within the black hole-neutron star mass gap [163]. To resolve this issue, models using modified gravity theories [15], quark matter EOS [34, 285], primordial black holes [342], other neutron star EOSs [340, 334, 122, 329, 145, 329, 97], rotation of the neutron star [85, 230], and combinations of these have been proposed [240]. There are also proposals based on admixture of DM in the neutron star recently [376].

Besides the iron-core collapse of massive stars, the accretion-induced collapse (AIC) of WDs has been proposed to be another channel for forming neutron stars. AIC occurs when the mass of a WD containing an Oxygen-Neon core increases towards the Chandrasekhar limit through stable accretion from a companion object [236, 345, 291], though a binary WD merger seems to be another possible scenario [207]. The collapse is triggered by electron capture in the degenerate matter [48]. On the other hand, pycnonuclear burning is also possible in such an extremely dense core.

Hence the ultimate fate of an Oxygen-Neon WD would depend on the competition between nuclear runaway and electron capture [347]. However, it was later found that the central temperature of Oxygen-Neon WDs is insufficient for explosive oxygen-neon burning [356]. Even if deflagration can take place, it fails to unbind the WD, and this directly leads to a collapse for a wide range of parameters [197, 374, 199].

Although its exact value is not clear [373], the typical runaway density should be $\sim 10^{10}$ g cm^{-3} [328, 297]. A critical density of a few times of 10^{10} g cm^{-3} has also been adopted in multi-dimensional simulations of rotating collapse [84, 3]. We see that DMRWD can be a suitable progenitor that none of the previous rotating WD models could produce. A 2.6 $M_\odot$ DMRWD with $\rho_{\rm Max2} = 10^{10.5}$ g cm^{-3} (which is just about the critical density) can be obtained, and it can be a progenitor for AIC. The collapse of such a WD can form a DM-admixed neutron star that is rapidly rotating while having a total mass of $\sim 2.6\ M_\odot$. This gives rise to another possible explanation of the origin of the 2.6 $M_\odot$ compact object. The AIC of a rapidly rotating WD [208, 83] and a rotating WD admixed with a point DM [201, 373] have been numerically investigated. It will be an interesting future research to analyze the possibilities of forming a 2.6 $M_\odot$ DM-admixed rotating neutron star through multi-dimensional simulations.

Non-Trivial Multi-pole Moments for the Dark Matter Component

A rigidly rotating DMRWD would have κ_2 greater than 0.65. Also, most of the NM is concentrated near the center. The DM remains highly spherical (see Figure 2.9). However, for differentially-rotating DMRWDs the NM would have a deformed structure with most of its mass shifted off from the rotational axis (see Figure 2.17).

The DM reacts to this and forms a deformed ellipsoidal structure (see Figure 2.18). Such a deformation would induce non-trivial higher-order moments for the DM component. The rapid changes of such high-order moments of the DM would imprint a gravitational-wave signature when the DMRWDs approach their end-stage of evolution. Some of the possible scenarios would be AIC [247, 111, 291] and thermonuclear supernovae [95, 302, 174, 377]. The gravitational-wave signatures from the DM component of a collapsing DMRWD were studied by [201] and [373][4]. It will be interesting to investigate the corresponding gravitational-wave signatures of a deformed and extended component of DM in a collapsing and rotating white dwarf.

2.4 Chapter Summary

In this chapter, we presented methods of obtaining the equilibrium models for time-independent 1. spherically symmetric DMWDs, and 2. axial-symmetric DMRWDs. We show that admixing sub-GeV DM particles to WDs could increase their total mass, provided that the amount of DM admixture is large enough. The resulting DM component would have comparable size and mass to those of the NM. These DM-admixed WDs may represent a new class of exotic objects. For DMRWDs, the admixture of DM contracts the NM to make it faster rotating, but with a reduction in the total angular momentum. The deformation of the rotating NM induces multipole moments for the DM even if it is not rotating. The admixture of DM does not break the universality of the $I-\text{Love}-Q$ relations with respect to different NM EOSs, but now they span bands above those without any DM admixture. They may be used as a tool to search for DM inside WDs. We could also construct ultra-massive

[4]They assumed a uniform rotation for the NM plus a small and spherical DM component.

DMRWDs that are way beyond the traditional Chandrasekhar limit to a value of at least 2.6 $M_\odot$. The accretion-induced collapse of such a DMRWD may lead to a 2.6 $M_\odot$ compact object, which may help explain the origin of the mysterious compact star discovered in the gravitational-wave event GW190814.

□ **End of chapter.**

Chapter 3

The Thermonuclear Explosion of White Dwarfs

In this chapter, we first describe how do we obtain the progenitors for DM-admixed Type Ia supernova. We then introduce the necessary tools for simulating the supernova explosion of spherically symmetric DMWDs. We present the simulation results and we discuss the physical implications of our findings. This chapter is based on part of the published article in The Astrophysical Journal, 914(2), 138.

3.1 Methods

3.1.1 The Hydrodynamic Solver

Since the DM only affects the dynamics of the NM by gravity, in this study we identify the primary effects of admixing DM to thermonuclear supernovae by considering the spherically symmetric Newtonian two-fluid hydrodynamics in the Eulerian framework. We show in Appendix D that the dynamics of DM are indeed neces-

sary for this scenario. Multi-dimensional two-fluid simulations in this scenario are computationally demanding because, during the late phase of the explosion, a large simulation box is required when the NM is extended to a much larger radius, while a sufficiently fine grid resolution is needed to resolve the central DM component. In a typical one-dimensional simulation, Lagrangian formalism is often used. We do not consider this formalism because a further interpolation of the local gravitational force by both fluid components becomes necessary when they do not overlap with each other. The two fluids may also have different masses and radii, which makes the definition of the mass coordinate difficult.

Our code is constructed based on the two-fluid hydrodynamics code developed by [160]. Unless otherwise noted, we use geometric units with $G = c = M_\odot = 1$. Different from the work by [193], we have adopted the finite-volume approach where the Euler equations in the spherical coordinate are given as [225]:

$$\frac{d}{dt}\vec{U}_i = -\frac{1}{r^2}\frac{d}{dr}(r^2\vec{F}_i) + \vec{S}_i + \vec{G}_i, \tag{3.1}$$

with the state vector $\vec{U}$ and the flux vector $\vec{F}$ given as

$$\vec{U}_i = \begin{pmatrix} \rho_i \\ \rho_i v_i \\ E_i \\ \Psi_i \end{pmatrix}, \tag{3.2}$$

$$\vec{F}_i = \begin{pmatrix} \rho_i v_i \\ \rho_i v_i^2 + p_i \\ (E_i + p_i) v_i \\ \rho_i \Psi_i \end{pmatrix}. \tag{3.3}$$

Here ϵ_i is the internal energy, v_i is the radial velocity and $E_i = \rho_i(\epsilon_i + \frac{1}{2}v_i^2)$ is the total energy density. Ψ_i is any passive scalar quantity. For example, Ψ_i could be the isotope mass fraction $X(^{12}\mathrm{C})$ of the element ^{12}C. The geometric source term $\vec{S}$ and the extra source term are given as

$$\vec{S}_i = \begin{pmatrix} 0 \\ 2p_i/r \\ 0 \\ 0 \end{pmatrix}, \tag{3.4}$$

$$\vec{G}_i = \begin{pmatrix} 0 \\ -\rho_i \frac{d\phi}{dr} \\ -\rho_i v_i \frac{d\phi}{dr} \\ 0 \end{pmatrix}, \tag{3.5}$$

where ϕ is the gravitational potential, governed by the two-fluid Poisson equation:

$$\nabla^2 \phi = 4\pi(\rho_1 + \rho_2). \tag{3.6}$$

We adopt the Monotonicity-Preserving 5th-Order (MP5) scheme [327] to reconstruct the primitive variables at the cell interfaces. We use the Lax-Friedrich Riemann

solver [156] to compute the interface numerical fluxes, and we discretize the temporal evolution using the method of lines where the strong stability-preserving 3rd-order Runge-Kutta method is implemented [123].

We adopt a modified monopole solver [74] for the gravitational potential because the error due to computing the potential at the cell center while using the mass density at that point could be reduced. We implement a moving-grid algorithm [284] to follow the expansion of the ejecta until it becomes homologous. The moving-grid equations contain a grid velocity v_f so that the fluxes and source term vectors are modified as follows [196]:

$$\vec{F_i} \rightarrow \vec{F_i} - \vec{U_i} v_f, \tag{3.7}$$

$$\vec{G_2} \rightarrow \vec{G_2} - \vec{U_2} \frac{1}{r^2} \frac{d}{dr}(r^2 \vec{v_f}). \tag{3.8}$$

To capture all exothermic reactions before the expanding material reaches the boundaries so that the moving-grid algorithm is triggered, we set the initial grid box size as 2.7×10^9 cm, which is more than 10 times the typical size of the progenitor.

3.1.2 A Simplified Nuclear Network

To reduce the computational time, we implement a reduced nuclear reaction network which was used by [196] and [198]. It was developed based on the original works by [337] and [53]. The nuclear network includes 7 isotopes - ^{4}He, ^{12}C, ^{16}O, ^{20}Ne, ^{24}Mg, ^{28}Si, ^{56}Ni. The nuclear network separates nuclear burning into 3 stages:

1. Combustion of ^{12}C to ^{24}Mg;

2. Burning of ^{16}O and ^{24}Mg to ^{28}Si;

3. Nuclear statistical equilibrium (NSE).

When the deflagration first sweeps through the fuel, step 1 is triggered. The burning proceeds to step 2 which is also called the nuclear quasi statistical equilibrium (NQSE) when the hydrodynamical time step δt is larger than the quasi-equilibrium time step $\tau_{\rm NQSE} = \exp(182.06/T_9 - 46.064)$. Here, T_9 is the temperature in 10^9 K. Finally the burning proceeds to step 3 if the hydrodynamical time step is larger than the NSE time scale $\tau_{\rm NSE} = \exp(196.02/T_9 - 41.645)$. These time scales are provided in, for example, the work by [337] and [53]. For any incomplete burning ($\delta t < \tau_{\rm NQSE}$ or $\tau_{\rm NSE}$), we will use linear interpolation to compute the resulting compositions and energy released. We will discuss the accuracy of the linear interpolation in the Appendix C.

3.1.3 Flame Capturing and Delayed Detonation

To capture the propagation of a subsonic deflagration, which has a width of $\sim 10^{-4}$ cm [41], we adopt the level-set method [304] as our flame capturing scheme. This method was used by several authors in their studies of multi-dimensional thermonuclear supernovae [280, 279, 278]. To initiate the deflagration, we plant a level-set enclosing $\sim 0.02\ M_\odot$ of NM for all models. The spherical symmetry does not allow us to compute the turbulence production explicitly. Therefore, we follow the method in the literature [239, 144, 351, 31, 29] to parameterize the deflagration speed in terms of the local speed of sound c_s. The typical value would be a fraction, possibly a few percent. After various numerical experiments on the pure NM explosions, we choose

the fraction to be 0.06, and the DDT is manually triggered once the deflagration front reaches a density of 1.7×10^7 g cm^{-3} [153] so that the production of ^{56}Ni lies within the acceptable range of 0.4 – 0.7 $M_\odot$. During the onset of the DDT, the speed of the level-set is immediately raised to that of the detonation. The detonation for a density lower than $\sim 2 \times 10^7$ g cm^{-3} is a CJ detonation with the speed of sound, while that for a density higher than $\sim 2 \times 10^7$ g cm^{-3} is a pathological one[1]. The latter one is solved by the method described in [309] and [198].

3.1.4 Supernova Observables

Recent studies on thermonuclear supernovae show that neutrino production could be a key to distinguish different explosion models [355, 354]. It is therefore likely that the neutrino signals will also play an important role in DM-admixed models. We use an open-source neutrino emission subroutine[2] which calculates the pair, photo-, bremsstrahlung, and recombination neutrinos with formulae derived in [150]. The plasmon neutrinos are computed using the method by [164]. To compute the differential production rate for high-energy neutrinos (1 – 5 MeV), we adopt the method by [226] to calculate the pair neutrino spectrum. In addition, the plasma neutrino spectrum is calculated using the method by [242]. These methods have also been applied in some previous works [194, 190]. The differential production rate is then integrated to obtain the total number of thermoneutrinos produced.

[1] Although the transition density is lower than 2×10^7 g cm^{-3}, the detonation front could achieve a density higher than this value because the NM is being compressed during the passage of the detonation.

[2] http://cococubed.asu.edu/

[284] found that the supernova ejecta would approach a homologous expansion in $\sim 5 - 10$ s. Furthermore, most of the exothermic nuclear reactions would come to an end after ~ 1 s, and the distribution of the isotope mass fractions does not change too much between 5 s and 10 s. Moreover, we performed several numerical experiments for the pure NM explosions, and we found that due to the significant increment in the grid size, the mass and energy conservations could become worse if we keep increasing the simulation time. Therefore, we terminate the simulation at 5 s after the runaway has started. The resulting density, temperature, velocity, and isotope profiles are then mapped from our one-dimensional Eulerian form into a one-dimensional Lagrangian form, which is then inputted to the SNEC code [228] to calculate the light curves.

3.2 Simulation Results

Table 3.1: The stellar parameters for different DM-admixed supernova progenitors. The ratios are computed as those of DM over NM. The DM particle mass is fixed at 0.1 GeV.

Model	NM	DM-1	DM0	DM1	DM2	DM3
DM ρ_c (10^8 g cm^{-3})	-	2.0	2.5	3.0	3.5	4.0
NM ρ_c (10^9 g cm^{-3})	3.0	3.0	3.0	3.0	3.0	3.0
DM Mass ($M_\odot$)	-	0.067	0.120	0.201	0.322	0.494
NM Mass ($M_\odot$)	1.374	1.242	1.183	1.124	1.067	1.015
DM Radius (km)	-	975	1160	1380	1640	1920
NM Radius (km)	1930	1890	1830	1740	1650	1560
Radius Ratio	-	0.52	0.63	0.79	0.99	1.23
Mass Ratio	-	0.05	0.10	0.18	0.30	0.47

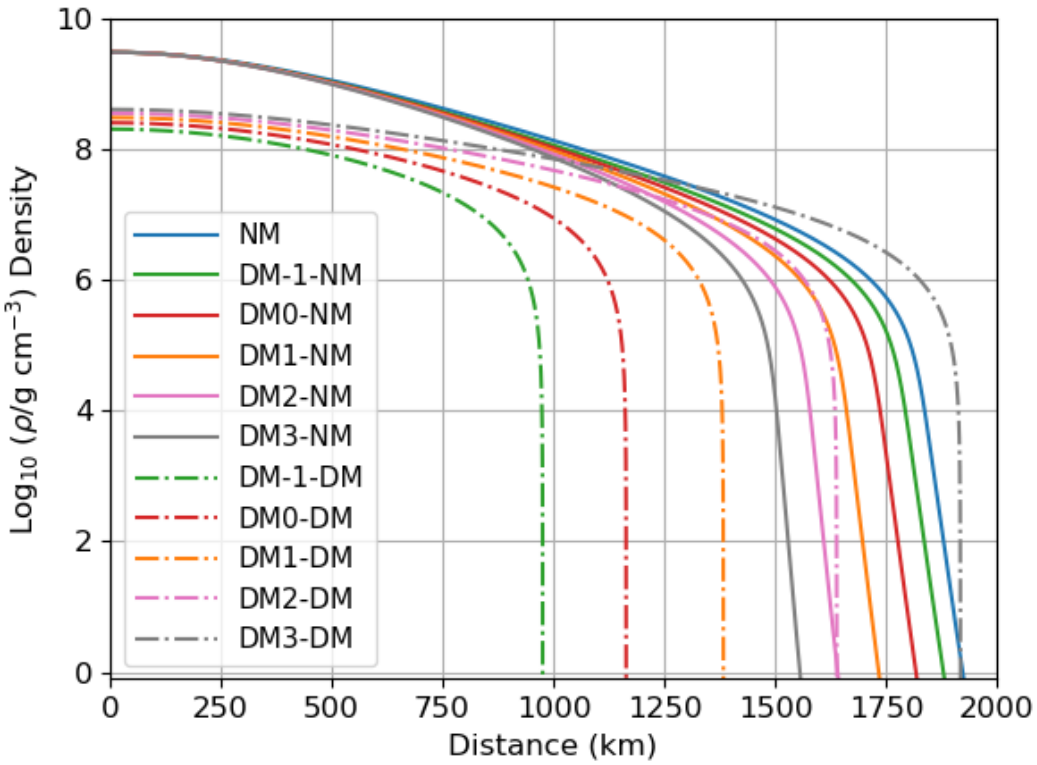

Figure 3.1: The density profiles for the DM-admixed thermonuclear supernova progenitors. The solid (dashed) lines represent the NM (DM) densities for different amounts of DM admixtures (see Table 3.1). The solid blue line is for the WD without DM.

3.2.1 Constructing Supernova Progenitors

We show in Section 2.2 the effects of admixing 0.1 GeV DM on the stellar parameters of the static WD, such as the masses and radii, are particularly interesting. We compute 5 configurations using this DM particle mass as the supernova progenitors: DM-1, DM0, DM1, DM2, DM3. The model with no DM admixture is named model NM. They are chosen with an increasing ratio of the DM to NM masses from 0.05 to $\sim$ 0.5. The parameters for the progenitors are shown in Table 3.1, while the

density profiles for the NM and DM of each model are shown in Figure 3.1. The NM radius of Model DM2 is nearly the same as its DM radius, while model DM3 has an extended DM component that covers the entire NM. Note that in all of the above models, the NM is more massive than the DM. We will show in Appendix A that admixing DM of the order of $O(10^{-1})\ M_{\odot}$ is indeed possible. We will investigate the thermonuclear explosions of these configurations. In particular, we are interested in how the extended DM component will affect the explosion dynamics and the supernova observables.

3.2.2 The Explosion Hydrodynamics

Table 3.2: Simulation results for different models. $t_{\rm DDT}$ is the time of DDT. The last two rows represent the NM and DM energies at the end of the simulations.

Model	NM	DM-1	DM0	DM1	DM2	DM3
$t_{\rm DDT}$ (s)	0.885	0.893	0.920	0.985	1.127	1.340
^{56}Ni Mass ($M_{\odot}$)	0.623	0.577	0.563	0.549	0.520	0.534
Energy (10^{51} erg)	1.650	1.503	1.442	1.383	1.336	1.321
NM Energy (10^{51} erg)	1.512	0.977	0.865	0.713	0.517	0.281
DM Energy (10^{50} erg)	-	-0.091	-0.178	-0.355	-0.758	-1.680

The simulation results are summarized in Table 3.2, where we list the energy, ^{56}Ni generation and time of the DDT. In general, the presence of the DM delays the transition time and reduces energy production. The DM gravitational potential and the interactions between the DM and NM prohibit the expansion of the NM during the deflagration phase. Therefore, the NM needs a longer time to reach the density necessary for a DDT. On the other hand, the ^{56}Ni masses synthesized are similar in magnitude when compared with the pure NM explosion. The ^{56}Ni mass

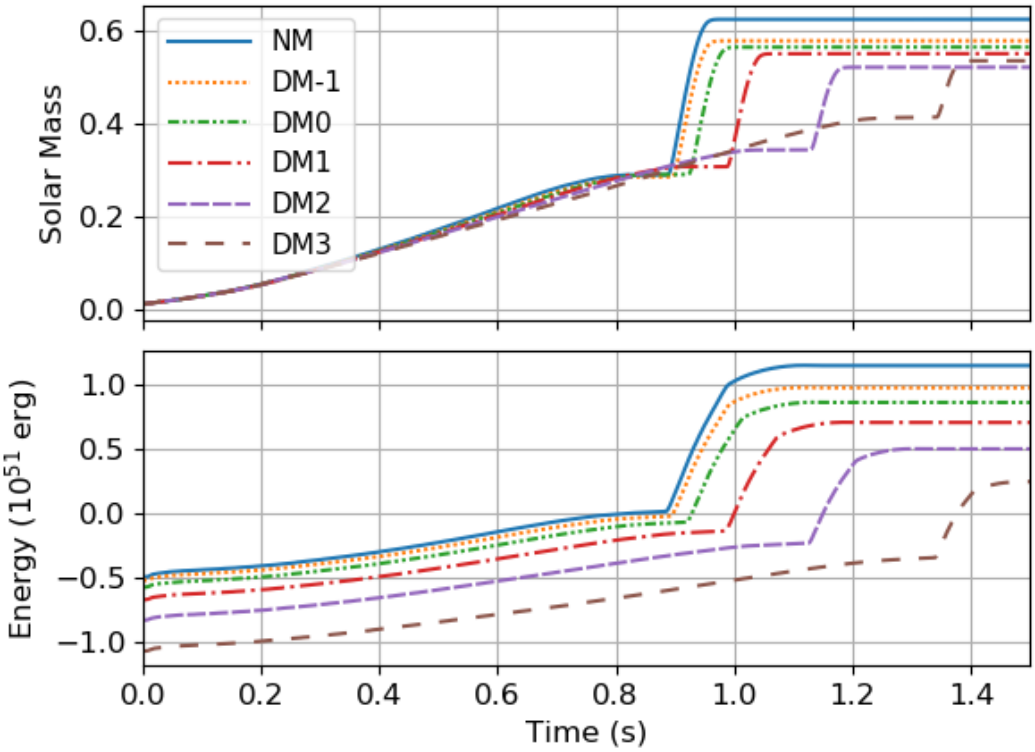

Figure 3.2: Total energy (bottom panel) and ^{56}Ni mass (top panel) vs. time for the DM-admixed models (DM-1, DM0, DM1, DM2, and DM3), compared with those of the pure NM one. See Table 3.1 for the description of the models.

first decreases with more DM admixture to a minimum of the model DM2, then it rebounds when we proceed to the model DM3. We plot the total ^{56}Ni mass variations in Figure 3.2. In general, models having more DM admixture would give lower ^{56}Ni production after the DDT. The steep density gradient would reduce the mass content at the outer envelope of the NM. The amount of ^{56}Ni for the DM-admixed models is compensated by a higher production before the DDT. The prolonged deflagration phase gives more time for the NM to synthesize ^{56}Ni. We also include the total energy variations in Figure 3.2. The energy production after the DDT is smaller for

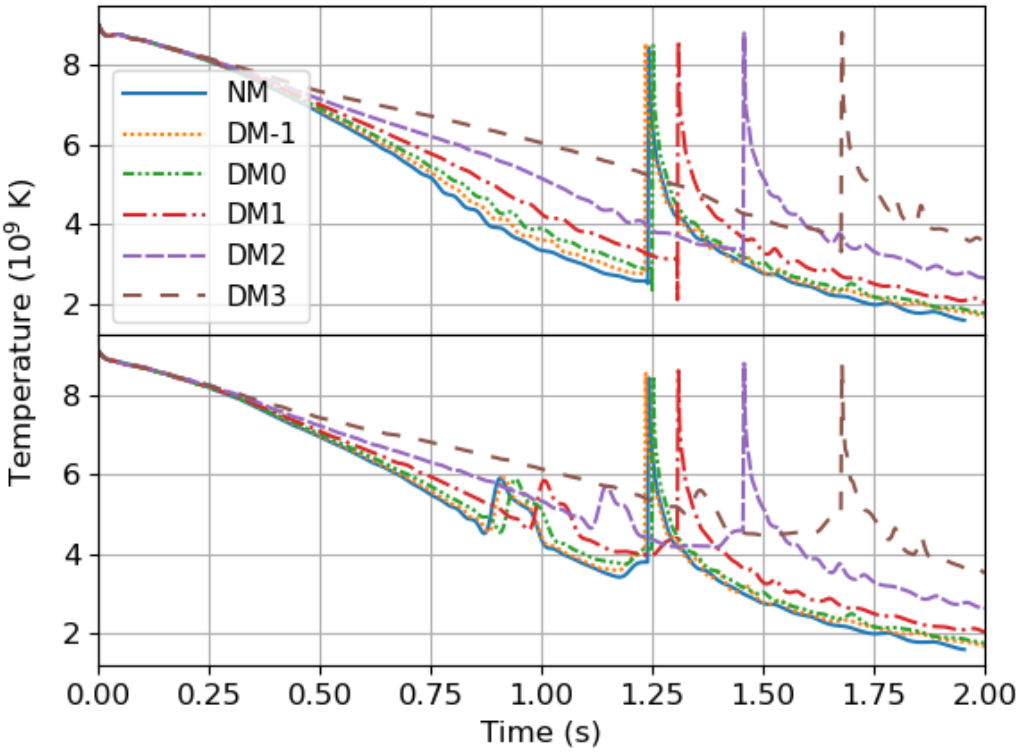

Figure 3.3: Same as Figure 3.2, but for the maximum (bottom panel) and the central temperature (top panel).

models with more DM admixture, which is consistent with the variations of the ^{56}Ni after the DDT.

We show the maximum and central temperatures in Figure 3.3. We find that the presence of the DM tends to keep the NM hotter. This can be explained by the suppressed expansion during the deflagration phase, and thus the NM cannot dissipate its internal energy by the pressure work done. Energy conservation suggests that the loss in the internal energy would be converted not only to kinetic energy but also to gravitational energy. Therefore, for models with more DM admixture, the

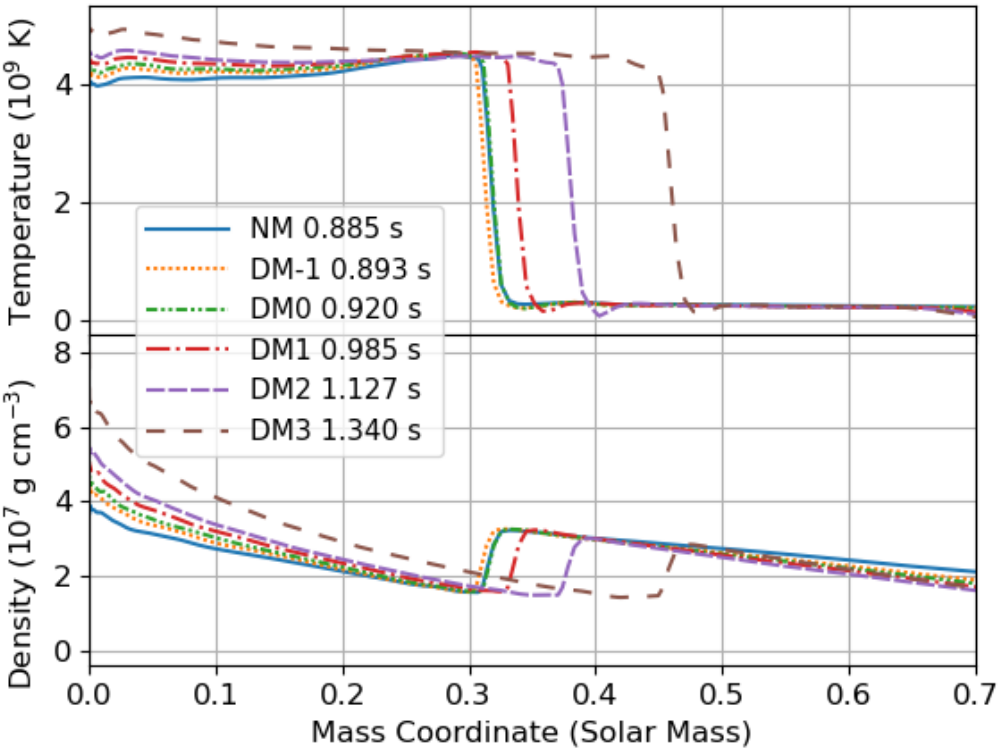

Figure 3.4: NM temperature (top panel) and density profiles (bottom panel) at the moment of DDT for different models. The number specified after each label gives the time of the DDT in seconds.

expansion velocity of the NM is lower. This can be seen in Figures 3.4 and 3.5, where the temperature, density, and velocity profiles for the NM of different models at the moment of the DDT is shown. This also explains why these models have later occurrences of the DDT. The first peak in the maximum temperature corresponds to the DDT, and it is consistent with the transition time $t_{\rm DDT}$ we have recorded in Table 3.2.

We plot the central densities of the DM and NM in Figure 3.6. The presence of DM tends to make the NM expand slower, which is similar to what we have found for

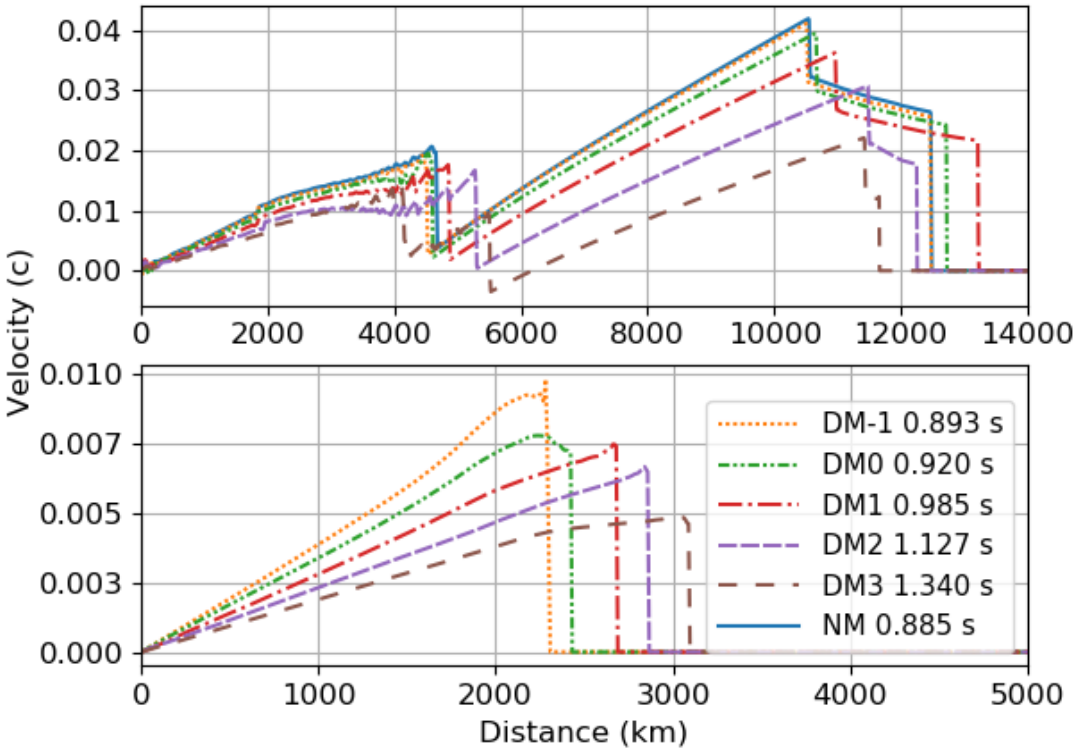

Figure 3.5: NM (top panel) and DM (bottom panel) velocity profiles at the moment of DDT for different models. Note the differences in the axis scales.

the central and maximum temperatures. The sudden increases in the DM and NM central densities lead to the second peaks of the central and maximum temperature. This is because a converging acoustic wave is generated during the DDT. The acoustic wave travels toward the center of the NM, compressing and heating the material.

We also tabulate the DM and the NM energies in Table 3.2 and show their variations in Figure 3.7. The energy E_i of the i^{th} component of the fluid is defined by

$$E_i = \sum_{\text{AllGrids}} \rho_i(\epsilon_i + \phi_j + \frac{1}{2}(v_i^2 + \phi_i)), \tag{3.9}$$

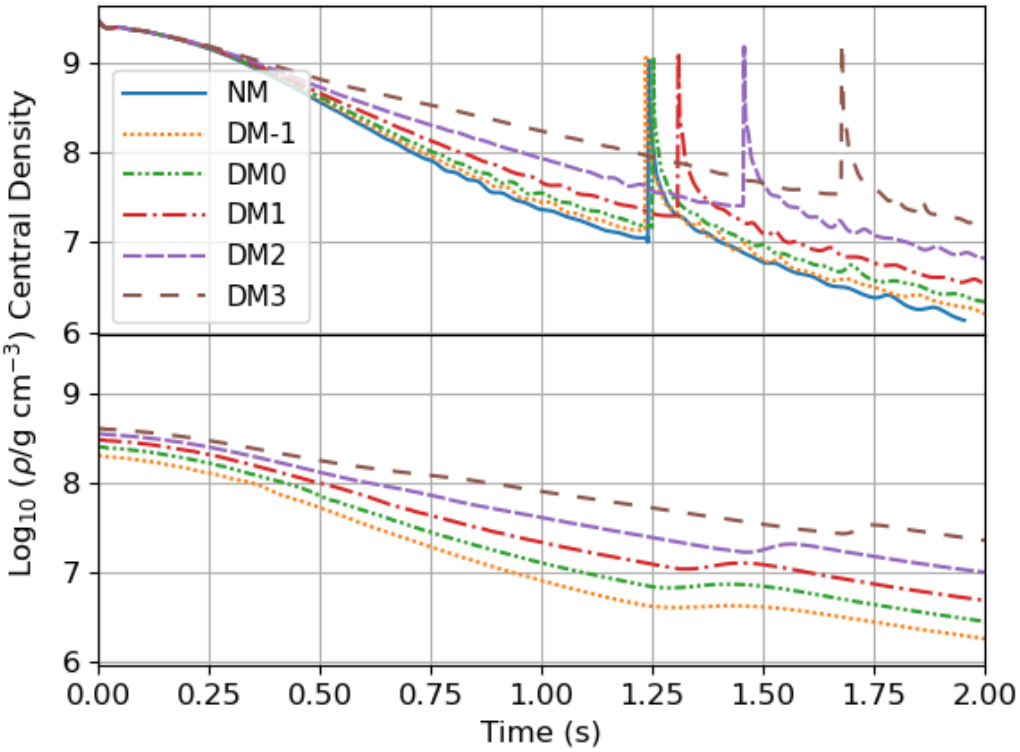

Figure 3.6: Same as Figure 3.2, but for the DM (bottom panel) and NM (top panel) central densities.

where $j \neq i$. The extended DM component has negative energy at the end of the simulations, for all of our considered models, which means that they remain bounded. Figure 3.7 shows that the NM and DM energies would eventually approach constants towards the ends of the simulations. The increase in the DM energy after all major exothermic nuclear reactions are completed is because the contribution from the NM gravitational potential is weaker when the NM expands to a larger size. It hints at the decoupling between some of the most energetic NM and all of the bound DM. The most energetic NM is governed by the explosion time scale which is much shorter than the dynamical time scale of the DM. They can no longer transfer energy to

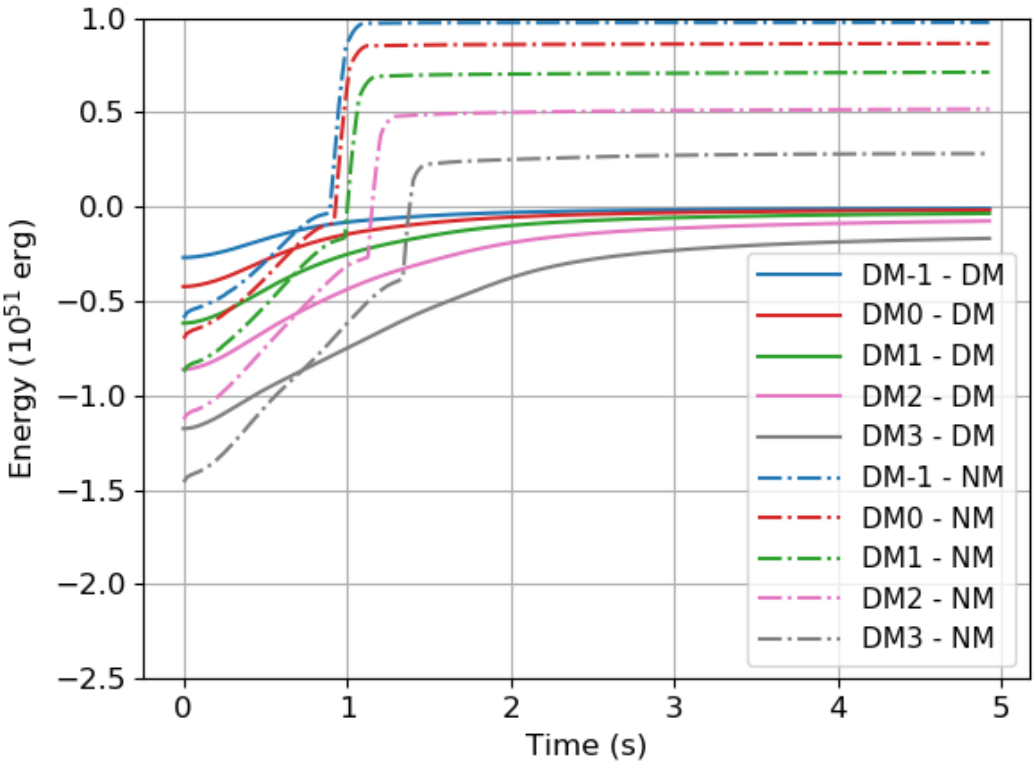

Figure 3.7: Same as Figure 3.2, but for the DM (solid lines) and NM (dot-dashed lines) total energy.

unbind the remaining DM through gravitational interaction.

3.2.3 Computing Supernova Observables

We tabulate the time-integrated total thermoneutrino production and the neutrino energy loss in Table 3.3. We find that models having more DM admixture tend to have a higher neutrino energy loss and more neutrino production in the 1 – 5 MeV channels. We plot the neutrino energy loss rate and the differential production rate for the 1 MeV and 2 MeV channels in Figures 3.8, 3.9 and 3.10. The sudden peaks in all neutrino observables at the transition time $t_{\rm DDT}$ are called 'neutrino bursts'

Table 3.3: Time-integrated neutrino energy loss and the production numbers for each MeV bin of neutrino energy from 1 – 5 MeV, the sum over all bins ('Total'), and the ratio of the total neutrino production of the DM-admixed models to that of the pure NM one.

Model	NM	DM-1	DM0	DM1	DM2	DM3
Energy (10^{47} erg)	0.970	0.958	0.998	1.234	1.426	2.133
1 MeV (10^{52})	1.232	1.176	1.204	1.316	1.595	2.191
2 MeV (10^{52})	1.944	1.911	1.993	2.253	2.875	4.303
3 MeV (10^{52})	1.264	1.265	1.329	1.521	1.981	3.076
4 MeV (10^{52})	0.605	0.612	0.643	0.737	0.959	1.505
5 MeV (10^{52})	0.249	0.254	0.266	0.302	0.389	0.607
Total (10^{52})	5.294	5.218	5.434	6.129	7.800	11.682
Ratio	1.000	0.986	1.027	1.158	1.473	2.207

and they have been observed in several previous studies [355, 354]. The neutrino burst signals are weaker for models that are admixed with DM, but the neutrino production for these models is compensated by the prolonged deflagration phase. This observation is consistent with what we have found for the production of the ^{56}Ni and energy. We sum up the contributions of the thermoneutrinos from the 1 – 5 MeV channels and compute the ratio of the total neutrino production of the DM-admixed models to that of the pure NM one. The total neutrino production for the DM-admixed models could at most increase by a factor of 2.2.

There is an exception to the above discussion, which is the model DM-1. The neutrino observables of this model are weaker when compared with those of the pure NM one. As we have discussed above that the DM gravitational potential traps the NM, which helps to suppress the thermal expansion of the hot NM. However, the DM mass in DM-1 is only 0.067 $M_\odot$. The gravitational potential of the DM is not deep

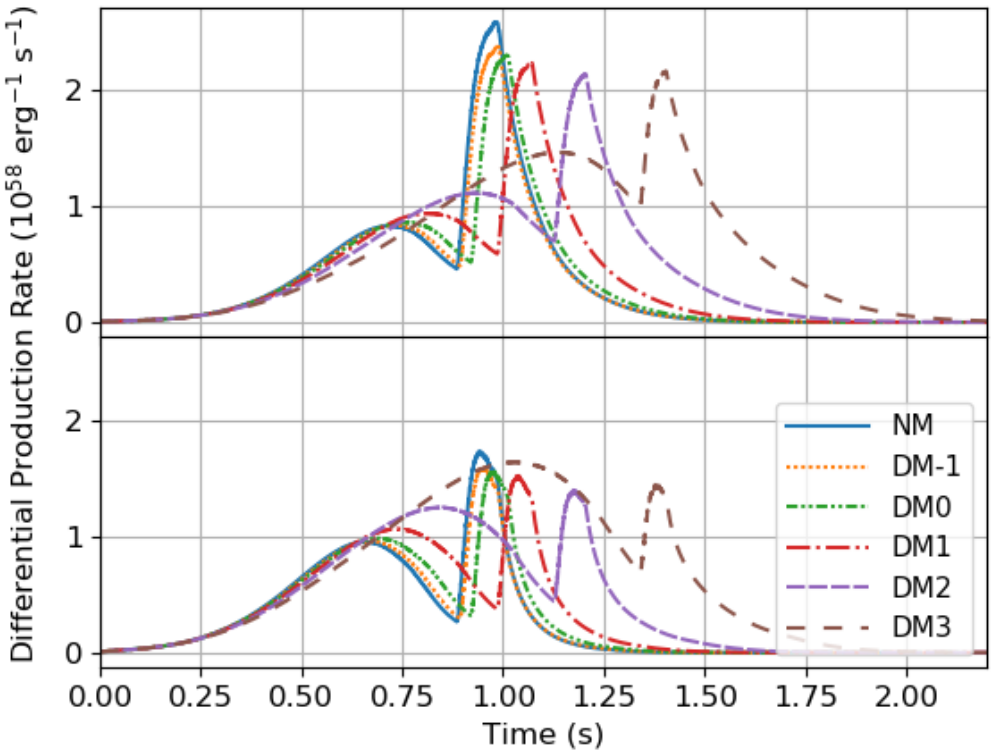

Figure 3.8: The 1 MeV (top panel) and 2 MeV (bottom panel) pair-neutrino differential production rates for different DM-admixed models (DM-1, DM0, DM1, DM2, DM3) compared to those of the pure NM model (solid blue line).

enough to trap the NM (see Figure 3.4). On the other hand, the initial NM mass is substantially decreased by 0.132 $M_{\odot}$. As a result, there is a much lower amount of NM contributing to the production of thermoneutrinos at a similar temperature, and hence the neutrino signal is substantially reduced.

After we terminate the simulation, we map the isotope, density, internal energy, electron fraction, and velocity profiles into a uniform Lagrangian grid. We then input them into the SNEC code. Since the hydrodynamic simulation shows that the DM

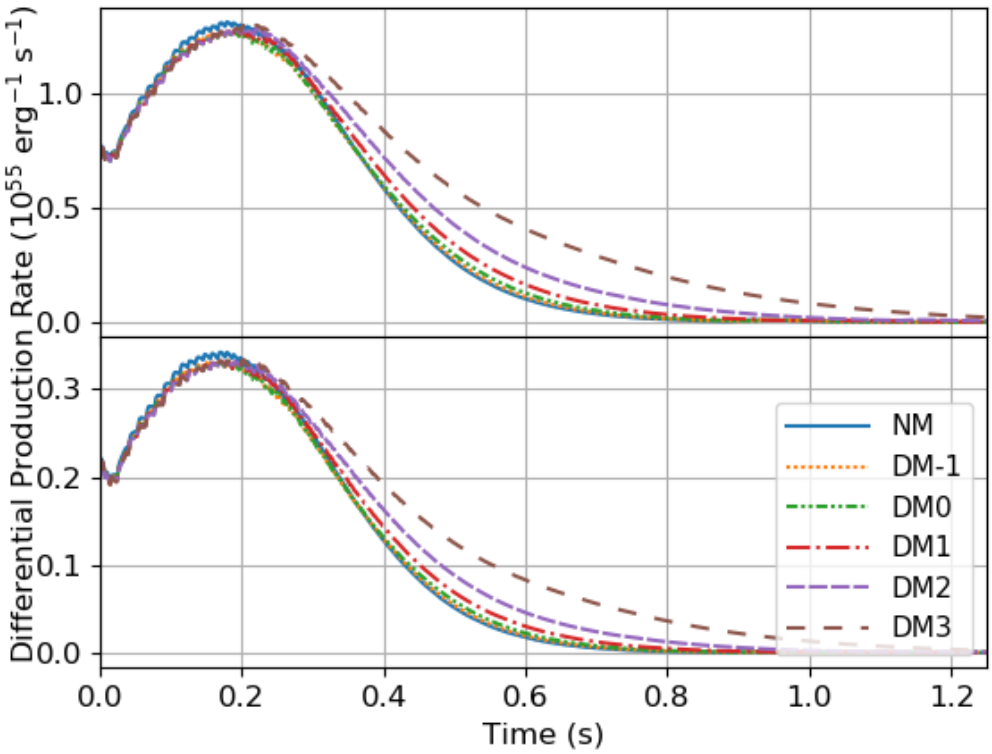

Figure 3.9: Same as Figure 3.8, but for the plasma-neutrino differential production rate.

remains bound while the most energetic NM component is decoupled and ejected, the NM has a typical size much larger than that of the DM at the end of the explosion. To approximate the gravitational effects from the DM, we include the DM gravitational field as a point source $g = -GM_{\rm DM}/r^2$ in the momentum equation of the SNEC code for all of the DM-admixed models.

The luminosity, radius and temperature of the photosphere are plotted in Figures 3.11 and 3.12. We find that the light curves of the DM-admixed models are similar in peak luminosities when compared with that of the pure NM one. In particular,

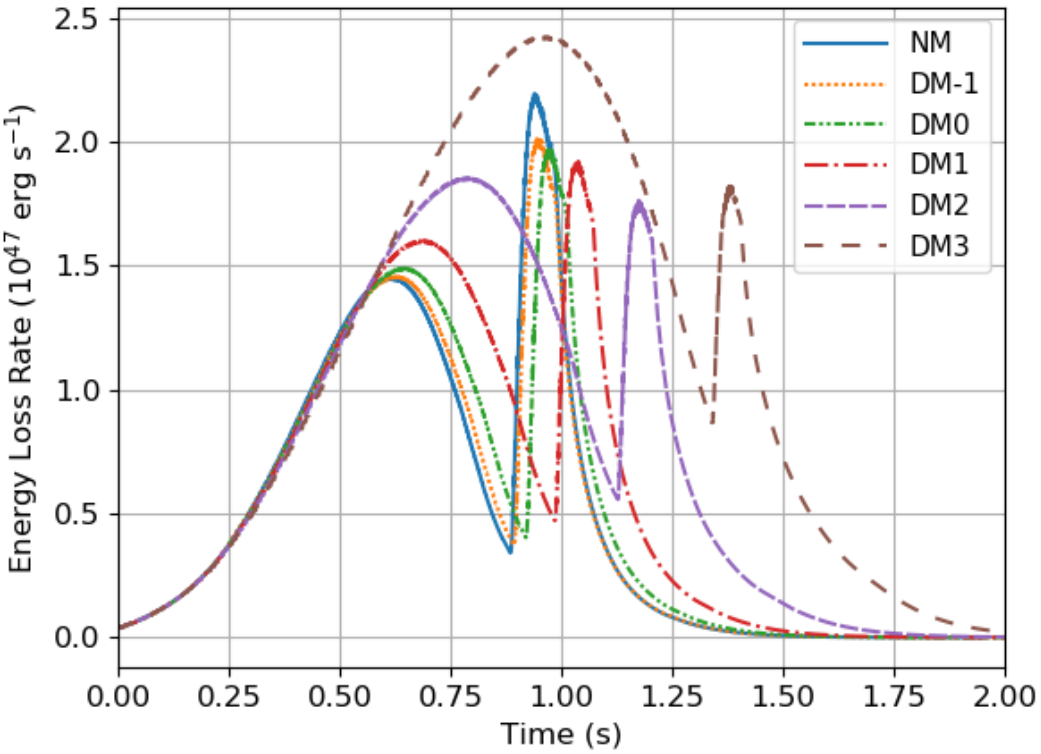

Figure 3.10: Same as Figure 3.8, but for the total thermoneutrino energy loss.

the peak luminosity of the model DM3 is only 2 times lower. This could be understood, as the amount of ^{56}Ni generated are similar. The peak luminosity decreases as more DM is admixed, even though the model DM3 generates slightly more ^{56}Ni than the model DM2. Models that have more DM-admixed produce light curves that are dimmer and slower in rising and decline. These light curves are therefore flatter and broader. Note that in general, there exists a point of inflection for a normal thermonuclear supernova light curve. We find that such a point disappears in the range of 0 – 100 days for those models that have a more massive DM component, such as DM2 and DM3.

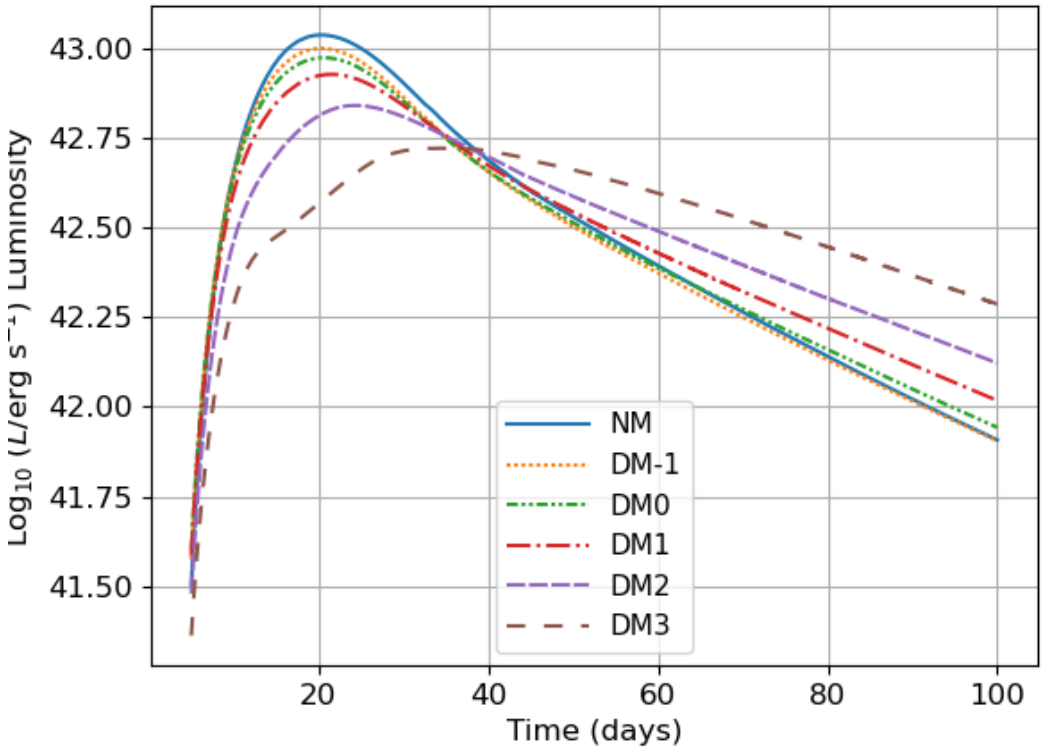

Figure 3.11: Light luminosity L for different DM-admixed models (DM-1, DM0, DM1, DM2, DM3) compared to that of the pure NM model (solid blue line).

DM-admixed models tend to give a higher luminosity, say after 60 days of the explosions. The increased luminosity can be explained by the radii of their photospheres. For the pure NM model, the photosphere shrinks to the center at around 50 days, earlier than all DM-admixed models. The radii of the photospheres even increase to a second peak for the models DM2 and DM3, contributing to their higher luminosities and effective temperatures.

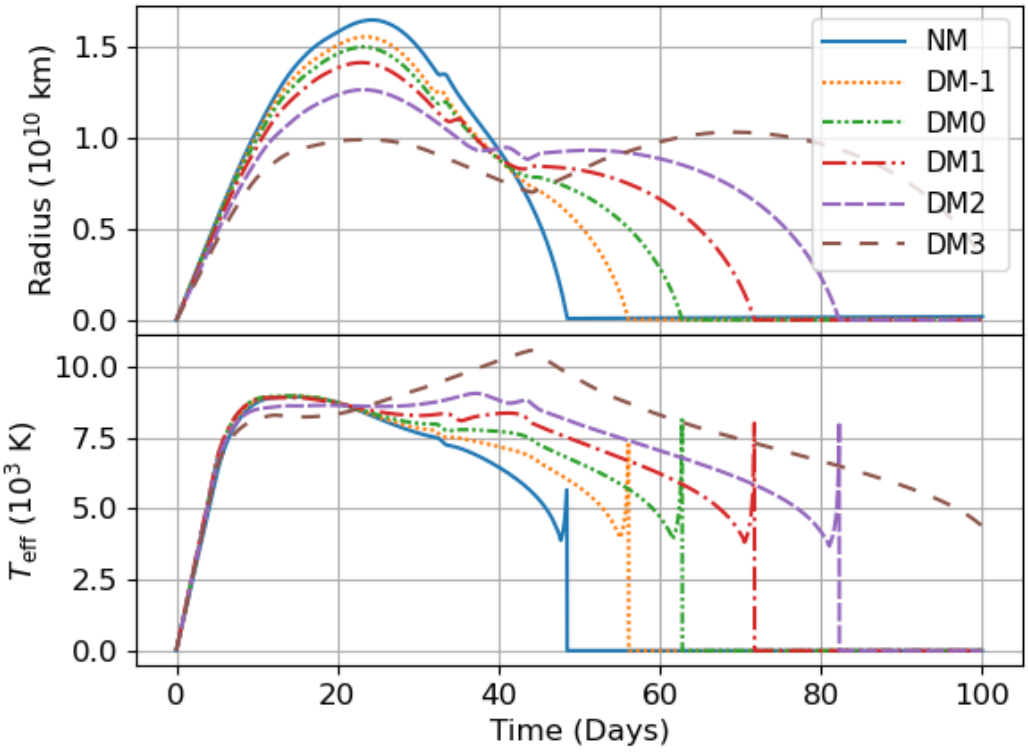

Figure 3.12: Same as Figure 3.8, but for the effective temperature $T_{\rm eff}$ (bottom panel) and the radius of the photosphere (top panel).

3.3 Discussion

3.3.1 Effects of the Extended Dark Matter Component

Admixing DM of 0.1 GeV to a WD could give rise to some interesting equilibrium structures. The DM component no longer acts as a stationary point mass, but it has an extended radius comparable to that of the NM. The subsequent supernova depends on the competition between the NM and DM components. If the DM is massive enough, the extra DM-NM gravitational interaction would have a significant impact on the expansion of the NM during the deflagration phase. It traps and keeps the NM hotter and denser, hence producing more fractions of ^{56}Ni. Though the model DM3 has less NM content compared to that of the model DM2, more ^{56}Ni is produced in the model DM3 than DM2. What if the DM content increases even further? Would it be possible to synthesize more ^{56}Ni than that of the pure NM model? We note that increasing the DM mass would reduce the NM mass. Hence there should be an upper bound of the amount of ^{56}Ni being produced. Furthermore, the DM content may become so massive that no NM could eventually escape from the deep gravitational potential. The explosions would then behave like a failed detonation [166, 263, 159] even though the DDT occurs. It's an interesting future work to model the thermonuclear flame reignition of such an explosion.

3.3.2 Formation of Compact Dark Stars

We show that the DM is left behind as a compact dark star with a mass ranging from ~ 0.07 to 0.5 $M_\odot$ in all of our considered models. This suggests an alternative way to search for astrophysical dark matter through thermonuclear supernovae - to look for any dark compact remnant in a thermonuclear supernova, through the micro-lensing

effect for example. We note that recent development in gravitational-wave astronomy has opened up a new window to search for astronomical compact objects, especially sub-solar-mass black holes [306, 235]. Our results show that if sub-solar-mass dark gravitational sources are observed, they could be compact dark stars remaining after DM-admixed thermonuclear supernovae. [3]

3.3.3 Computing Neutrino Signals

Table 3.4: Estimated total number of neutrino events for different models. The supernova is assumed to be at a distance of 1 kpc away from Earth. The first column lists 4 different detectors. For the LENA detectors, two different detection methods are presented, one using the elastic scattering of electrons (ES0) and the other the elastic scattering of protons (PES). The calculations of the neutrino event rate for different detectors are based on the work of [241]. No neutrino threshold energy is assumed in our rough estimations.

-	NM	DM-1	DM0	DM1	DM2	DM3
Hyper-K, Memphys	3.3	3.3	3.4	3.8	4.9	7.3
Glacier	4.2	4.1	4.3	4.9	6.2	9.3
LENA (ES0)	2.9	2.9	3.0	3.4	4.3	6.4
LENA (PES)	12.0	11.8	12.3	13.9	17.7	26.5

Models with a more massive DM component tend to produce more thermoneutrinos. It would be interesting to estimate the number of expected neutrino events for the models considered in this work. It was shown that the number of events N scale as [57]:

$$N = N_t \times \sigma_\nu \times \frac{\dot{N}_\nu}{4\pi d^2} \times \tau, \tag{3.10}$$

where N_t is the number of targets, σ_ν is the neutrino interaction cross-section, $\dot{N}_\nu$

[3] However, one distinctive feature to distinguish between a dark star and a black hole will be the absence of the event horizon in the former one.

is the number of neutrinos produced per second, d is the distance of the supernova event from Earth, and τ is the time elapsed. There are previous results on estimating the event counts for some neutrino detectors proposed or under constructions [241]. They include the Hyper-Kamiokande [146], Memphys [17, 256], Glacier [17, 287] and LENA [17, 357]. Here, we use Equation (3.10) to estimate the ratios in Table 3.3. The total number of neutrino events is presented in Table 3.4. In general, the neutrino production is distinguishable from that of the pure NM model only for the models DM2 and DM3. We have not done post-processing on the weak interaction neutrinos due to the limited number of isotopes. This together with a more detailed analysis in nucleosynthesis using a full nuclear network will be an interesting research direction in the future.

3.3.4 Effects of the Dark Matter Gravity

Although the amount of ^{56}Ni generated for the model DM3 is more than that of model DM2, the corresponding peak luminosity is lower. Moreover, the light curves for models that have a massive DM component (DM1 – DM3) are flatter and broader, and the corresponding points of inflection disappear. It is interesting to investigate factors governing the peak luminosity and the shape of the light curve. In particular, the major difference between the models DM2 and DM3 is the amount of the DM remnant. To explore the effect of the DM gravity, we add one more light curve for each of the models DM0 – DM3 in Figure 3.13. They are labeled as the model 'NoDM', and the DM gravity is not included in the momentum equation of the SNEC code. We find that the presence of the DM gravitational force significantly alters the peak luminosity and the shape of the light curve. After switching off the DM gravity, the resulting light curves become narrower, brighter, and their points of inflection

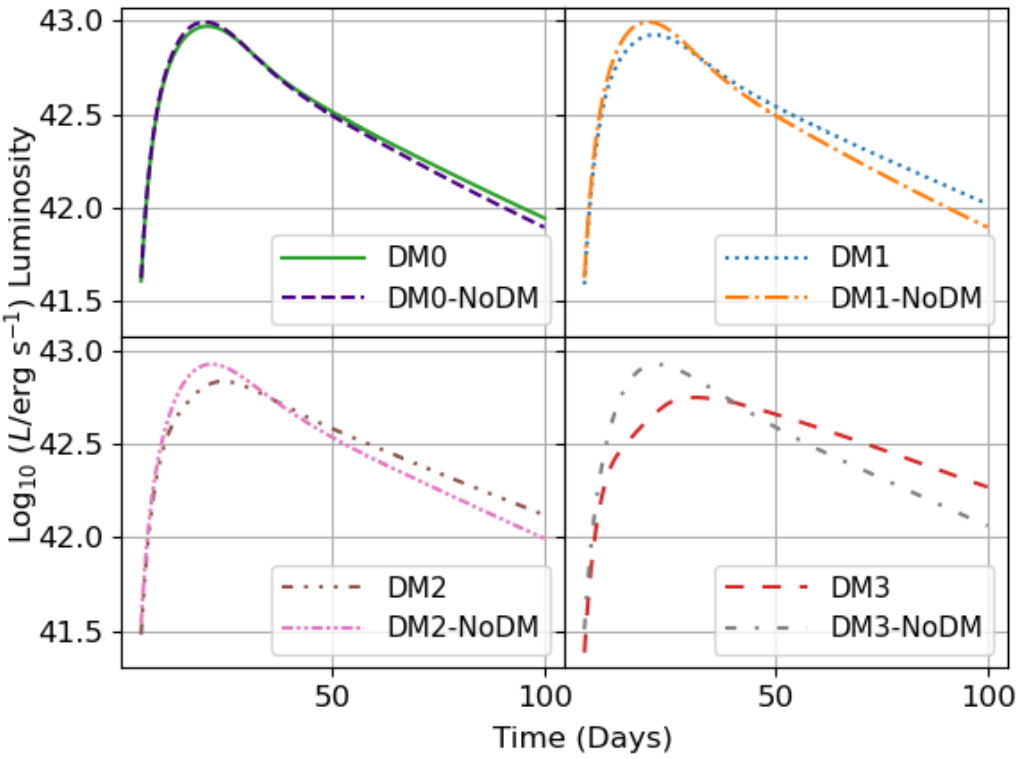

Figure 3.13: Luminosities with and without (labeled NoDM) including the DM gravity in the momentum equation of the SNEC code.

re-appear, especially for the models DM2 and DM3. Thus, we conclude that the effects of DM gravity cannot be neglected in the light curve calculation.

3.3.5 Could there be Any Trapped Normal Matter?

Although the NM in all of the models has positive energies at the end of the simulation, some NM at the tail of the ejecta may remain bound, especially in the zone that is overlapping with the DM remnant. Nevertheless, we are ultimately interested in the supernova observables, and the amount of the free NM is important only in calculating the light curves using an analytic approach [75]. In our studies, we

have already added the effect from the DM consistently in the SNEC's momentum equation, and so the SNEC code would keep track of the falling NM, which makes estimating the amount of unbound NM mass not necessary. Moreover, the fate of the NM in the post-explosion phase is governed by the ^{56}Ni and ^{56}Co decays and the γ-ray deposition. The kinetic energy transfer from the photons would also help to increase the kinetic energy of the NM so that it can escape the DM gravitational potential. However, modeling the radiative transfer of such a model will require a more realistic two-fluid radiative transfer code, involving complex gamma-ray heating in the bound core, which is beyond the scope of this study.

3.3.6 Relation to Peculiar Thermonuclear Supernovae

Peculiar thermonuclear supernovae had been observed in the past few decades. Depending on their luminosities and spectra, they can be further classified as the super-luminous (e.g, SN 1991T, [261]), sub-luminous (e.g, SN 1991bg, [99]), and sub-luminous with strong mixing (also known as Type Iax supernovae). Among many observed Type Iax supernovae, SN 2002cx is one of the classical examples [202]. In particular, some of these events show a slower decline rate than that of a normal supernova. We extract the R-band light curves[4] of the following supernova events: SN 1999ac [55, 115, 315], SN 2002cx, SN 2002es [116], SN 2005hk [67, 260, 315, 319], SN 2012Z [315, 319], from The Open Supernova Catalog [348], and we show them together with the R-band light curves of our models in Figure 3.14. We find that some of the events, for instance, SN 1999ac and SN 2002cx are well fitted by the

[4]We follow the treatment in [348] to consider only the R-band magnitude, so as to be consistent with the discussion in the next section.

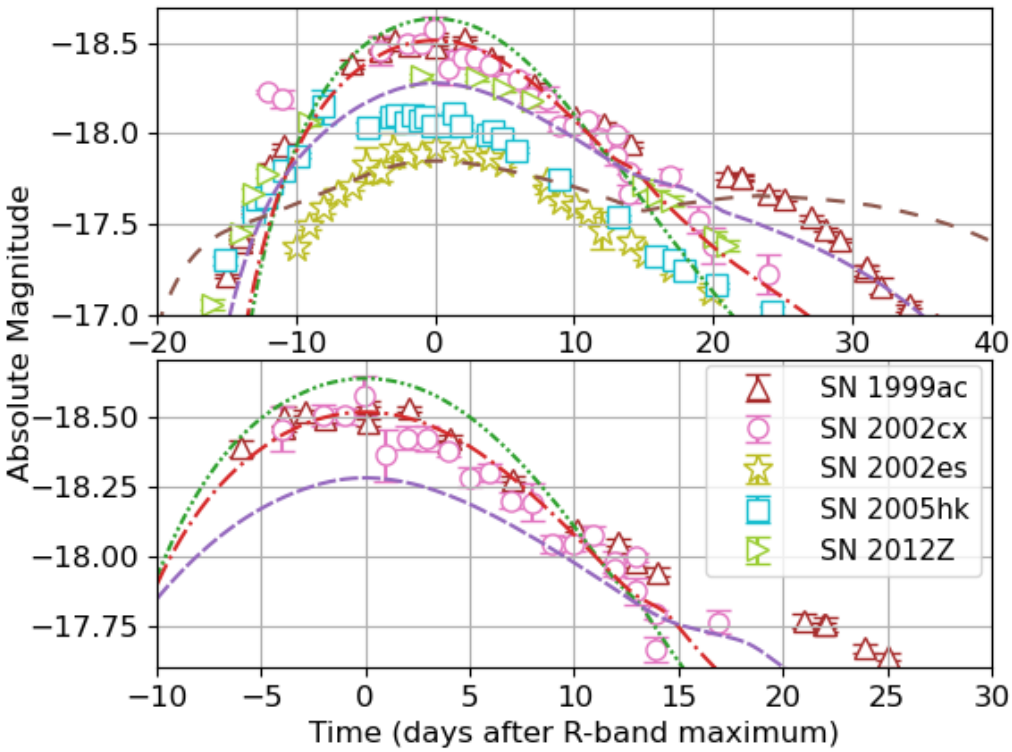

Figure 3.14: Comparison of the R-band light curves of our models with those from the observed peculiar thermonuclear supernovae. Data are extracted from The Open Supernova Catalog [128]. Note that we offset the data in time so that the moment $t = 0$ corresponds to the R-band maximum. See the caption of Figure 3.11 for the description of the light curves of our models. The lower panel is the zoom-in light curves for the models DM0, DM1, and DM2.

model DM1 before 15 days post-R-band maximum[5], suggesting that other than some non-Chandrasekhar models, these two events may also be explained by thermonuclear supernovae having DM admixtures.

[5]In general a multi-frequency radiative transfer code is necessary for a consistent prediction of the band-specific luminosity. In this work, we use the embedded R-band filter implemented in the SNEC code to isolate the R-band luminosity based on the black-body distribution. We only consider the period where the photosphere is hot and dense so that the local thermodynamical equilibrium approximation is valid. The frequency-dependent opacity, for example, will be needed to capture the later evolution, such as the second maximum in the R-band light curve.

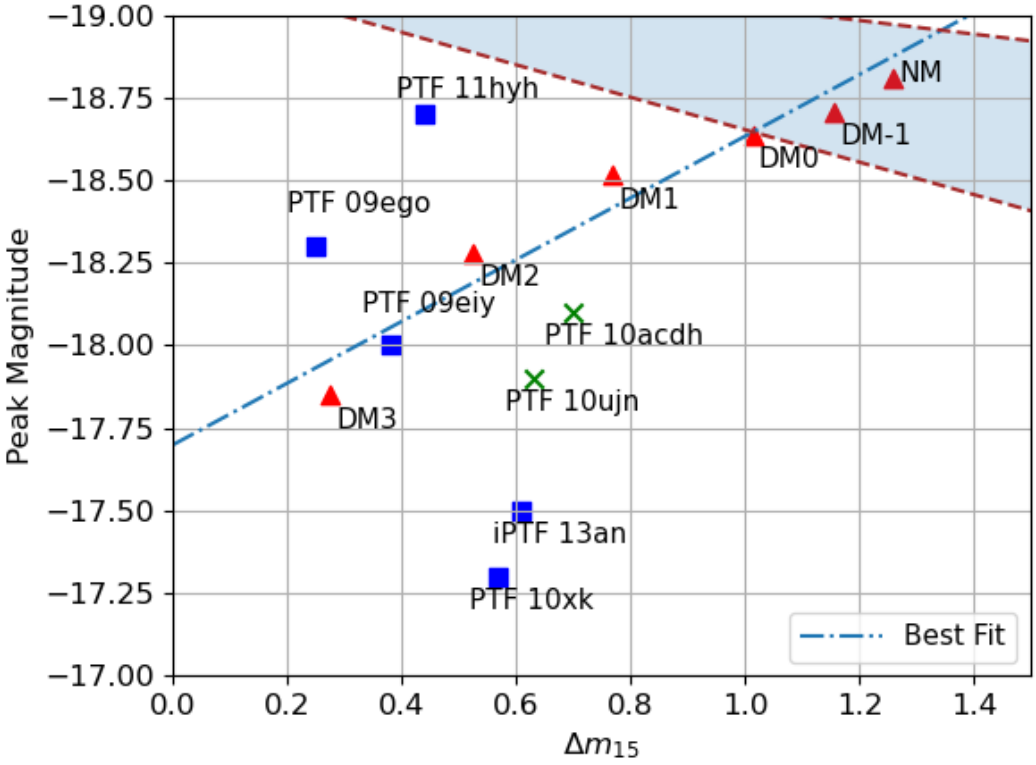

Figure 3.15: Light curve peak magnitudes against decline rates Δm_{15} for our models and some of the observed supernovae taken from [348]. We classify the observed supernovae according to the treatment of the original text. The blue-marked events are the SN 2002cx-like, while the green ones are the SN 2002es-like. Error bars are not shown since they are not given in the original text. The best-fit line gives a slope of -0.934 and an intercept -17.698. The shaded area is spanned by the Phillips relation in the R-Band, computed by [268] using several supernova samples taken from [155].

Recent studies using observational data from the Palomar Transient Factory (PTF, [189]) also found some peculiar thermonuclear supernovae that have a lower luminosity, longer rise time, and a slower decline rate [348]. Such features resemble the drop of the peak luminosity and the flattened light curve in our DM-admixed

models. We plot the peak magnitudes of the R-band light curve[6] against the decline rate Δm_{15}, for the PTF-observed supernovae: PTF 09ego, PTF 09eiy, PTF 10xk, PTF 11hyh, iPTF 13an, PTF 10ujn, and PTF 10acdh, together with those of our models in Figure 3.15. Our models show a wide range of peak magnitudes ranging from -17.8 to -18.8, and decline rates from 0.28 to 1.26. We find that the data of PTF 09eiy are closest to the best-fit line for the series of the DM-admixed models in Figure 3.15, followed by PTF 09ego, PTF 10acdh, and PTF 10ujn. These events seem to be possible candidates for DM-admixed thermonuclear supernovae.

We show that DM-admixed models give rise to orthogonal deviations from the Phillips relation. The prevailing view on thermonuclear supernovae is that they are a group of diverse objects corresponding to multiple explosive models and progenitors, e.g, the Single-Degenerate and Chandrashekhar scenario. Even the Single-Degenerate scenario fails to produce the entire observed width-luminosity relation [317, 243]. Therefore, not only the observed normal supernovae but also peculiar supernovae that deviate from the mainstream of the width-luminosity relation are now believed to be caused by other explosion mechanisms, such as the Double-Degenerate and sub-Chandrashekhar scenarios [332]. We note that there is a recent simulation study on double-detonation explosion models and non-LTE light curve calculations [310]. Their theoretical B-Band data that are generated by progenitors of different masses and compositions could span the observed B-Band Phillips relation. This indicates that non-peculiar supernovae can correspond to explosive models in the sub-Chandrasekhar mass regime, and it also implies that other progenitors or explosion mechanisms are needed to account for peculiar supernovae. We note that several

[6]The discovery paper provides only the light curves data in the R band.

PTF entities presented in Figure 3.15 deviate significantly from the Phillips relation, being slightly dimmer but declining very slowly. We will show in Section 3.3.7 that most canonical models, including Single-Degenerate and Double-Degenerate models, cannot account for this observed feature. DM-admixed models may provide an alternative path to explain some of these peculiar events and to span the parameter space that is not reachable by canonical models. However, we do not intend to claim that all peculiar supernovae are caused by a Single Degenerate progenitor admixed with DM, particularly since we have only done a preliminary analysis through the bolometric light curve here. Instead, we propose the DM-admixed model as an alternative to span the possibilities for some peculiar supernovae.

3.3.7 Comparison with Other Explosion Models

In Chapter 1.4.2, we introduce several alternative explosion models for Type Ia supernovae. Here, we show the distinctive features of DM-admixed models when compared with the pure NM models with a different explosive condition or mechanism. As we have discussed, the explosions of Chandrashekhar WDs using the DDT model failed to produce the observed Phillips relation. Instead, they produce an orthogonal width-luminosity relation, either by varying the compositions or the ignition conditions of the progenitors [317, 243]. However, we show in Figure 3.16 that none of these results could reach the parameter space that is spanned by the massive DM models, say DM1 – DM3. Results from the Double-Degenerate prompt explosions, on the other hand, could give slowly declining light curves, but they are then too bright [353, 227, 311]. On the other hand, the Double-Degenerate scenario with a Carbon-Oxygen companion, rather than a Helium companion, is proposed to account for some peculiar supernovae that have low luminosities but slowly evolving

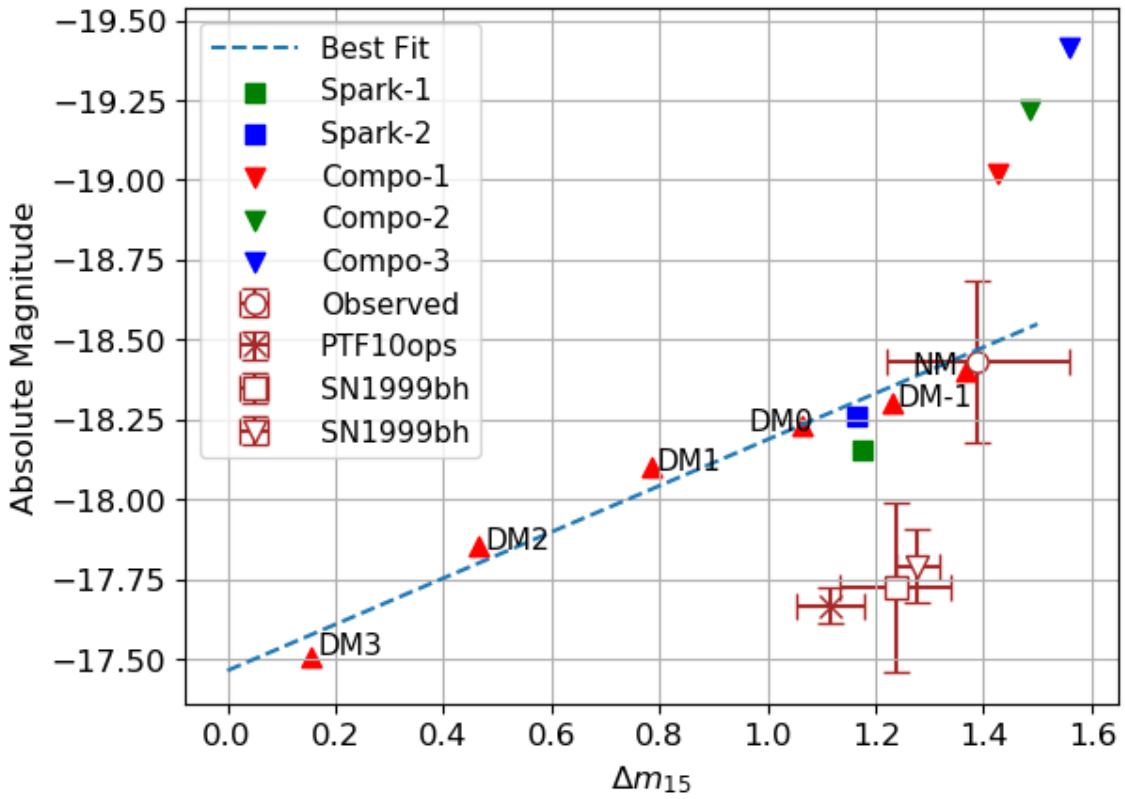

Figure 3.16: Light curve peak magnitudes against the decline rate Δm_{15} for different models in the B Band. The data for the normal supernovae are named as 'Observed', and are taken from [248] and [332] to show that our pure NM model is consistent with observations. Those data that have orthogonal trends for varying compositions in the progenitors are named Compo-1, Compo-2, and Compo-3. They are taken from [243]. Those of varying ignition conditions are taken from [317]. They are named Spark-1 and Spark-2. Data for PTF 10ops, SN 1999bh and SN 2002es are taken from [248] and [332]. Data from theoretical Double-Degenerate explosions are omitted since they lie on the parameter space that is way outside the plot.

light curves, such as SN 2002es and PTF10ops [248]. However, these theoretical and observational results are declining too fast when compared with the massive DM model.

3.4 Chapter Summary

In this chapter, we presented the necessary tools for simulating the one-dimensional supernova explosion of DMWDs. We show that the dynamical interaction between the DM and NM could significantly affect the simulation outcome. The presence of the DM lengthens the deflagration phase to produce more thermoneutrions than and similar amounts of iron peak element to that of ordinary explosions. The resulting light curves are dimmer but slowly declining, which may explain some peculiar supernova events. The DM component is left behind as compact dark stars in all of our considered models, and it may point to a formation path for dark compact objects that could mimic sub-solar-mass black holes as dark gravitational sources.

□ End of chapter.

Chapter 4

Limitations

In this chapter, we briefly enumerate the current limitations of our study, and we discuss some possible improvements that could be made.

4.1 Hydrostatic Equilibrium

4.1.1 The Non-Rotating Approximation for Dark Matter

We have assumed that the DM is non-rotating for two reasons. First, we are considering non-interacting DM particles. Such particles have independent orbits such as rotation with respect to the stellar center, but they would not have a collective motion. Second, even though accretion can change the collective motion of the DM component, it was pointed out by [149] that a neutron star in the galaxy could accrete DM at a rate of 10^7 kg s^{-1}, which is so small that there could be no considerable amount of DM build-up at the outer envelope in the time scale of the age of the Universe. We expect that the change of the angular momentum which scales as $\sim \rho v r$ should be negligible so that the non-rotation approximation is also valid throughout

the evolution from the zero-age main-sequence to the formation of DMRWD. Yet the rotational motion of DM should be considered if one studies DMRWD with a self-interacting DM EOS.

4.1.2 The Onset of Secular Instability

We have estimated the onset of secular instability in terms of the stability parameter $\sigma = 0.14$ for a two-fluid star, in which the DM is non-rotating. A more careful analysis would require performing perturbative analysis (numerically) on the criteria that govern the onset of secular instability in terms of σ. We leave such a study for the future. Furthermore, we have naively generalized Radau's equation (Equation 2.3.2) to a two-fluid star. The legitimacy of such a generalization should also be verified. We will show in Appendix E that we obtain Equation 2.3.2 by taking the Newtonian limit from a relativistic version of a similar differential equation that had been established for the two-fluid case.

4.1.3 Maximum Mass of Dark Matter-Admixed White Dwarfs

We have discussed the maximum mass of DMRWDs in the Newtonian framework. Since the maximum rotational speed of DMRWDs is much below the speed of light, the relativistic effect of the fluid motion can be neglected. However, the relativistic gravitational effect cannot be neglected when $\rho_{\rm Max2} \to 10^{14}$ g cm^{-3}. General relativistic corrections should be calculated for the maximum mass and $I-{\rm Love}-Q$ relations. Such a future study can also help reveal whether the $I-{\rm Love}-Q$ universality holds for a DMRWD under strong gravity.

4.1.4 The 2.6 $M_\odot$ Dark Matter-Admixed Neutron Star

We hypothesize that the 2.6 $M_\odot$ compact object discovered in the gravitational-wave event GW190814 could be a 2.6 $M_\odot$ DM-admixed rotating neutron star formed by the AIC of a DMRWD. However, further analysis will be needed to confirm two key assumptions used: 1. A 2.6 $M_\odot$ DM-admixed rotating neutron star exists for some realistic neutron star EOSs, and 2. the AIC of such a DMRWD leads to a stable neutron star supported by rotation. We leave such a study for the future.

4.2 Dynamical Evolution

4.2.1 Spanning the Parameter Space

Besides the 1D modeling of the explosive dynamics, several limitations of this work should be noted. We constructed a series of thermonuclear supernova models based on a model without DM admixture. To match the diversified thermonuclear supernova data, a wide range of 'normal' models, coupled with different amounts of DM admixture, are needed to span the parameter space. Given that the effects of the DM observed in this work are generic, we expect that when DM is admixed with other ordinary thermonuclear supernova models, the trend will be similar.

4.2.2 Lacking Detailed Nucleosynthesis

Another caveat is that the Type Iax supernova spectra show a strong mixing feature and weak intermediate-mass element lines. Our DM-admixed models show that the delayed DDT can strongly suppress the strength of the detonation. This suggests that fewer intermediate-mass elements are produced. However, a firm conclusion will

require a combination of radiative transfer coupled with an extended network of nuclear reactions to capture the explosive nucleosynthesis, which will be an interesting project in the future.

4.2.3 More Realistic Light Curve Modelling

Last but not least, we note that our calculations do not include a full radiation transport, and the multi-color light curve is unclear. It would be interesting to investigate the post-explosion light curve using a multi-band radiative transfer model. We have shown that including the gravitational force from the DM in the radiative transfer phase is necessary for more accurate treatment.

Chapter 5

Conclusion

We investigated the effects of admixing sub-GeV, Fermionic DM to WDs and thermonuclear supernovae.

Our semi-analytic calculations show that admixing such kind of DM particles could increase the total mass of the WD while having a DM component that is comparable in size and mass to those of the NM. These DMWDs may represent a new class of exotic compact objects. In addition, the inclusion of such kind of DM particles to a rotating WD would not break the well-known universality of the $I-$Love$-Q$ relations. The $I-$Love$-Q$ relations remain universal with respect to different NM equations of states,but they span bands above those without any DM admixtures. These results provide a new method to search for astrophysical DM inside WDs through, for instance, gravitational-wave parameter extraction. We can also construct models of ultra-massive DMRWD that is way beyond the traditional Chandrasekhar limit to a value of at least 2.6 $M_{\odot}$, which may help explain the origin of the mysterious compact object discovered in the gravitational-wave event GW190814.

We also investigated the subsequent supernova explosion of DMWDs using a 1D hydrodynamical solver. We found that the gravitational interactions between the NM and DM would significantly affect the explosion dynamics, creating more thermoneutrinos and a comparable amount of iron peak elements to that of ordinary explosions. The resulting light curves are dimmer but slowly declining, which may serve as an alternative explanation to some anomalous supernovae. Our results could provide hints to search for astrophysical DM in the future.

□ End of chapter.

Appendix A

How to Admix Dark Matter to White Dwarfs?

We consider a scenario similar to that presented in [195], where the star is born with an inherent admixture of DM, contributing an extra gravitational force to the zero-age main-sequence star. We assume a spherically symmetric cloud of NM and DM having constant densities ρ_1 and ρ_2 respectively. Their individual radii could be computed by $R = (3M/4\pi\rho)^3$. In particular, we consider the situation with the DM radius R_1 being larger than that of the NM, R_2. The total energy E (gravitational + kinetic) is:

$$E = -(\frac{3}{5}\frac{GM_1^2}{R_1} + \frac{3}{5}\frac{GM_2^2}{R_2} + \frac{3}{2}\frac{GM_1M_2}{R_1} - \frac{3}{10}\frac{GM_1^2R_1^2}{R_1^3}) + \frac{3}{2}NkT + \frac{1}{2}M_1v_1^2. \quad \text{(A.1)}$$

Here, v_1 is the DM thermal velocity, $N = M_2/m_{\rm H}$ is the total number of NM nuclei, and m_H is the molecular mass of hydrogen. Furthermore, we assume $M_1 \sim 0.1$ $M_\odot$, $M_2 \sim 10.0$ $M_\odot$. For a typical collapsing molecular cloud, we have $T \sim 150$ K

and $\rho_2 \sim 10^8 m_{\rm H}$ cm^{-3}, and hence $R_2 = 3.05 \times 10^{16}$ cm is smaller than the Jeans radius. The maximum velocity of DM $v_{1\rm max}$ for it to be bounded by the combined gravitational force is obtained by solving $E(R_2) = 0$. We find $v_{1\rm max} \sim 1.27 \times 10^6$ cm s^{-1}. For a given $v_1 < v_{1\rm max}$, we would fix R_2 and vary R_1 to look for solution where $E < 0$. However, the most probable DM speed (assuming a Maxwell distribution) is $v_{\rm p1} \sim 10^7$ cm s^{-1}. To take this into account, the bounded DM fraction is given by f:

$$f = \frac{\int_0^{u_1} u^2 \exp(-u^2) du}{\int_0^{\infty} u^2 \exp(-u^2) du}. \tag{A.2}$$

Here, $u = v/v_{\rm p1}$, and $u_1 = v_1/v_{\rm p1}$. We take a particular $v_1 = 1.23 \times 10^6$ cm s^{-1}, and give two sets of solutions in terms of (R_1, ρ_1) to show that the requirement of $E < 0$ could be satisfied: (1.71×10^{18} cm, 3860 GeV/cm^3) and (6.10×10^{16} cm, 8.48×10^7 GeV/cm^3). The required DM density in the first set of solutions is based on the state-of-the-art simulations, which showed that the DM density at the galactic bulge could be ~ 3600 GeV cm^{-3} [262]. The required DM density in the other set of solution is much larger. However, such a value is possible near the galactic center, and values with a similar order of magnitude have been adopted in studying the effect of DM annihilation on main-sequence stars [229, 148]. In conclusion, our estimations that take into account the DM velocity disperson show that it is possible to trap a DM of 0.1 $M_\odot$ during the star-forming phase, provided that the molecular cloud is in the vicinity of the galactic center. Note that the DM and NM have different ambient densities, implying that they have different free-fall times, and in principle, the DM would not follow the trajectory of the NM.

Appendix B

The General Relativistic Formalism

In Chapter 2.2.1, we show that admixing with DM that has a particle mass of 0.1 GeV does not necessarily reduce the total mass of a static DMWD. Here, we show that such a result also holds in the general relativistic framework. The two-fluid, hydrostatic equations are given as [296, 70, 200]:

$$\begin{aligned} \frac{dp_i}{dr} &= -\frac{m + 4\pi r^3 (p_1 + p_2)}{r^2 (1 - 2(m_1 + m_2)/r)} (\rho_i + p_i), \\ \frac{dm_i}{dr} &= 4\pi r^2 \rho_i. \end{aligned} \tag{B.1}$$

Here, ρ_i is the total energy density (mass + internal energy) of individual components. We show the mass-radius relations for DMWDs in Figure B.1. We find that the maximum total mass of the DMWD is reduced when we start to admix DM to the WD. The maximum total mass reaches a minimum of $\approx 1.3\ M_\odot$ when we admix $0.05\ M_\odot$ of DM. The maximum total mass then starts to increase, and it exceeds the

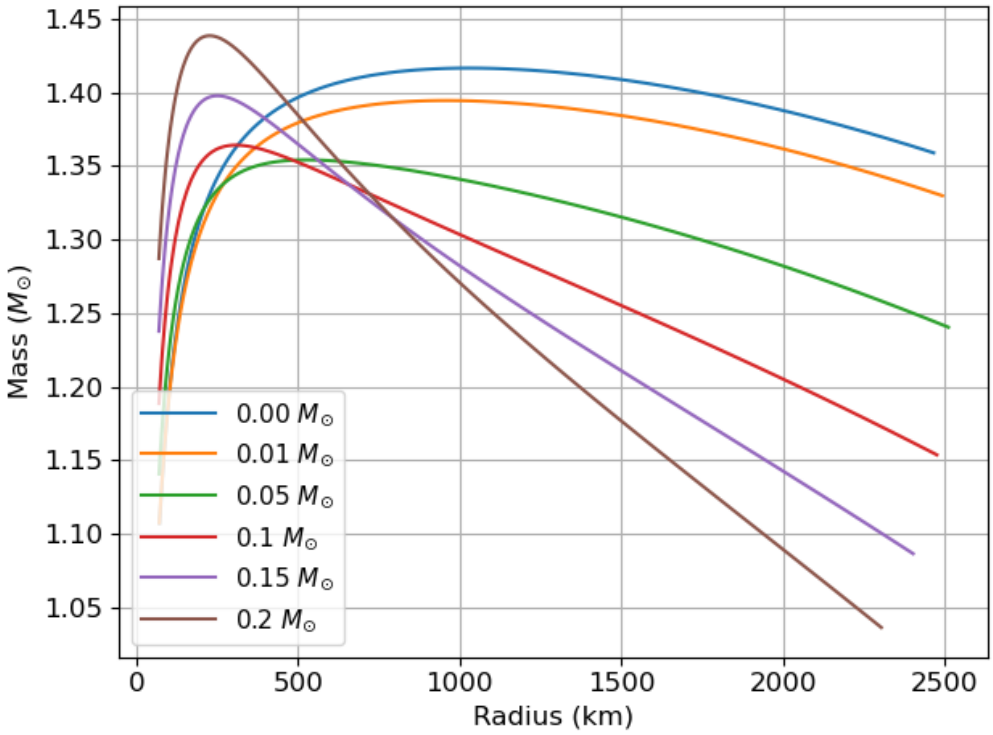

Figure B.1: Mass-radius relations for a pure NM WD and five models of DMWDs that have a DM particle mass of 0.1 GeV under general relativity. The number listed after each colored line in the legend indicates the amount of DM mass being admixed.

maximum total mass of a pure NM WD when we admix 0.2 $M_\odot$ of DM. Hence, we showed that the increase in the total mass when more DM is being admixed is also true under a more accurate treatment of gravity.

□ End of chapter.

Appendix C

The Accuracy of Linear Interpolation

Table C.1: Simulation results for models NM, NM-Quad, DM3, and DM3-Quad.

Model	NM	NM-Quad	DM3	DM3-Quad
t_{DDT} (s)	0.885	0.883	1.340	1.340
^{56}Ni ($M_{\odot}$)	0.623	0.632	0.534	0.534
Energy Production (10^{51} erg)	1.650	1.655	1.321	1.321
Neutrino Loss (10^{47} erg)	0.970	0.976	2.133	2.133
Total Neutrino Production (10^{52})	5.294	5.329	11.682	11.694

We have mentioned in Section 3.1.2 that in case there is any incomplete burning ($\delta t < \tau_{\mathrm{NQSE}}$ or τ_{NSE}), we will use linear interpolation to compute the resulting compositions and energy released. We can go one step further to consider quadratic

fitting. That is for a given quantity O:

$$O\left(\frac{\delta t}{\tau}\right) = O_0 + (O_1 - O_0)\left[\alpha\left(\frac{\delta t}{\tau}\right)^2 + \beta\left(\frac{\delta t}{\tau}\right)\right] \tag{C.1}$$

Here, O_1 is the state of O when the material is completely burnt, and O_0 is that when there is no burning occur. Furthermore, $\tau = \tau_{\rm NQSE}$ or $\tau = \tau_{\rm NSE}$. α and β are fitted from direct nuclear reactions in the relevant ranges of density and temperature. The parameter is chosen such that the formula satisfies the limit $O(0) = O_0$ and $O(1) = O_1$ as similar to the linear approximation. To compare the performance of linear and quadratic fitting, we repeat the simulations for models NM and DM3 but with the linear interpolation replaced by the quadratic one. These two new models are named as NM-Quad and DM3-Quad. We present global quantities of models NM-Quad and DM3-Quad such as the time of DDT, Ni^{56} mass, energy production, neutrino energy loss, and total neutrino production together with those of models NM and DM3 in Table C.1. We show that the results from the quadratic fitting agree within 2 % from those with the linear one. This confirms that the linear interpolation is accurate enough to model incomplete burning in the reduced nuclear reaction network.

□ End of chapter.

Appendix D

Effects of Having a Movable DM Component

Extended from the previous work by [193] where the DM is assumed to be a stationary point mass, this work takes into account the DM dynamics. Here, we explain why, even when the DM couples to the NM only by gravity, the motion of the DM that has comparable size to the NM is still an important factor for the prolonged deflagration phase. To illustrate the effects, we repeat the simulations for the models DM-1 and DM3, but with the motion of the DM frozen. These models are named: DM-1-Static, DM3-Static. These two models stand for the two extremes in how the DM affects the explosions. Model DM-1 is approaching the limit in the work by [193], where an increasing DM admixture can reduce the ^{56}Ni production in the PTD explosion. The simulation results are presented in Table D.1. Our results show that freezing the DM motion tends to under-produce some of the crucial supernova observables. Hence, not only the DM gravity but also the dynamical interactions between the DM and the NM are important in our studies.

Table D.1: Simulation results for frozen DM models DM-1-Static and DM3-Static, compared with their movable counterparts.

Model	DM-1	DM-1-Static	DM3	DM3-Static
t_{DDT} (s)	0.893	0.639	1.340	0.404
^{56}Ni ($M_{\odot}$)	0.577	0.430	0.534	0.232
Neutrino Loss (10^{47} erg)	0.958	0.499	2.133	2.037
Total Neutrino Production (10^{52})	5.218	2.784	11.682	1.141

□ End of chapter.

Appendix E

Generalizing the Tidal Equation to Two-Fluid

Radau's equation which gives the tidal love number can be obtained in an alternative way by considering the Poisson equation [142]:

$$H''(r) + \frac{2}{r}H'(r) - \left[\frac{6}{r^2} - 4\pi G\rho(r)\frac{d\rho(r)}{dP(r)}\right]H(r) = 0. \tag{E.1}$$

Here, $H(r)$ represents the Eulerian change of the Newtonian gravitational potential [363]. A change of the variable $Y(r) = r\frac{H'(r)}{H(r)}$ transforms the second-order equation to a first-order equation [363]:

$$Y'(r) + \frac{Y(r)}{r} + \frac{Y(r)^2}{r} = \frac{6}{r} + \frac{4\pi r^3}{m(r)}\frac{d\rho(r)}{dr}, \tag{E.2}$$

where we have made use of the chain rule $\frac{d\rho(r)}{dP(r)} = \frac{d\rho(r)}{dr}\frac{dr}{dP(r)}$ and the hydrostatic equation $\frac{dp(r)}{dr} = -\frac{Gm(r)\rho(r)}{r^2}$. We can define $y(r) = Y(r) - \frac{4\pi r^3}{m(r)}$ to obtain [363]:

$$y'(r) + \left[\frac{1}{r} + \frac{8\pi r^2\rho(r)}{m(r)}\right] y(r) + \frac{y(r)^2}{r} = \frac{6}{r} - \frac{16\pi r^2\rho(r)}{m(r)}. \tag{E.3}$$

Rearranging terms, and denoting $D(r) = \frac{4\pi r^3\rho(r)}{3m(r)}$, we have:

$$ry'(r) + y(r)^2 + y + 6D(r)(y(r) + 2) - 6 = 0, \tag{E.4}$$

This is to be solved with initial condition $y(0) = -1$, and the tidal deformability is given as $k_2 = \frac{2-y(R)}{2[3+y(R)]}$, where R is the stellar radius. By inspection, we make a substitution $y = \eta - 1$ to transform the equation as:

$$r\eta(r)' + \eta(r)(\eta(r) - 1) + 6D(r)(\eta(r) + 1) - 6 = 0, \tag{E.5}$$

for which we recover Radau's equation with $\eta = \eta_2$. We notice that there are two-fluid generalizations to calculate the tidal love number of hybrid stars under the general relativistic framework [375]. Therefore, the key to justifying our naive generalization of Equation 2.3.2 to the two-fluid situation is to take the Newtonian limit of the relativistic version of Equation E.1 that has been established for the two-fluid system. The relativistic version of the equation is [142]:

$$\begin{aligned} &rY'(r) + Y(r)^2 + Y(r)e^{\lambda(r)}[1 + 4\pi r^2(p(r) - \rho(r))] + r^2Q(r) = 0, \\ &Q(r) = 4\pi e^{\lambda(r)}\left[5\rho(r) + 9p(r) + \frac{\rho(r) + p(r)}{dp/d\rho}\right] - 6\frac{e^{\lambda(r)}}{r^2} - (\nu'(r))^2, \end{aligned} \tag{E.6}$$

where we have adopted geometric units $c = G = 1$. Here, $\lambda(r)$ and $\nu(r)$ are related to the metric elements. The term $\frac{\rho(r)+p(r)}{dp/d\rho}$ should be treated carefully in the two-fluid case. Fortunately, it can be decomposed into the contributions from NM and DM if they do not interact with each other [375]:

$$\frac{\rho(r)+p(r)}{dp/d\rho} = \frac{\rho_1(r)+p_1(r)}{dp_1/d\rho_1} + \frac{\rho_2(r)+p_2(r)}{dp_2/d\rho_2}. \tag{E.7}$$

In the Newtonian limit $e^{\lambda(r)} \approx 1$, $\nu'(r) \approx 0$ and $p \lll \rho$, we have:

$$Q(r) \approx 4\pi \left[\rho_1(r)\frac{d\rho_1(r)}{dp_1} + \rho_2(r)\frac{d\rho_2(r)}{dp_2}\right] - \frac{6}{r^2}. \tag{E.8}$$

We make use of the hydrostatic equation $\frac{dp_i(r)}{dr} = -\frac{Gm(r)\rho_i(r)}{r^2}$ to obtain:

$$Q(r) \approx -4\pi\frac{r^2}{m(r)}\left[\frac{d\rho_1(r)}{dr} + \frac{d\rho_2(r)}{dr}\right] - \frac{6}{r^2}. \tag{E.9}$$

Since the densities of DM and NM can be added as scalars, we substitute this expression into Equation E.6 and use $4\pi r^2(p(r) - \rho(r)) \approx 0$ to get:

$$rY'(r) + Y(r)^2 + Y(r) - \left(4\pi\frac{r^4}{m(r)}\frac{d\rho(r)}{dr} + 6\right) = 0, \tag{E.10}$$

which is just Equation E.1 with $\rho = \rho_1 + \rho_2$ and $m(r)$ the total enclosed mass.

□ End of chapter.

Bibliography

[1] M. G. Aartsen et al. Search for neutrinos from decaying dark matter with IceCube. *European Physical Journal C*, 78(10):831, Oct. 2018.

[2] R. Abbott et al. GW190814: Gravitational Waves from the Coalescence of a 23 Solar Mass Black Hole with a 2.6 Solar Mass Compact Object. ApJ, 896(2):L44, June 2020.

[3] E. B. Abdikamalov, C. D. Ott, L. Rezzolla, L. Dessart, H. Dimmelmeier, A. Marek, and H. T. Janka. Axisymmetric general relativistic simulations of the accretion-induced collapse of white dwarfs. Phys. Rev. D, 81(4):044012, Feb. 2010.

[4] T. Abe et al. LHC Dark Matter Working Group: Next-generation spin-0 dark matter models. *Physics of the Dark Universe*, 27:100351, Jan. 2020.

[5] J. F. Acevedo and J. Bramante. Supernovae sparked by dark matter in white dwarfs. *Phys. Rev. D*, 100:043020, Aug 2019.

[6] C. Adam, A. G. Martín-Caro, M. Huidobro, R. Vázquez, and A. Wereszczynski. Quasiuniversal relations for generalized Skyrme stars. Phys. Rev. D, 103(2):023022, Jan. 2021.

[7] A. G. Aksenov and S. I. Blinnikov. A Newton iteration method for obtaining equilibria of rapidly rotating stars. A&A, 290:674–681, Oct. 1994.

[8] P. M. and. Dark matter searches at super-kamiokande. *Journal of Physics: Conference Series*, 1342:012075, jan 2020.

[9] E. Aprile et al. Light Dark Matter Search with Ionization Signals in XENON1T. Phys. Rev. Lett., 123(25):251801, Dec. 2019.

[10] E. Aprile et al. XENON1T dark matter data analysis: Signal and background models and statistical inference. Phys. Rev. D, 99(11):112009, June 2019.

[11] W. D. Arnett. A possible model of supernovae: Detonation of12c. *Astrophysics and space science*, 5(2):180–212, 1969.

[12] K. Arun, S. B. Gudennavar, A. Prasad, and C. Sivaram. Effects of dark matter in star formation. Ap&SS, 364(2):24, Feb. 2019.

[13] K. Arun, S. B. Gudennavar, A. Prasad, and C. Sivaram. Effects of dark matter in star formation. *Astrophysics and Space Science*, 364(2), Feb 2019.

[14] G. G. Arutyunyan, D. M. Sedrakyan, and É. V. Chubaryan. Rotating white dwarfs in the general relativity theory. *Astrophysics*, 7(3):274–280, July 1971.

[15] A. V. Astashenok, S. Capozziello, S. D. Odintsov, and V. K. Oikonomou. Extended gravity description for the GW190814 supermassive neutron star. *Physics Letters B*, 811:135910, Dec. 2020.

[16] C. N. Augustine, D. E. Willcox, J. Brooks, D. M. Townsley, and A. C. Calder. SN ia explosions from hybrid carbon–oxygen–neon white dwarf progenitors

that have mixed during cooling. *The Astrophysical Journal*, 887(2):188, dec 2019.

[17] D. Autiero et al. Large underground, liquid based detectors for astro-particle physics in europe: scientific case and prospects. *Journal of Cosmology and Astroparticle Physics*, 2007(11):011–011, nov 2007.

[18] D. Bandyopadhyay, S. A. Bhat, P. Char, and D. Chatterjee. Moment of inertia, quadrupole moment, Love number of neutron star and their relations with strange-matter equations of state. *European Physical Journal A*, 54(2):26, Feb. 2018.

[19] S. Baur. Dark Matter Searches with the IceCube Upgrade. In *36th International Cosmic Ray Conference (ICRC2019)*, volume 36 of *International Cosmic Ray Conference*, page 506, July 2019.

[20] A. Bauswein, N.-U. F. Bastian, D. B. Blaschke, K. Chatziioannou, J. A. Clark, T. Fischer, and M. Oertel. Identifying a first-order phase transition in neutron-star mergers through gravitational waves. *Phys. Rev. Lett.*, 122:061102, Feb 2019.

[21] L. Becerra, J. A. Rueda, P. Lorén-Aguilar, and E. García-Berro. The Spin Evolution of Fast-rotating, Magnetized Super-Chandrasekhar White Dwarfs in the Aftermath of White Dwarf Mergers. ApJ, 857(2):134, Apr. 2018.

[22] N. F. Bell, A. Melatos, and K. Petraki. Realistic neutron star constraints on bosonic asymmetric dark matter. Phys. Rev. D, 87(12):123507, June 2013.

[23] E. Benitez, J. Weller, V. Guedes, C. Chirenti, and M. C. Miller. Investigating the I-Love-Q and w -mode universal relations using piecewise polytropes. Phys. Rev. D, 103(2):023007, Jan. 2021.

[24] P. Bera and D. Bhattacharya. Mass-radius relation of strongly magnetized white dwarfs: dependence on field geometry, GR effects and electrostatic corrections to the EOS. MNRAS, 456(3):3375–3385, Mar. 2016.

[25] G. Bertone and M. Fairbairn. Compact stars as dark matter probes. Phys. Rev. D, 77(4):043515, Feb. 2008.

[26] M. Bezares and C. Palenzuela. Gravitational waves from dark boson star binary mergers. *Classical and Quantum Gravity*, 35(23):234002, Dec. 2018.

[27] M. Bezares, C. Palenzuela, and C. Bona. Final fate of compact boson star mergers. Phys. Rev. D, 95(12):124005, June 2017.

[28] G. S. Bisnovatyi-Kogan and S. I. Blinnikov. Static Criteria for Stability of Arbitrarily Rotating Stars. A&A, 31:391, Apr. 1974.

[29] S. Blondin, L. Dessart, and D. J. Hillier. A one-dimensional Chandrasekhar-mass delayed-detonation model for the broad-lined Type Ia supernova 2002bo. *Monthly Notices of the Royal Astronomical Society*, 448(3):2766–2797, 03 2015.

[30] S. Blondin, L. Dessart, D. J. Hillier, and A. M. Khokhlov. One-dimensional delayed-detonation models of Type Ia supernovae: confrontation to observations at bolometric maximum. *Monthly Notices of the Royal Astronomical Society*, 429(3):2127–2142, 12 2012.

[31] S. Blondin, L. Dessart, D. J. Hillier, and A. M. Khokhlov. One-dimensional delayed-detonation models of Type Ia supernovae: confrontation to observations at bolometric maximum. *Monthly Notices of the Royal Astronomical Society*, 429(3):2127–2142, 12 2012.

[32] S. Blondin, D. Kasen, F. K. Röpke, R. P. Kirshner, and K. S. Mandel. Confronting 2D delayed-detonation models with light curves and spectra of Type Ia supernovae. *Monthly Notices of the Royal Astronomical Society*, 417(2):1280–1302, 10 2011.

[33] G. R. Blumenthal, S. M. Faber, J. R. Primack, and M. J. Rees. Formation of galaxies and large-scale structure with cold dark matter. Nature, 311:517–525, Oct. 1984.

[34] I. Bombaci, A. Drago, D. Logoteta, G. Pagliara, and I. Vidana. Was GW190814 a black hole – strange quark star system? *arXiv e-prints*, page arXiv:2010.01509, Oct. 2020.

[35] K. Boshkayev. Equilibrium Configurations of Rotating White Dwarfs at Finite Temperatures. *Astronomy Reports*, 62(12):847–852, Dec. 2018.

[36] K. Boshkayev and H. Quevedo. Non-validity of I-Love-Q Relations for Hot White Dwarf Stars. MNRAS, 478(2):1893–1899, Aug. 2018.

[37] K. Boshkayev, H. Quevedo, and B. Zhami. I -Love- Q relations for white dwarf stars. MNRAS, 464(4):4349–4359, Feb. 2017.

[38] J. Bouvier. Observational studies of stellar rotation. In P. Hennebelle and C. Charbonnel, editors, *EAS Publications Series*, volume 62 of *EAS Publications Series*, pages 143–168, Sept. 2013.

[39] J. Bramante. Dark matter ignition of type ia supernovae. *Phys. Rev. Lett.*, 115:141301, Sep 2015.

[40] J. Bramante, K. Fukushima, and J. Kumar. Constraints on bosonic dark matter from observation of old neutron stars. Phys. Rev. D, 87(5):055012, Mar. 2013.

[41] D. Branch. *Supernova explosions*. Astronomy and astrophysics library. Springer, Berlin, Germany, 2017.

[42] E. Bravo and D. García-Senz. Beyond the bubble catastrophe of type ia supernovae: Pulsating reverse detonation models. *The Astrophysical Journal*, 642(2):L157–L160, apr 2006.

[43] E. Bravo and D. García-Senz. PULSATING REVERSE DETONATION MODELS OF TYPE ia SUPERNOVAE. i. DETONATION IGNITION. *The Astrophysical Journal*, 695(2):1244–1256, apr 2009.

[44] E. Bravo, D. García-Senz, R. M. Cabezón, and I. Domínguez. PULSATING REVERSE DETONATION MODELS OF TYPE ia SUPERNOVAE. II. EXPLOSION. *The Astrophysical Journal*, 695(2):1257–1272, apr 2009.

[45] Bravo, E., Gil-Pons, P., Gutiérrez, J. L., and Doherty, C. L. Explosion of white dwarfs harboring hybrid cone cores. *A&A*, 589:A38, 2016.

[46] E. Brooker, T. Plewa, and D. Fenn. SN Ia DDT Explosions Powered by the Zeldovich Reactivity Gradient Mechanism. *arXiv e-prints*, page arXiv:2008.05010, Aug. 2020.

[47] E. Brooker, T. Plewa, and D. Fenn. Type Ia supernovae deflagration-to-detonation transition explosions powered by the Zel'dovich reactivity gradi-

ent mechanism. *Monthly Notices of the Royal Astronomical Society: Letters*, 501(1):L23–L27, 12 2020.

[48] J. Brooks, J. Schwab, L. Bildsten, E. Quataert, and B. Paxton. Accretion-induced Collapse from Helium Star + White Dwarf Binaries. ApJ, 843(2):151, July 2017.

[49] J. Brooks, J. Schwab, L. Bildsten, E. Quataert, and B. Paxton. Convection destroys the core/mantle structure in hybrid c/o/ne white dwarfs. *The Astrophysical Journal*, 834(2):L9, jan 2017.

[50] A. Burkert. The Structure of Dark Matter Halos in Dwarf Galaxies. ApJ, 447:L25–L28, July 1995.

[51] R. M. Cabezón, K.-C. Pan, M. Liebendörfer, T. Kuroda, K. Ebinger, O. Heinimann, A. Perego, and F.-K. Thielemann. Core-collapse supernovae in the hall of mirrors. *Astronomy and Astrophysics*, 619:A118, Nov 2018.

[52] A. C. Calder, T. Plewa, N. Vladimirova, D. Q. Lamb, and J. W. Truran. Type Ia Supernovae: An Asymmetric Deflagration Model. *arXiv e-prints*, pages astro–ph/0405162, May 2004.

[53] A. C. Calder, D. M. Townsley, I. R. Seitenzahl, F. Peng, O. E. B. Messer, N. Vladimirova, E. F. Brown, J. W. Truran, and D. Q. Lamb. Capturing the fire: Flame energetics and neutronization for type ia supernova simulations. *The Astrophysical Journal*, 656(1):313–332, feb 2007.

[54] M. Camenzind. *Compact objects in astrophysics : white dwarfs, neutron stars, and black holes*. 2007.

[55] P. Candia et al. Optical and infrared photometry of the unusual type ia supernova 2000cx. *Publications of the Astronomical Society of the Pacific*, 115(805):277–294, mar 2003.

[56] J. Casanellas and I. Lopes. The Formation and Evolution of Young Low-mass Stars within Halos with High Concentration of Dark Matter Particles. ApJ, 705(1):135–143, Nov. 2009.

[57] F. Cavanna, M. L. Costantini, O. Palamara, and F. Vissani. Neutrinos as astrophysical probes. *Surveys in High Energy Physics*, 19(1):35–54, 2004.

[58] J. M. Centrella, K. C. B. New, L. L. Lowe, and J. D. Brown. Dynamical Rotational Instability at Low T/W. ApJ, 550(2):L193–L196, Apr. 2001.

[59] K. Chakravarti, S. Chakraborty, K. S. Phukon, S. Bose, and S. SenGupta. Constraining extra-spatial dimensions with observations of GW170817. *Classical and Quantum Gravity*, 37(10):105004, apr 2020.

[60] H.-S. Chan, M. chung Chu, S.-C. Leung, and L.-M. Lin. Delayed detonation thermonuclear supernovae with an extended dark matter component. *The Astrophysical Journal*, 914(2):138, jun 2021.

[61] T. K. Chan, A. P. O. Chan, and P. T. Leung. I-Love relations for incompressible stars and realistic stars. Phys. Rev. D, 91(4):044017, Feb. 2015.

[62] Charignon, C. and Chièze, J.-P. Deflagration-to-detonation transition by amplification of acoustic waves in type ia supernovae. *A&A*, 550:A105, 2013.

[63] D. Chatterjee, A. F. Fantina, N. Chamel, J. Novak, and M. Oertel. On the maximum mass of magnetized white dwarfs. MNRAS, 469(1):95–109, July 2017.

[64] K. Chatziioannou, C.-J. Haster, and A. Zimmerman. Measuring the neutron star tidal deformability with equation-of-state-independent relations and gravitational waves. *Phys. Rev. D*, 97:104036, May 2018.

[65] W.-C. Chen and X.-D. Li. ON THE PROGENITORS OF SUPER-CHANDRASEKHAR MASS TYPE ia SUPERNOVAE. *The Astrophysical Journal*, 702(1):686–691, aug 2009.

[66] S. Cheng, J. D. Cummings, B. Ménard, and S. Toonen. Double white dwarf merger products among high-mass white dwarfs. *The Astrophysical Journal*, 891(2):160, mar 2020.

[67] R. Chornock, A. V. Filippenko, D. Branch, R. J. Foley, S. Jha, and W. Li. Spectropolarimetry of the peculiar type ia supernova 2005hk. *Publications of the Astronomical Society of the Pacific*, 118(843):722–732, may 2006.

[68] Ciaraldi-Schoolmann, F., Seitenzahl, I. R., and Röpke, F. K. A subgrid-scale model for deflagration-to-detonation transitions in type ia supernova explosion simulations - numerical implementation. *A&A*, 559:A117, 2013.

[69] P. Ciarcelluti and F. Sandin. Have neutron stars a dark matter core? *Physics Letters B*, 695(1-4):19–21, Jan. 2011.

[70] P. Ciarcelluti and F. Sandin. Have neutron stars a dark matter core? *Physics Letters B*, 695(1):19–21, 2011.

[71] M. Cirelli, N. Fornengo, B. J. Kavanagh, and E. Pinetti. Integral x-ray constraints on sub-gev dark matter. *Phys. Rev. D*, 103:063022, Mar 2021.

[72] D. Clowe, M. Bradač, A. H. Gonzalez, M. Markevitch, S. W. Randall, C. Jones, and D. Zaritsky. A direct empirical proof of the existence of dark matter. *The Astrophysical Journal*, 648(2):L109–L113, aug 2006.

[73] D. Clowe, M. Bradač, A. H. Gonzalez, M. Markevitch, S. W. Randall, C. Jones, and D. Zaritsky. A Direct Empirical Proof of the Existence of Dark Matter. ApJ, 648(2):L109–L113, Sept. 2006.

[74] S. M. Couch, C. Graziani, and N. Flocke. AN IMPROVED MULTIPOLE APPROXIMATION FOR SELF-GRAVITY AND ITS IMPORTANCE FOR CORE-COLLAPSE SUPERNOVA SIMULATIONS. *The Astrophysical Journal*, 778(2):181, nov 2013.

[75] S. Dado and A. Dar. ANALYTICAL EXPRESSIONS FOR LIGHT CURVES OF ORDINARY AND SUPERLUMINOUS TYPE ia SUPERNOVAE. *The Astrophysical Journal*, 809(1):32, aug 2015.

[76] U. Das and B. Mukhopadhyay. Strongly magnetized cold degenerate electron gas: Mass-radius relation of the magnetized white dwarf. *Phys. Rev. D*, 86:042001, Aug 2012.

[77] U. Das and B. Mukhopadhyay. New mass limit for white dwarfs: Super-chandrasekhar type ia supernova as a new standard candle. *Phys. Rev. Lett.*, 110:071102, Feb 2013.

[78] U. Das, B. Mukhopadhyay, and A. R. Rao. A POSSIBLE EVOLUTIONARY SCENARIO OF HIGHLY MAGNETIZED SUPER-CHANDRASEKHAR

WHITE DWARFS: PROGENITORS OF PECULIAR TYPE ia SUPERNOVAE. *The Astrophysical Journal*, 767(1):L14, mar 2013.

[79] M. Davis, G. Efstathiou, C. S. Frenk, and S. D. M. White. The evolution of large-scale structure in a universe dominated by cold dark matter. ApJ, 292:371–394, May 1985.

[80] A. de Lavallaz and M. Fairbairn. Neutron stars as dark matter probes. Phys. Rev. D, 81(12):123521, June 2010.

[81] P. Denissenkov, J. Truran, F. Herwig, S. Jones, B. Paxton, K. Nomoto, T. Suzuki, and H. Toki. Hybrid C-O-Ne White Dwarfs as Progenitors of Diverse SNe Ia. *arXiv e-prints*, page arXiv:1411.1471, Nov. 2014.

[82] P. A. Denissenkov, J. W. Truran, F. Herwig, S. Jones, B. Paxton, K. Nomoto, T. Suzuki, and H. Toki. Hybrid C–O–Ne white dwarfs as progenitors of Type Ia supernovae: dependence on Urca process and mixing assumptions. *Monthly Notices of the Royal Astronomical Society*, 447(3):2696–2705, 01 2015.

[83] L. Dessart, A. Burrows, E. Livne, and C. D. Ott. Magnetically Driven Explosions of Rapidly Rotating White Dwarfs Following Accretion-Induced Collapse. ApJ, 669(1):585–599, Nov. 2007.

[84] L. Dessart, A. Burrows, C. D. Ott, E. Livne, S. C. Yoon, and N. Langer. Multidimensional Simulations of the Accretion-induced Collapse of White Dwarfs to Neutron Stars. ApJ, 644(2):1063–1084, June 2006.

[85] V. Dexheimer, R. O. Gomes, T. Klähn, S. Han, and M. Salinas. GW190814 as a massive rapidly rotating neutron star with exotic degrees of freedom. Phys. Rev. C, 103(2):025808, Feb. 2021.

[86] M. J. Dolan, F. J. Hiskens, and R. R. Volkas. Constraining axion-like particles using the white dwarf initial-final mass relation, 2021.

[87] D. D. Doneva, S. S. Yazadjiev, and K. D. Kokkotas. I-q relations for rapidly rotating neutron stars in $f(r)$ gravity. *Phys. Rev. D*, 92:064015, Sep 2015.

[88] R. H. Durisen. Upper mass limits for stable rotating white dwarfs. ApJ, 199:179–183, July 1975.

[89] B. Dutta, S. Ghosh, and J. Kumar. Sub-gev dark matter model. *Phys. Rev. D*, 100:075028, Oct 2019.

[90] J. Eby, C. Kouvaris, N. G. Nielsen, and L. C. R. Wijewardhana. Boson stars from self-interacting dark matter. *Journal of High Energy Physics*, 2016:28, Feb. 2016.

[91] J. Ellis, G. Hütsi, K. Kannike, L. Marzola, M. Raidal, and V. Vaskonen. Dark matter effects on neutron star properties. Phys. Rev. D, 97(12):123007, June 2018.

[92] Y. Eriguchi. Hydrostatic Equilibria of Rotating Polytropes. PASJ, 30:507–518, Jan. 1978.

[93] Y. Eriguchi and E. Mueller. A general computational method for obtaining equilibria of self-gravitating and rotating gases. A&A, 146(2):260–268, May 1985.

[94] Y. Eriguchi and E. Mueller. Structure and Circulation of Self-gravitating Toroids. ApJ, 416:666, Oct. 1993.

[95] D. Falta, R. Fisher, and G. Khanna. Gravitational Wave Emission from the Single-Degenerate Channel of Type Ia Supernovae. Phys. Rev. Lett., 106(20):201103, May 2011.

[96] N. J. Fantin, P. Côté, and A. W. McConnachie. White dwarfs in the era of the LSST and its synergies with space-based missions. *The Astrophysical Journal*, 900(2):139, sep 2020.

[97] F. J. Fattoyev, C. J. Horowitz, J. Piekarewicz, and B. Reed. Gw190814: Impact of a 2.6 solar mass neutron star on the nucleonic equations of state. *Physical Review C*, 102(6), Dec 2020.

[98] J. L. Feng. Dark Matter Candidates from Particle Physics and Methods of Detection. ARA&A, 48:495–545, Sept. 2010.

[99] A. V. Filippenko, M. W. Richmond, D. Branch, M. Gaskell, W. Herbst, C. H. Ford, R. R. Treffers, T. Matheson, L. C. Ho, A. Dey, W. L. W. Sargent, T. A. Small, and W. J. M. van Breugel. The Subluminous, Spectroscopically Peculiar Type 1a Supernova 1991bg in the Elliptical Galaxy NGC 4374. AJ, 104:1543, Oct. 1992.

[100] M. Fink, M. Kromer, W. Hillebrandt, F. K. Röpke, R. Pakmor, I. R. Seitenzahl, and S. A. Sim. Thermonuclear explosions of rapidly differentially rotating white dwarfs: Candidates for superluminous Type Ia supernovae? A&A, 618:A124, Oct. 2018.

[101] M. Fink, M. Kromer, I. R. Seitenzahl, F. Ciaraldi-Schoolmann, F. K. Röpke, S. A. Sim, R. Pakmor, A. J. Ruiter, and W. Hillebrandt. Three-dimensional pure deflagration models with nucleosynthesis and synthetic observables for

Type Ia supernovae. *Monthly Notices of the Royal Astronomical Society*, 438(2):1762–1783, 12 2013.

[102] E. E. Flanagan and T. Hinderer. Constraining neutron-star tidal love numbers with gravitational-wave detectors. *Phys. Rev. D*, 77:021502, Jan 2008.

[103] A. Flörs, J. Spyromilio, S. Taubenberger, S. Blondin, R. Cartier, B. Leibundgut, L. Dessart, S. Dhawan, and W. Hillebrandt. Sub-Chandrasekhar progenitors favoured for Type Ia supernovae: evidence from late-time spectroscopy. *Monthly Notices of the Royal Astronomical Society*, 491(2):2902–2918, 11 2019.

[104] K. Frankiewicz and Super-Kamiokande Collaboration. Dark matter searches with the Super-Kamiokande detector. In *Journal of Physics Conference Series*, volume 888 of *Journal of Physics Conference Series*, page 012210, Sept. 2017.

[105] B. Franzon and S. Schramm. Effects of strong magnetic fields and rotation on white dwarf structure. Phys. Rev. D, 92(8):083006, Oct. 2015.

[106] K. Freese. Status of dark matter in the universe. *International Journal of Modern Physics D*, 26(6):1730012–223, Jan. 2017.

[107] K. Freese, T. Rindler-Daller, D. Spolyar, and M. Valluri. Dark stars: a review. *Reports on Progress in Physics*, 79(6):066902, June 2016.

[108] K. Freese, T. Rindler-Daller, D. Spolyar, and M. Valluri. Dark stars: a review. *Reports on Progress in Physics*, 79(6):066902, May 2016.

[109] J. L. Friedman and B. F. Schutz. Gravitational radiation instability in rotating stars. ApJ, 199:L157–L159, Aug. 1975.

[110] J. L. Friedman and B. F. Schutz. Secular instability of rotating Newtonian stars. ApJ, 222:281–296, May 1978.

[111] C. L. Fryer and K. C. B. New. Gravitational Waves from Gravitational Collapse. *Living Reviews in Relativity*, 14(1):1, Jan. 2011.

[112] T. Fukushima, Y. Eriguchi, D. Sugimoto, and G. S. Bisnovatyi-Kogan. Concave Hamburger Equilibrium of Rotating Bodies. In D. Sugimoto, D. Q. Lamb, and D. N. Schramm, editors, *Fundamental Problems in the Theory of Stellar Evolution*, volume 93, page 273, Jan. 1981.

[113] J. Fuller and L. Ma. Most Black Holes Are Born Very Slowly Rotating. ApJ, 881(1):L1, Aug. 2019.

[114] V. N. Gamezo, A. M. Khokhlov, E. S. Oran, A. Y. Chtchelkanova, and R. O. Rosenberg. Thermonuclear supernovae: Simulations of the deflagration stage and their implications. *Science*, 299(5603):77–81, 2003.

[115] M. Ganeshalingam, W. Li, A. V. Filippenko, C. Anderson, G. Foster, E. L. Gates, C. V. Griffith, B. J. Grigsby, N. Joubert, J. Leja, T. B. Lowe, B. Macomber, T. Pritchard, P. Thrasher, and D. Winslow. RESULTS OF THE LICK OBSERVATORY SUPERNOVA SEARCH FOLLOW-UP PHOTOMETRY PROGRAM: BVRI LIGHT CURVES OF 165 TYPE ia SUPERNOVAE. *The Astrophysical Journal Supplement Series*, 190(2):418–448, sep 2010.

[116] M. Ganeshalingam, W. Li, A. V. Filippenko, J. M. Silverman, R. Chornock, R. J. Foley, T. Matheson, R. P. Kirshner, P. Milne, M. Calkins, and et al. The low-velocity, rapidly fading type ia supernova 2002es. *The Astrophysical Journal*, 751(2):142, May 2012.

[117] V. S. Geroyannis and A. A. Hadjopoulos. Models of White Dwarfs under Rapid Uniform or Differential Rotation: Numerical Results. ApJS, 70:661, July 1989.

[118] V. S. Geroyannis and A. A. Hadjopoulos. Models of White Dwarfs under Rapid Uniform or Differential Rotation: Numerical Results. II. ApJS, 75:499, Feb. 1991.

[119] P. Ghosh and J. C. Wheeler. Differentially rotating white dwarfs. i. regimes of internal rotation. *The Astrophysical Journal*, 834(1):93, Jan 2017.

[120] A. Gianninas, P. Dufour, M. Kilic, W. R. Brown, P. Bergeron, and J. J. Hermes. Precise Atmospheric Parameters for the Shortest-period Binary White Dwarfs: Gravitational Waves, Metals, and Pulsations. ApJ, 794(1):35, Oct. 2014.

[121] S. A. Glasner, E. Livne, E. Steinberg, A. Yalinewich, and J. W. Truran. Ignition of detonation in accreted helium envelopes. MNRAS, 476(2):2238–2248, May 2018.

[122] D. A. Godzieba, D. Radice, and S. Bernuzzi. On the maximum mass of neutron stars and gw190814. *The Astrophysical Journal*, 908(2):122, Feb 2021.

[123] S. Gottlieb, D. Ketcheson, and C.-W. Shu. *Strong Stability Preserving Runge-Kutta and Multistep Time Discretizations*. WORLD SCIENTIFIC, 2011.

[124] P. W. Graham, R. Janish, V. Narayan, S. Rajendran, and P. Riggins. White dwarfs as dark matter detectors. Phys. Rev. D, 98(11):115027, Dec. 2018.

[125] S. Gronow, C. Collins, S. T. Ohlmann, R. Pakmor, M. Kromer, I. R. Seitenzahl, S. A. Sim, and F. K. Röpke. Sne ia from double detonations: Impact of core-

shell mixing on the carbon ignition mechanism. *Astronomy & Astrophysics*, 635:A169, Mar 2020.

[126] J. Guedes, S. Callegari, P. Madau, and L. Mayer. Forming Realistic Late-type Spirals in a ΛCDM Universe: The Eris Simulation. ApJ, 742(2):76, Dec. 2011.

[127] M. W. Guidry. Stars and stellar processes, 2019.

[128] J. Guillochon, J. Parrent, L. Z. Kelley, and R. Margutti. An open catalog for supernova data. *The Astrophysical Journal*, 835(1):64, jan 2017.

[129] V. V. Gvaramadze, G. Gräfener, N. Langer, O. V. Maryeva, A. Y. Kniazev, A. S. Moskvitin, and O. I. Spiridonova. A massive white-dwarf merger product before final collapse. Nature, 569(7758):684–687, May 2019.

[130] I. Hachisu. A Versatile Method for Obtaining Structures of Rapidly Rotating Stars. ApJS, 61:479, July 1986.

[131] I. Hachisu, Y. Eriguchi, and D. Sugimoto. Rapidly Rotating Polytropes and Concave Hamburger Equilibrium. *Progress of Theoretical Physics*, 68(1):191–205, July 1982.

[132] I. Hachisu, M. Kato, and K. Nomoto. Final Fates of Rotating White Dwarfs and Their Companions in the Single Degenerate Model of Type Ia Supernovae. ApJ, 756(1):L4, Sept. 2012.

[133] I. Hachisu, M. Kato, H. Saio, and K. Nomoto. A Single Degenerate Progenitor Model for Type Ia Supernovae Highly Exceeding the Chandrasekhar Mass Limit. ApJ, 744(1):69, Jan. 2012.

[134] C. J. Hansen, S. D. Kawaler, and V. Trimble. *Stellar interiors : physical principles, structure, and evolution*. 2004.

[135] B. K. Harrison, K. S. Thorne, M. Wakano, and J. A. Wheeler. *Gravitation Theory and Gravitational Collapse*. 1965.

[136] L. Hartmann and J. R. Stauffer. Additional Measurements of Pre-Main-Sequence Stellar Rotation. AJ, 97:873, Mar. 1989.

[137] B. Haskell, R. Ciolfi, F. Pannarale, and L. Rezzolla. On the universality of I-Love-Q relations in magnetized neutron stars. MNRAS, 438(1):L71–L75, Feb. 2014.

[138] A. Hayashi, Y. Eriguchi, and M.-a. Hashimoto. On the Possibility of the Nonexplosive Core Contraction of Massive Stars: New Evolutionary Paths from Rotating White Dwarfs to Rotating Neutron Stars. ApJ, 492(1):286–297, Jan. 1998.

[139] A. Hayashi, Y. Eriguchi, and M.-a. Hashimoto. On the Possibility of the Non-explosive Core Contraction of Massive Stars. II. General Relativistic Analysis. ApJ, 521(1):376–381, Aug. 1999.

[140] A. Heger and N. Langer. Presupernova Evolution of Rotating Massive Stars. II. Evolution of the Surface Properties. ApJ, 544(2):1016–1035, Dec. 2000.

[141] W. Hillebrandt, M. Kromer, F. K. Röpke, and A. J. Ruiter. Towards an understanding of type ia supernovae from a synthesis of theory and observations. *Frontiers of Physics*, 8(2):116–143, Apr 2013.

[142] T. Hinderer. Tidal Love Numbers of Neutron Stars. ApJ, 677(2):1216–1220, Apr. 2008.

[143] T. Hinderer, B. D. Lackey, R. N. Lang, and J. S. Read. Tidal deformability of neutron stars with realistic equations of state and their gravitational wave signatures in binary inspiral. *Phys. Rev. D*, 81:123016, Jun 2010.

[144] P. Hoeflich, A. M. Khokhlov, and J. C. Wheeler. Delayed Detonation Models for Normal and Subluminous Type IA Supernovae: Absolute Brightness, Light Curves, and Molecule Formation. ApJ, 444:831, May 1995.

[145] K. Huang, J. Hu, Y. Zhang, and H. Shen. The Possibility of the Secondary Object in GW190814 as a Neutron Star. ApJ, 904(1):39, Nov. 2020.

[146] Hyper-Kamiokande Proto-Collaboration, :, K. Abe, et al. Hyper-Kamiokande Design Report. *arXiv e-prints*, page arXiv:1805.04163, May 2018.

[147] M. Ilkov and N. Soker. Type Ia supernovae from very long delayed explosion of core-white dwarf merger. MNRAS, 419(2):1695–1700, Jan. 2012.

[148] F. Iocco. Dark Matter Capture and Annihilation on the First Stars: Preliminary Estimates. ApJ, 677(1):L1, Apr. 2008.

[149] L. Iorio. Phenomenological constraints on accretion of non-annihilating dark matter on the psr b1257+12 pulsar from orbital dynamics of its planets. *Journal of Cosmology and Astroparticle Physics*, 2010(11):046–046, Nov 2010.

[150] N. Itoh, H. Hayashi, A. Nishikawa, and Y. Kohyama. Neutrino Energy Loss in Stellar Interiors. VII. Pair, Photo-, Plasma, Bremsstrahlung, and Recombination Neutrino Processes. ApJS, 102:411, Feb. 1996.

[151] O. Ivanytskyi, V. Sagun, and I. Lopes. Neutron stars: New constraints on asymmetric dark matter. Phys. Rev. D, 102(6):063028, Sept. 2020.

[152] O. Ivanytskyi, V. Sagun, and I. Lopes. Neutron stars: New constraints on asymmetric dark matter. *Phys. Rev. D*, 102:063028, Sep 2020.

[153] K. Iwamoto, F. Brachwitz, K. Nomoto, N. Kishimoto, H. Umeda, W. R. Hix, and F.-K. Thielemann. Nucleosynthesis in chandrasekhar mass models for type ia supernovae and constraints on progenitor systems and burning-front propagation. *The Astrophysical Journal Supplement Series*, 125(2):439–462, dec 1999.

[154] R. Janish, V. Narayan, and P. Riggins. Type ia supernovae from dark matter core collapse. *Phys. Rev. D*, 100:035008, Aug 2019.

[155] S. Jha, A. G. Riess, and R. P. Kirshner. Improved distances to type ia supernovae with multicolor light-curve shapes: MLCS2k2. *The Astrophysical Journal*, 659(1):122–148, apr 2007.

[156] G.-S. Jiang and C.-W. Shu. Efficient implementation of weighted eno schemes. *Journal of Computational Physics*, 126(1):202–228, 1996.

[157] N. Jiang and K. Yagi. Analytic I-Love-C relations for realistic neutron stars. Phys. Rev. D, 101(12):124006, June 2020.

[158] G. C. Jordan, C. Graziani, R. T. Fisher, D. M. Townsley, C. Meakin, K. Weide, L. B. Reid, J. Norris, R. Hudson, and D. Q. Lamb. THE DETONATION MECHANISM OF THE PULSATIONALLY ASSISTED GRAVITATIONALLY CONFINED DETONATION MODEL OF type ia SUPERNOVAE. *The Astrophysical Journal*, 759(1):53, oct 2012.

[159] G. C. Jordan, H. B. Perets, R. T. Fisher, and D. R. van Rossum. FAILED-DETONATION SUPERNOVAE: SUBLUMINOUS LOW-VELOCITY ia SUPERNOVAE AND THEIR KICKED REMNANT WHITE DWARFS WITH IRON-RICH CORES. *The Astrophysical Journal*, 761(2):L23, dec 2012.

[160] L.-M. L. Ka-Wing Wong, Ming-Chung Chu. Physical properties of white dwarf with a dark matter core. Master's thesis, The Chinese University of Hong Kong, Hong Kong, 2011.

[161] F. Kahlhoefer. Review of LHC dark matter searches. *International Journal of Modern Physics A*, 32(13):1730006, May 2017.

[162] B. Kain. Dark matter admixed neutron stars. Phys. Rev. D, 103(4):043009, Feb. 2021.

[163] A. Kanakis-Pegios, P. S. Koliogiannis, and C. C. Moustakidis. Probing the nuclear equation of state from the existence of a 2.6 m neutron star: The gw190814 puzzle. *Symmetry*, 13(2):183, Jan 2021.

[164] E. M. Kantor and M. E. Gusakov. The neutrino emission due to plasmon decay and neutrino luminosity of white dwarfs. *Monthly Notices of the Royal Astronomical Society*, 381(4):1702–1710, 10 2007.

[165] S. Karino and Y. Eriguchi. Gravitational Radiation Reaction Driven Secular Instability of f-Mode Oscillations in Differentially Rotating Newtonian Stars. ApJ, 578(1):413–419, Oct. 2002.

[166] D. Kasen and T. Plewa. Detonating failed deflagration model of thermonuclear supernovae. II. comparison to observations. *The Astrophysical Journal*, 662(1):459–471, jun 2007.

[167] S. D. Kawaler. White Dwarf Rotation: Observations and Theory. *arXiv e-prints*, pages astro–ph/0301539, Jan. 2003.

[168] S. M. Kent. Dark matter in spiral galaxies. I. Galaxies with optical rotation curves. AJ, 91:1301–1327, June 1986.

[169] S. M. Kent. Dark Matter in Spiral Galaxies. II. Galaxies with H I Rotation Curves. AJ, 93:816, Apr. 1987.

[170] S. M. Kent. Dark Matter in Spiral Galaxies. III. The SA Galaxies. AJ, 96:514, Aug. 1988.

[171] D. Kereš, N. Katz, R. Davé, M. Fardal, and D. H. Weinberg. Galaxies in a simulated ΛCDM universe - II. Observable properties and constraints on feedback. MNRAS, 396(4):2332–2344, July 2009.

[172] D. Kereš, N. Katz, M. Fardal, R. Davé, and D. H. Weinberg. Galaxies in a simulated ΛCDM Universe - I. Cold mode and hot cores. MNRAS, 395(1):160–179, May 2009.

[173] A. M. Khokhlov. Delayed detonation model for type IA supernovae. A&A, 245(1):114–128, May 1991.

[174] T. Kinugawa, H. Takeda, and H. Yamaguchi. Probe for type ia supernova progenitor in decihertz gravitational wave astronomy, 2019.

[175] R. Kippenhahn, A. Weigert, and A. Weiss. *Stellar Structure and Evolution*. 2012.

[176] C. Kobayashi, S.-C. Leung, and K. Nomoto. New type ia supernova yields and the manganese and nickel problems in the milky way and dwarf spheroidal galaxies. *The Astrophysical Journal*, 895(2):138, jun 2020.

[177] V. Korol, E. M. Rossi, P. J. Groot, G. Nelemans, S. Toonen, and A. G. A. Brown. Prospects for detection of detached double white dwarf binaries with Gaia, LSST and LISA. *Monthly Notices of the Royal Astronomical Society*, 470(2):1894–1910, 05 2017.

[178] Korol, V., Toonen, S., Klein, A., Belokurov, V., Vincenzo, F., Buscicchio, R., Gerosa, D., Moore, C. J., Roebber, E., Rossi, E. M., and Vecchio, A. Populations of double white dwarfs in milky way satellites and their detectability with lisa. *A&A*, 638:A153, 2020.

[179] C. Kouvaris. WIMP annihilation and cooling of neutron stars. Phys. Rev. D, 77(2):023006, Jan. 2008.

[180] C. Kouvaris and P. Tinyakov. Constraining asymmetric dark matter through observations of compact stars. Phys. Rev. D, 83(8):083512, Apr. 2011.

[181] S. Kriminski, V. Bychkov, and M. Liberman. On the stability of thermonuclear detonation in supernovae events. *New Astronomy*, 3(6):363–377, 1998.

[182] M. Kromer, M. Fink, V. Stanishev, S. Taubenberger, F. Ciaraldi-Schoolman, R. Pakmor, F. K. Röpke, A. J. Ruiter, I. R. Seitenzahl, S. A. Sim, and et al. 3d deflagration simulations leaving bound remnants: a model for 2002cx-like type ia supernovae. *Monthly Notices of the Royal Astronomical Society*, 429(3):2287–2297, Dec 2012.

[183] B. Kumar and P. Landry. Inferring neutron star properties from gw170817 with universal relations. *Phys. Rev. D*, 99:123026, Jun 2019.

[184] D. Kushnir, N. Wygoda, and A. Sharon. Sub-Chandrasekhar-mass detonations are in tension with the observed t0MNi56 relation of type Ia supernovae. *Monthly Notices of the Royal Astronomical Society*, 499(4):4725–4747, 10 2020.

[185] P. Landry and B. Kumar. Constraints on the moment of inertia of PSR j0737-3039a from GW170817. *The Astrophysical Journal*, 868(2):L22, nov 2018.

[186] N. Langer, S. C. Yoon, J. Petrovic, and A. Heger. Binary evolution models with rotation. *arXiv e-prints*, pages astro–ph/0302232, Feb. 2003.

[187] S. L. Larson, W. A. Hiscock, J. R. Routzahn, and B. Kulick. Low Frequency Gravitational Waves from White Dwarf MACHO Binaries. In *APS April Meeting Abstracts*, APS Meeting Abstracts, page H20.014, Apr. 2000.

[188] H. K. Lau, P. T. Leung, and L. M. Lin. INFERRING PHYSICAL PARAMETERS OF COMPACT STARS FROM THEIRf-MODE GRAVITATIONAL WAVE SIGNALS. *The Astrophysical Journal*, 714(2):1234–1238, apr 2010.

[189] N. M. Law, S. R. Kulkarni, R. G. Dekany, E. O. Ofek, R. M. Quimby, P. E. Nugent, J. Surace, C. C. Grillmair, J. S. Bloom, M. M. Kasliwal, and et al. The palomar transient factory: System overview, performance, and first results. *Publications of the Astronomical Society of the Pacific*, 121(886):1395–1408, Dec 2009.

[190] S.-C. Leung, S. Blinnikov, K. Ishidoshiro, A. Kozlov, and K. Nomoto. Pulsational pair-instability supernovae. II. neutrino signals from pulsations and

their detection by terrestrial neutrino detectors. *The Astrophysical Journal*, 889(2):75, jan 2020.

[191] S. C. Leung, M. C. Chu, and L. M. Lin. Dark-matter admixed neutron stars. Phys. Rev. D, 84(10):107301, Nov. 2011.

[192] S. C. Leung, M. C. Chu, and L. M. Lin. Equilibrium structure and radial oscillations of dark matter admixed neutron stars. Phys. Rev. D, 85(10):103528, May 2012.

[193] S.-C. Leung, M.-C. Chu, and L.-M. Lin. DARK MATTER ADMIXED TYPE ia SUPERNOVAE. *The Astrophysical Journal*, 812(2):110, oct 2015.

[194] S.-C. Leung, M.-C. Chu, and L.-M. Lin. A new hydrodynamics code for type ia supernovae. *Monthly Notices of the Royal Astronomical Society*, 454(2):1238–1259, Oct 2015.

[195] S.-C. Leung, M.-C. Chu, L.-M. Lin, and K.-W. Wong. Dark-matter admixed white dwarfs. *Physical Review D*, 87(12):123506, Jun 2013.

[196] S.-C. Leung and K. Nomoto. Explosive nucleosynthesis in near-chandrasekhar-mass white dwarf models for type ia supernovae: Dependence on model parameters. *The Astrophysical Journal*, 861(2):143, jul 2018.

[197] S.-C. Leung and K. Nomoto. Final evolution of super-AGB stars and supernovae triggered by electron capture. PASA, 36:e006, Feb. 2019.

[198] S.-C. Leung and K. Nomoto. Explosive nucleosynthesis in sub-chandrasekhar-mass white dwarf models for type ia supernovae: Dependence on model parameters. *The Astrophysical Journal*, 888(2):80, jan 2020.

[199] S.-C. Leung, K. Nomoto, and T. Suzuki. Electron-capture Supernovae of Super-AGB Stars: Sensitivity on Input Physics. ApJ, 889(1):34, Jan. 2020.

[200] S.-C. Leung, S. Zha, M.-C. Chu, L.-M. Lin, and K. Nomoto. Accretion-induced collapse of dark matter admixed white dwarfs. i. formation of low-mass neutron stars. *The Astrophysical Journal*, 884(1):9, oct 2019.

[201] S.-C. Leung, S. Zha, M.-C. Chu, L.-M. Lin, and K. Nomoto. Accretion-induced Collapse of Dark Matter Admixed White Dwarfs. I. Formation of Low-mass Neutron Stars. ApJ, 884(1):9, Oct. 2019.

[202] W. Li, A. V. Filippenko, R. Chornock, E. Berger, P. Berlind, M. L. Calkins, P. Challis, C. Fassnacht, S. Jha, R. P. Kirshner, T. Matheson, W. L. W. Sargent, R. A. Simcoe, G. H. Smith, and G. Squires. SN 2002cx: The most peculiar known type ia supernova. *Publications of the Astronomical Society of the Pacific*, 115(806):453–473, apr 2003.

[203] W. Li, X. Wang, M. Bulla, Y.-C. Pan, L. Wang, J. Mo, J. Zhang, C. Wu, J. Zhang, T. Zhang, D. Xiang, H. Lin, H. Sai, X. Zhang, Z. Chen, and S. Yan. Can the helium-detonation model explain the observed diversity of type ia supernovae? *The Astrophysical Journal*, 906(2):99, jan 2021.

[204] X. Y. Li, F. Y. Wang, and K. S. Cheng. Gravitational effects of condensate dark matter on compact stellar objects. J. Cosmology Astropart. Phys., 2012(10):031, Oct. 2012.

[205] M. Liebendorfer. A simple parameterization of the consequences of deleptonization for simulations of stellar core collapse. *The Astrophysical Journal*, 633(2):1042–1051, Nov 2005.

[206] A. M. Lisewski, W. Hillebrandt, and S. E. Woosley. Constraints on the delayed transition to detonation in type ia supernovae. *The Astrophysical Journal*, 538(2):831–836, aug 2000.

[207] D. Liu and B. Wang. The formation of single neutron stars from double white-dwarf mergers via accretion-induced collapse. MNRAS, 494(3):3422–3431, May 2020.

[208] Y. T. Liu and L. Lindblom. Models of rapidly rotating neutron stars: remnants of accretion-induced collapse. MNRAS, 324(4):1063–1073, July 2001.

[209] M. Livio and P. Mazzali. On the progenitors of type ia supernovae. *Physics Reports*, 736:1–23, Mar 2018.

[210] M. Livio and P. Mazzali. On the progenitors of type ia supernovae. *Physics Reports*, 736:1–23, 2018. On the progenitors of Type Ia supernovae.

[211] I. Lopes and G. Panotopoulos. Dark matter admixed strange quark stars in the Starobinsky model. Phys. Rev. D, 97(2):024030, Jan. 2018.

[212] J. Lopes and I. Lopes. Asymmetric Dark Matter Imprint on Low-mass Main-sequence Stars in the Milky Way Nuclear Star Cluster. ApJ, 879(1):50, July 2019.

[213] J. Lopes and I. Lopes. Asymmetric dark matter imprint on low-mass main-sequence stars in the milky way nuclear star cluster. *The Astrophysical Journal*, 879(1):50, Jul 2019.

[214] H. Ma, S. E. Woosley, C. M. Malone, A. Almgren, and J. Bell. CARBON DEFLAGRATION IN TYPE ia SUPERNOVA. i. CENTRALLY IGNITED MODELS. *The Astrophysical Journal*, 771(1):58, jun 2013.

[215] K. Maeda, F. Röpke, M. Fink, W. Hillebrandt, C. Travaglio, and F.-K. Thielemann. Nucleosynthesis in two-dimensional delayed detonation models of type ia supernova explosions. *The Astrophysical Journal*, 712(1):624–638, Mar 2010.

[216] D. Manreza Paret, J. E. Horvath, and A. Perez Martínez. Maximum mass of magnetic white dwarfs. *Research in Astronomy and Astrophysics*, 15(10):1735, Oct. 2015.

[217] D. Maoz, F. Mannucci, and G. Nelemans. Observational clues to the progenitors of type ia supernovae. *Annual Review of Astronomy and Astrophysics*, 52(1):107–170, 2014.

[218] Marquardt, Kai S., Sim, Stuart A., Ruiter, Ashley J., Seitenzahl, Ivo R., Ohlmann, Sebastian T., Kromer, Markus, Pakmor, Rüdiger, and Röpke, Friedrich K. Type ia supernovae from exploding oxygen-neon white dwarfs. *A&A*, 580:A118, 2015.

[219] G. Martinon, A. Maselli, L. Gualtieri, and V. Ferrari. Rotating protoneutron stars: Spin evolution, maximum mass, and I-Love-Q relations. Phys. Rev. D, 90(6):064026, Sept. 2014.

[220] A. Maselli, P. Pnigouras, N. G. Nielsen, C. Kouvaris, and K. D. Kokkotas. Dark stars: Gravitational and electromagnetic observables. *Phys. Rev. D*, 96:023005, Jul 2017.

[221] L. O. McNeill, R. A. Mardling, and B. Müller. Gravitational waves from dynamical tides in white-dwarf binaries. MNRAS, 491(2):3000–3012, Jan. 2020.

[222] R. F. P. Mendes and H. Yang. Tidal deformability of boson stars and dark matter clumps. *Classical and Quantum Gravity*, 34(18):185001, Sept. 2017.

[223] D. Merritt. The Distribution of Dark Matter in the Coma Cluster. ApJ, 313:121, Feb. 1987.

[224] G. Meynet and A. Maeder. Stellar evolution with rotation. I. The computational method and the inhibiting effect of the μ-gradient. A&A, 321:465–476, May 1997.

[225] A. Mignone. High-order conservative reconstruction schemes for finite volume methods in cylindrical and spherical coordinates. *Journal of Computational Physics*, 270:784–814, 2014.

[226] M. Misiaszek, A. Odrzywołek, and M. Kutschera. Neutrino spectrum from the pair-annihilation process in the hot stellar plasma. *Phys. Rev. D*, 74:043006, Aug 2006.

[227] R. Moll, C. Raskin, D. Kasen, and S. E. Woosley. TYPE ia SUPERNOVAE FROM MERGING WHITE DWARFS. i. PROMPT DETONATIONS. *The Astrophysical Journal*, 785(2):105, apr 2014.

[228] V. Morozova, A. L. Piro, M. Renzo, C. D. Ott, D. Clausen, S. M. Couch, J. Ellis, and L. F. Roberts. LIGHT CURVES OF CORE-COLLAPSE SUPERNOVAE WITH SUBSTANTIAL MASS LOSS USING THE NEW OPEN-SOURCE SUPERNOVA EXPLOSION CODE (SNEC). *The Astrophysical Journal*, 814(1):63, nov 2015.

[229] I. V. Moskalenko and L. L. Wai. Dark matter burners: Preliminary estimates. *arXiv e-prints*, pages astro–ph/0608535, Aug. 2006.

[230] E. R. Most, L. J. Papenfort, L. R. Weih, and L. Rezzolla. A lower bound on the maximum mass if the secondary in GW190814 was once a rapidly spinning neutron star. MNRAS, 499(1):L82–L86, Dec. 2020.

[231] P. Mukhopadhyay and J. Schaffner-Bielich. Quark stars admixed with dark matter. Phys. Rev. D, 93(8):083009, Apr. 2016.

[232] K. C. B. New and J. M. Centrella. Rotational instabilities and Centrifugal hangup. In J. M. Centrella, editor, *Astrophysical Sources for Ground-Based Gravitational Wave Detectors*, volume 575 of *American Institute of Physics Conference Series*, pages 221–233, June 2001.

[233] J. C. Niemeyer. Can deflagration-detonation transitions occur in type ia supernovae? *The Astrophysical Journal*, 523(1):L57–L60, sep 1999.

[234] R. Nityananda and S. Konar. Strong constraints on magnetized white dwarfs surpassing the chandrasekhar mass limit. *Phys. Rev. D*, 89:103017, May 2014.

[235] A. H. Nitz and Y.-F. Wang. Search for gravitational waves from high-mass-ratio compact-binary mergers of stellar mass and subsolar mass black holes. *Phys. Rev. Lett.*, 126:021103, Jan 2021.

[236] K. Nomoto and Y. Kondo. Conditions for Accretion-induced Collapse of White Dwarfs. ApJ, 367:L19, Jan. 1991.

[237] K. Nomoto and S.-C. Leung. *in Handbook of Supernovae*, pages 1275–1313. Springer International Publishing, Cham, 2017.

[238] K. Nomoto, D. Sugimoto, and S. Neo. Carbon Deflagration Supernova, an Alternative to Carbon Detonation. Ap&SS, 39:L37, Feb. 1976.

[239] K. Nomoto, F. K. Thielemann, and K. Yokoi. Accreting white dwarf models for type I supern. III. Carbon deflagration supernovae. ApJ, 286:644–658, Nov. 1984.

[240] R. C. Nunes, J. G. Coelho, and J. C. N. de Araujo. Weighing massive neutron star with screening gravity: a look on PSR J0740 + 6620 and GW190814 secondary component. *European Physical Journal C*, 80(12):1115, Dec. 2020.

[241] Odrzywolek, A. and Plewa, T. Probing thermonuclear supernova explosions with neutrinos. *A&A*, 529:A156, 2011.

[242] A. Odrzywołek. Plasmaneutrino spectrum. *The European Physical Journal C*, 52(2):425–434, 2007.

[243] S. T. Ohlmann, M. Kromer, M. Fink, R. Pakmor, I. R. Seitenzahl, S. A. Sim, and F. K. Röpke. The white dwarf's carbon fraction as a secondary parameter of type ia supernovae. *Astronomy and Astrophysics*, 572:A57, Nov 2014.

[244] B. R. Oppenheimer, N. C. Hambly, A. P. Digby, S. T. Hodgkin, and D. Saumon. Direct detection of galactic halo dark matter. *Science*, 292(5517):698–702, 2001.

[245] J. P. Ostriker and P. Bodenheimer. Rapidly Rotating Stars. II. Massive White Dwarfs. ApJ, 151:1089, Mar. 1968.

[246] E. Otoniel, B. Franzon, G. A. Carvalho, M. Malheiro, S. Schramm, and F. Weber. Strongly magnetized white dwarfs and their instability due to nuclear processes. *The Astrophysical Journal*, 879(1):46, jul 2019.

[247] C. D. Ott. TOPICAL REVIEW: The gravitational-wave signature of core-collapse supernovae. *Classical and Quantum Gravity*, 26(6):063001, Mar. 2009.

[248] R. Pakmor, M. Kromer, S. Taubenberger, and V. Springel. HELIUM-IGNITED VIOLENT MERGERS AS a UNIFIED MODEL FOR NORMAL AND RAPIDLY DECLINING TYPE ia SUPERNOVAE. *The Astrophysical Journal*, 770(1):L8, may 2013.

[249] L. Pan, J. C. Wheeler, and J. Scalo. The effect of turbulent intermittency on the deflagration to detonation transition in supernova ia explosions. *The Astrophysical Journal*, 681(1):470–481, jul 2008.

[250] G. Panotopoulos and I. Lopes. Dark matter effect on realistic equation of state in neutron stars. Phys. Rev. D, 96(8):083004, Oct. 2017.

[251] G. Panotopoulos and I. Lopes. Radial oscillations of strange quark stars admixed with condensed dark matter. Phys. Rev. D, 96(8):083013, Oct. 2017.

[252] G. Panotopoulos and I. Lopes. Millisecond pulsars modeled as strange quark stars admixed with condensed dark matter. *International Journal of Modern Physics D*, 27(9):1850093, Jan. 2018.

[253] G. Panotopoulos and I. Lopes. Radial oscillations of strange quark stars admixed with fermionic dark matter. Phys. Rev. D, 98(8):083001, Oct. 2018.

[254] G. Pappas, D. D. Doneva, T. P. Sotiriou, S. S. Yazadjiev, and K. D. Kokkotas. Multipole moments and universal relations for scalarized neutron stars. Phys. Rev. D, 99(10):104014, May 2019.

[255] V. Paschalidis, K. Yagi, D. Alvarez-Castillo, D. B. Blaschke, and A. Sedrakian. Implications from GW170817 and I-Love-Q relations for relativistic hybrid stars. Phys. Rev. D, 97(8):084038, Apr. 2018.

[256] T. Patzak and the MEMPHYS collaboration. MEMPHYS: A next generation megaton scale water cherenkov detector in europe. *Journal of Physics: Conference Series*, 375(4):042055, jul 2012.

[257] A. H. G. Peter. Dark Matter: A Brief Review. *arXiv e-prints*, page arXiv:1201.3942, Jan. 2012.

[258] J. M. M. Pfannes, J. C. Niemeyer, and W. Schmidt. Thermonuclear explosions of rapidly rotating white dwarfs. II. Detonations. A&A, 509:A75, Jan. 2010.

[259] J. M. M. Pfannes, J. C. Niemeyer, W. Schmidt, and C. Klingenberg. Thermonuclear explosions of rapidly rotating white dwarfs. I. Deflagrations. A&A, 509:A74, Jan. 2010.

[260] M. M. Phillips et al. The peculiar SN 2005hk: Do some type ia supernovae explode as deflagrations? *Publications of the Astronomical Society of the Pacific*, 119(854):360–387, apr 2007.

[261] M. M. Phillips, L. A. Wells, N. B. Suntzeff, M. Hamuy, B. Leibundgut, R. P. Kirshner, and C. B. Foltz. SN 1991T: Further Evidence of the Heterogeneous Nature of Type IA Supernovae. AJ, 103:1632, May 1992.

[262] T. Piffl, J. Binney, P. J. McMillan, M. Steinmetz, A. Helmi, R. F. G. Wyse, O. Bienaymé, J. Bland-Hawthorn, K. Freeman, B. Gibson, G. Gilmore, E. K. Grebel, G. Kordopatis, J. F. Navarro, Q. Parker, W. A. Reid, G. Seabroke, A. Siebert, F. Watson, and T. Zwitter. Constraining the Galaxy's dark halo with RAVE stars. MNRAS, 445(3):3133–3151, Dec. 2014.

[263] T. Plewa. Detonating failed deflagration model of thermonuclear supernovae. i. explosion dynamics. *The Astrophysical Journal*, 657(2):942–960, mar 2007.

[264] T. Plewa, A. C. Calder, and D. Q. Lamb. Type ia supernova explosion: Gravitationally confined detonation. *The Astrophysical Journal*, 612(1):L37–L40, aug 2004.

[265] E. Poisson. Gravitational waves from inspiraling compact binaries: The quadrupole-moment term. *Phys. Rev. D*, 57:5287–5290, Apr 1998.

[266] E. Poisson and C. M. Will. *Gravity: Newtonian, Post-Newtonian, Relativistic*. 2014.

[267] A. Y. Poludnenko, J. Chambers, K. Ahmed, V. N. Gamezo, and B. D. Taylor. A unified mechanism for unconfined deflagration-to-detonation transition in terrestrial chemical systems and type ia supernovae. *Science*, 366(6465):eaau7365, Oct 2019.

[268] J. L. Prieto, A. Rest, and N. B. Suntzeff. A new method to calibrate the magnitudes of type ia supernovae at maximum light. *The Astrophysical Journal*, 647(1):501–512, aug 2006.

[269] M. S. Pshirkov, A. V. Dodin, A. A. Belinski, S. G. Zheltoukhov, A. A. Fedoteva, O. V. Voziakova, S. A. Potanin, S. I. Blinnikov, and K. A. Postnov. Discovery

of a hot ultramassive rapidly rotating DBA white dwarf. MNRAS, 499(1):L21–L25, Dec. 2020.

[270] T. J. Raen, H. Martínez-Rodríguez, T. J. Hurst, A. R. Zentner, C. Badenes, and R. Tao. The effects of asymmetric dark matter on stellar Evolution I: Spin-dependent scattering. MNRAS, Mar. 2021.

[271] C. A. Raithel. Constraints on the neutron star equation of state from gw170817. *The European Physical Journal A*, 55(5):80, May 2019.

[272] C. Raskin, D. Kasen, R. Moll, J. Schwab, and S. Woosley. TYPE ia SUPERNOVAE FROM MERGING WHITE DWARFS. II. POST-MERGER DETONATIONS. *The Astrophysical Journal*, 788(1):75, may 2014.

[273] P. B. Rau and A. Sedrakian. Oscillations of Hypermassive Compact Stars with Gravitational Radiation and Viscosity. ApJ, 902(2):L41, Oct. 2020.

[274] J. I. Read, M. G. Walker, and P. Steger. Dark matter heats up in dwarf galaxies. MNRAS, 484(1):1401–1420, Mar. 2019.

[275] L. M. Rebull, S. C. Wolff, and S. E. Strom. Stellar Rotation in Young Clusters: The First 4 Million Years. AJ, 127(2):1029–1051, Feb. 2004.

[276] B. Reina, N. Sanchis-Gual, R. Vera, and J. A. Font. Completion of the universal I-Love-Q relations in compact stars including the mass. MNRAS, 470(1):L54–L58, Sept. 2017.

[277] M. Reinecke, W. Hillebrandt, and J. C. Niemeyer. Thermonuclear explosions of Chandrasekhar-mass C+O white dwarfs. A&A, 347:739–747, July 1999.

[278] M. Reinecke, W. Hillebrandt, and J. C. Niemeyer. Refined numerical models for multidimensional type ia supernova simulations. *A&A*, 386(3):936–943, 2002.

[279] M. Reinecke, W. Hillebrandt, and J. C. Niemeyer. Three-dimensional simulations of type ia supernovae. *A&A*, 391(3):1167–1172, 2002.

[280] M. Reinecke, W. Hillebrandt, J. C. Niemeyer, R. Klein, and A. Gröbl. A new model for deflagration fronts in reactive fluids. A&A, 347:724–733, July 1999.

[281] Z. Rezaei. Double dark matter admixed neutron star. *International Journal of Modern Physics D*, 27(16):1950002, Jan. 2018.

[282] F. K. Roepke. Flame-driven deflagration-to-detonation transitions in type ia supernovae? *The Astrophysical Journal*, 668(2):1103–1108, oct 2007.

[283] F. K. Röpke and S. A. Sim. Models for type ia supernovae and related astrophysical transients. *Space Science Reviews*, 214(4):72, Apr 2018.

[284] Röpke, F. K. Following multi-dimensional type ia supernova explosion models to homologous expansion. *A&A*, 432(3):969–983, 2005.

[285] Z. Roupas, G. Panotopoulos, and I. Lopes. QCD color superconductivity in compact stars: color-flavor locked quark star candidate for the gravitational-wave signal GW190814. *arXiv e-prints*, page arXiv:2010.11020, Oct. 2020.

[286] S. K. Roy, S. Mukhopadhyay, and D. N. Basu. Compact star deformation and universal relationship for magnetized white dwarfs, 2020.

[287] A. Rubbia. Underground neutrino detectors for particle and astroparticle science: The giant liquid argon charge imaging ExpeRiment (GLACIER). *Journal of Physics: Conference Series*, 171:012020, jun 2009.

[288] V. C. Rubin. The rotation of spiral galaxies. *Science*, 220(4604):1339–1344, 1983.

[289] V. C. Rubin and J. Ford, W. Kent. Rotation of the Andromeda Nebula from a Spectroscopic Survey of Emission Regions. ApJ, 159:379, Feb. 1970.

[290] A. J. Ruiter. Type ia supernova sub-classes and progenitor origin. *Proceedings of the International Astronomical Union*, 15(S357):1–15, Oct 2019.

[291] A. J. Ruiter, L. Ferrario, K. Belczynski, I. R. Seitenzahl, R. M. Crocker, and A. I. Karakas. On the formation of neutron stars via accretion-induced collapse in binaries. MNRAS, 484(1):698–711, Mar. 2019.

[292] F. K. Röpke. Combustion in thermonuclear supernova explosions. *Handbook of Supernovae*, page 1185–1209, 2017.

[293] F. K. Röpke and W. Hillebrandt. Full-star type ia supernova explosion models. *Astronomy and astrophysics (Berlin)*, 431(2):635–645, 2005.

[294] F. K. Röpke, W. Hillebrandt, W. Schmidt, J. C. Niemeyer, S. I. Blinnikov, and P. A. Mazzali. A three-dimensional deflagration model for type ia supernovae compared with observations. *The Astrophysical Journal*, 668(2):1132–1139, 2007.

[295] A. Samajdar and T. Dietrich. Constructing Love-Q relations with gravitational wave detections. Phys. Rev. D, 101(12):124014, June 2020.

[296] F. Sandin and P. Ciarcelluti. Effects of mirror dark matter on neutron stars. *Astroparticle Physics*, 32(5):278–284, 2009.

[297] J. Schwab and K. A. Rocha. Residual Carbon in Oxygen-Neon White Dwarfs and Its Implications for Accretion-induced Collapse. ApJ, 872(2):131, Feb. 2019.

[298] P. Scott, M. Fairbairn, and J. Edsjo. Impacts of WIMP dark matter upon stellar evolution: main-sequence stars. In *Identification of Dark Matter 2008*, page 73, Jan. 2008.

[299] P. SCOTT, M. Fairbairn, and J. Edsjo. Impacts of WIMP dark matter upon stellar evolution: main-sequence stars. *PoS*, idm2008:073, 2009.

[300] I. R. Seitenzahl, F. Ciaraldi-Schoolmann, and F. K. Röpke. Type Ia supernova diversity: white dwarf central density as a secondary parameter in three-dimensional delayed detonation models. *Monthly Notices of the Royal Astronomical Society*, 414(3):2709–2715, 06 2011.

[301] I. R. Seitenzahl et al. Three-dimensional delayed-detonation models with nucleosynthesis for Type Ia supernovae. *Monthly Notices of the Royal Astronomical Society*, 429(2):1156–1172, 2 2013.

[302] I. R. Seitenzahl, M. Herzog, A. J. Ruiter, K. Marquardt, S. T. Ohlmann, and F. K. Röpke. Neutrino and gravitational wave signal of a delayed-detonation model of type Ia supernovae. Phys. Rev. D, 92(12):124013, Dec. 2015.

[303] Seitenzahl, Ivo R., Kromer, Markus, Ohlmann, Sebastian T., Ciaraldi-Schoolmann, Franco, Marquardt, Kai, Fink, Michael, Hillebrandt, Wolfgang,

Pakmor, Rüdiger, Röpke, Friedrich K., Ruiter, Ashley J., Sim, Stuart A., and Taubenberger, Stefan. Three-dimensional simulations of gravitationally confined detonations compared to observations of sn 1991t. *A&A*, 592:A57, 2016.

[304] J. A. Sethian. *Level set methods and fast marching methods : evolving interfaces in computational geometry, fluid mechanics, computer vision, and materials science*. Cambridge monographs on applied and computational mathematics ; 3. Cambridge University Press, Cambridge, U.K. ; New York, 2nd ed edition, 1999.

[305] Y. H. Sham, T. K. Chan, L. M. Lin, and P. T. Leung. Unveiling the Universality of I-Love-Q Relations. ApJ, 798(2):121, Jan. 2015.

[306] S. Shandera, D. Jeong, and H. S. G. Gebhardt. Gravitational waves from binary mergers of subsolar mass dark black holes. *Physical Review Letters*, 120(24), Jun 2018.

[307] S. L. Shapiro and S. A. Teukolsky. *Black holes, white dwarfs, and neutron stars : the physics of compact objects*. 1983.

[308] R. Sharma, S. Karmakar, and S. Mukherjee. Boson star and dark matter. *arXiv e-prints*, page arXiv:0812.3470, Dec. 2008.

[309] G. J. Sharpe. The structure of steady detonation waves in Type Ia supernovae: pathological detonations in C—O cores. *Monthly Notices of the Royal Astronomical Society*, 310(4):1039–1052, 12 1999.

[310] K. J. Shen, S. Blondin, D. Kasen, L. Dessart, D. M. Townsley, S. Boos, and D. J. Hillier. Non-local thermodynamic equilibrium radiative transfer simula-

tions of sub-chandrasekhar-mass white dwarf detonations. *The Astrophysical Journal Letters*, 909(2):L18, mar 2021.

[311] K. J. Shen, D. Kasen, B. J. Miles, and D. M. Townsley. Sub-chandrasekhar-mass white dwarf detonations revisited. *The Astrophysical Journal*, 854(1):52, Feb 2018.

[312] T. Shu, Y. Gao, and C. K. Law. Flame Acceleration in SN Ia Induced by the Burning of Local Unreacted Islands. ApJ, 889(2):82, Feb. 2020.

[313] H. O. Silva, A. M. Holgado, A. Cárdenas-Avendaño, and N. Yunes. Astrophysical and theoretical physics implications from multimessenger neutron star observations. *Phys. Rev. Lett.*, 126:181101, May 2021.

[314] H. O. Silva and N. Yunes. I-Love-Q to the extreme. *Classical and Quantum Gravity*, 35(1):015005, Jan. 2018.

[315] J. M. Silverman, R. J. Foley, A. V. Filippenko, M. Ganeshalingam, A. J. Barth, R. Chornock, C. V. Griffith, J. J. Kong, N. Lee, D. C. Leonard, and et al. Berkeley supernova ia program - i. observations, data reduction and spectroscopic sample of 582 low-redshift type ia supernovae. *Monthly Notices of the Royal Astronomical Society*, 425(3):1789–1818, Aug 2012.

[316] S. A. Sim, M. Fink, M. Kromer, F. K. Röpke, A. J. Ruiter, and W. Hillebrandt. 2D simulations of the double-detonation model for thermonuclear transients from low-mass carbon–oxygen white dwarfs. *Monthly Notices of the Royal Astronomical Society*, 420(4):3003–3016, 03 2012.

[317] S. A. Sim, I. R. Seitenzahl, M. Kromer, F. Ciaraldi-Schoolmann, F. K. Röpke, M. Fink, W. Hillebrandt, R. Pakmor, A. J. Ruiter, and S. Taubenberger. Syn-

thetic light curves and spectra for three-dimensional delayed-detonation models of Type Ia supernovae. *Monthly Notices of the Royal Astronomical Society*, 436(1):333–347, 09 2013.

[318] H. C. Spruit. Origin of the rotation rates of single white dwarfs. A&A, 333:603–612, May 1998.

[319] B. E. Stahl et al. Lick Observatory Supernova Search follow-up program: photometry data release of 93 Type Ia supernovae. *Monthly Notices of the Royal Astronomical Society*, 490(3):3882–3907, 10 2019.

[320] F. D. Steffen. Dark-matter candidates. Axions, neutralinos, gravitinos, and axinos. *European Physical Journal C*, 59(2):557–588, Jan. 2009.

[321] H. Steigerwald, S. Profumo, D. Rodrigues, and V. Marra. Dark Matter Thermonuclear Supernova Ignition. *arXiv e-prints*, page arXiv:1912.12417, Dec. 2019.

[322] M. Steinmetz, E. Muller, and W. Hillebrandt. Carbon Detonations in Rapidly Rotating White Dwarfs. A&A, 254:177, Feb. 1992.

[323] R. Stoeckly. Polytropic Models with Fast, Non-Uniform Rotation. ApJ, 142:208–228, July 1965.

[324] S. Subramanian and B. Mukhopadhyay. GRMHD formulation of highly super-Chandrasekhar rotating magnetized white dwarfs: stable configurations of non-spherical white dwarfs. *Monthly Notices of the Royal Astronomical Society*, 454(1):752–765, 09 2015.

[325] Sulistiyowati, H. Wulandari, B. Dermawan, M. I. Arifyanto, and I. Ibrahim. Effects of dark matter on interior and evolution of main sequence stars. *AIP Conference Proceedings*, 1589(1):33–36, 2014.

[326] C. Sunny, A. Kenath, C. Sivaram, and S. B. Gudennavar. Effects of Dark Matter in Red Giants. *arXiv e-prints*, page arXiv:2009.04302, Sept. 2020.

[327] A. Suresh and H. Huynh. Accurate monotonicity-preserving schemes with runge–kutta time stepping. *Journal of Computational Physics*, 136(1):83–99, 1997.

[328] T. Suzuki, S. Zha, S.-C. Leung, and K. Nomoto. Electron-capture Rates in ^{20}Ne for a Forbidden Transition to the Ground State of ^{20}F Relevant to the Final Evolution of High-density O-Ne-Mg Cores. ApJ, 881(1):64, Aug. 2019.

[329] H. Tan, J. Noronha-Hostler, and N. Yunes. Neutron star equation of state in light of gw190814. *Physical Review Letters*, 125(26):261104, Dec 2020.

[330] A. Tanikawa, K. Nomoto, N. Nakasato, and K. Maeda. Double-detonation models for type ia supernovae: Trigger of detonation in companion white dwarfs and signatures of companions' stripped-off materials. *The Astrophysical Journal*, 885(2):103, nov 2019.

[331] J.-L. Tassoul. *Stellar Rotation*. 2000.

[332] S. Taubenberger. The extremes of thermonuclear supernovae. pages 317–373, 2017.

[333] A. J. Taylor, K. Yagi, and P. L. Arras. I-Love-Q relations for realistic white dwarfs. MNRAS, 492(1):978–992, Feb. 2020.

[334] I. Tews, P. T. H. Pang, T. Dietrich, M. W. Coughlin, S. Antier, M. Bulla, J. Heinzel, and L. Issa. On the Nature of GW190814 and Its Impact on the Understanding of Supranuclear Matter. ApJ, 908(1):L1, Feb. 2021.

[335] F. X. Timmes and F. D. Swesty. The accuracy, consistency, and speed of an electron-positron equation of state based on table interpolation of the helmholtz free energy. *The Astrophysical Journal Supplement Series*, 126(2):501–516, feb 2000.

[336] D. M. Townsley, A. C. Calder, S. M. Asida, I. R. Seitenzahl, F. Peng, N. Vladimirova, D. Q. Lamb, and J. W. Truran. Flame evolution during type ia supernovae and the deflagration phase in the gravitationally confined detonation scenario. *The Astrophysical Journal*, 668(2):1118–1131, oct 2007.

[337] D. M. Townsley, A. C. Calder, S. M. Asida, I. R. Seitenzahl, F. Peng, N. Vladimirova, D. Q. Lamb, and J. W. Truran. Flame evolution during type ia supernovae and the deflagration phase in the gravitationally confined detonation scenario. *The Astrophysical Journal*, 668(2):1118–1131, oct 2007.

[338] D. M. Townsley, B. J. Miles, K. J. Shen, and D. Kasen. Double detonations with thin, modestly enriched helium layers can make normal type ia supernovae. *The Astrophysical Journal*, 878(2):L38, jun 2019.

[339] T. Tröster, A. G. Sánchez, M. Asgari, C. Blake, M. Crocce, C. Heymans, H. Hildebrandt, B. Joachimi, S. Joudaki, A. Kannawadi, C.-A. Lin, and A. Wright. Cosmology from large-scale structure. Constraining ΛCDM with BOSS. A&A, 633:L10, Jan. 2020.

[340] A. Tsokaros, M. Ruiz, and S. L. Shapiro. GW190814: Spin and Equation of State of a Neutron Star Companion. ApJ, 905(1):48, Dec. 2020.

[341] J. L. van Saders and M. H. Pinsonneault. Fast Star, Slow Star; Old Star, Young Star: Subgiant Rotation as a Population and Stellar Physics Diagnostic. ApJ, 776(2):67, Oct. 2013.

[342] K. Vattis, I. S. Goldstein, and S. M. Koushiappas. Could the 2.6 $M_\odot$ object in GW190814 be a primordial black hole? Phys. Rev. D, 102(6):061301, Sept. 2020.

[343] V. A. Villar, M. Nicholl, and E. Berger. Superluminous supernovae in LSST: Rates, detection metrics, and light-curve modeling. *The Astrophysical Journal*, 869(2):166, dec 2018.

[344] M. Vogel. Astrophysics in a nutshell (2nd edition), by Dan Maoz. *Contemporary Physics*, 58(2):193–193, Apr. 2017.

[345] B. Wang. The single-degenerate model for the progenitors of accretion-induced collapse events. MNRAS, 481(1):439–446, Nov. 2018.

[346] B. Wang, S. Justham, Z. W. Liu, J. J. Zhang, D. D. Liu, and Z. Han. On the evolution of rotating accreting white dwarfs and Type Ia supernovae. MNRAS, 445(3):2340–2352, Dec. 2014.

[347] B. Wang and D. Liu. The formation of neutron star systems through accretion-induced collapse in white-dwarf binaries. *Research in Astronomy and Astrophysics*, 20(9):135, Sept. 2020.

[348] C. J. White, M. M. Kasliwal, P. E. Nugent, A. Gal-Yam, D. A. Howell, M. Sullivan, A. Goobar, A. L. Piro, J. S. Bloom, S. R. Kulkarni, R. R. Laher, F. Masci, E. O. Ofek, J. Surace, S. Ben-Ami, Y. Cao, S. B. Cenko, I. M. Hook, J. Jönsson, T. Matheson, A. Sternberg, R. M. Quimby, and O. Yaron. SLOW-SPEED SUPERNOVAE FROM THE PALOMAR TRANSIENT FACTORY: TWO CHANNELS. *The Astrophysical Journal*, 799(1):52, jan 2015.

[349] D. E. Willcox, D. M. Townsley, A. C. Calder, P. A. Denissenkov, and F. Herwig. TYPE ia SUPERNOVA EXPLOSIONS FROM HYBRID CARBON–OXYGEN–NEON WHITE DWARF PROGENITORS. *The Astrophysical Journal*, 832(1):13, nov 2016.

[350] A. Wolz, K. Yagi, N. Anderson, and A. J. Taylor. Measuring individual masses of binary white dwarfs with space-based gravitational-wave interferometers. *Monthly Notices of the Royal Astronomical Society: Letters*, 500(1):L52–L56, 11 2020.

[351] S. E. Woosley. Neutron-rich nucleosynthesis in carbon deflagration supernovae. *The Astrophysical Journal*, 476(2):801–810, feb 1997.

[352] S. E. Woosley. Type ia supernovae: Burning and detonation in the distributed regime. *The Astrophysical Journal*, 668(2):1109–1117, oct 2007.

[353] S. E. Woosley and D. Kasen. Sub-chandrasekhar mass models for supernovae. *The Astrophysical Journal*, 734(1):38, May 2011.

[354] W. P. Wright, J. P. Kneller, S. T. Ohlmann, F. K. Röpke, K. Scholberg, and I. R. Seitenzahl. Neutrinos from type ia supernovae: The gravitationally confined detonation scenario. *Phys. Rev. D*, 95:043006, Feb 2017.

[355] W. P. Wright, G. Nagaraj, J. P. Kneller, K. Scholberg, and I. R. Seitenzahl. Neutrinos from type ia supernovae: The deflagration-to-detonation transition scenario. *Phys. Rev. D*, 94:025026, Jul 2016.

[356] C.-Y. Wu and B. Wang. Accreting CO material onto ONe white dwarfs towards accretion-induced collapse. *Research in Astronomy and Astrophysics*, 18(3):036, Mar. 2018.

[357] M. Wurm, D. Bick, T. Enqvist, D. Hellgartner, M. Kaiser, K. Loo, S. Lorenz, M. Meloni, M. Meyer, R. Möllenberg, L. Oberauer, M. Soiron, M. Smirnov, W. Trzaska, and B. Wonsak. Low-energy neutrino astronomy in lena. *Physics Procedia*, 61:376–383, 2015. 13th International Conference on Topics in Astroparticle and Underground Physics, TAUP 2013.

[358] Q.-F. Xiang, W.-Z. Jiang, D.-R. Zhang, and R.-Y. Yang. Effects of fermionic dark matter on properties of neutron stars. Phys. Rev. C, 89(2):025803, Feb. 2014.

[359] K. Yagi, L. C. Stein, G. Pappas, N. Yunes, and T. A. Apostolatos. Why I-Love-Q: Explaining why universality emerges in compact objects. Phys. Rev. D, 90(6):063010, Sept. 2014.

[360] K. Yagi and N. Yunes. I-Love-Q relations in neutron stars and their applications to astrophysics, gravitational waves, and fundamental physics. Phys. Rev. D, 88(2):023009, July 2013.

[361] K. Yagi and N. Yunes. I-Love-Q anisotropically: Universal relations for compact stars with scalar pressure anisotropy. Phys. Rev. D, 91(12):123008, June 2015.

[362] K. Yagi and N. Yunes. Approximate universal relations for neutron stars and quark stars. Phys. Rep., 681:1–72, Apr. 2017.

[363] K. L. S. Yip and P. T. Leung. Tidal Love numbers and moment-Love relations of polytropic stars. MNRAS, 472(4):4965–4981, Dec. 2017.

[364] S. C. Yoon and N. Langer. Presupernova evolution of accreting white dwarfs with rotation. A&A, 419(2):623–644, May 2004.

[365] S. C. Yoon and N. Langer. On the evolution of rapidly rotating massive white dwarfs towards supernovae or collapses. A&A, 435(3):967–985, June 2005.

[366] S. C. Yoon, P. Podsiadlowski, and S. Rosswog. Remnant evolution after a carbon-oxygen white dwarf merger. MNRAS, 380(3):933–948, Sept. 2007.

[367] S. Yoshida. Rotating white dwarf models with finite-temperature envelope. MNRAS, 486(3):2982–2994, July 2019.

[368] S. Yoshida. Decihertz Gravitational Waves from Double White Dwarf Merger Remnants. ApJ, 906(1):29, Jan. 2021.

[369] Yu, S. and Jeffery, C. S. The gravitational wave signal from diverse populations of double white dwarf binaries in the galaxy. *A&A*, 521:A85, 2010.

[370] Y. B. Zel'dovich, V. B. Librovich, G. M. Makhviladze, and G. I. Sivashinskil. On the onset of detonation in a nonuniformly heated gas. *Journal of applied mechanics and technical physics*, 11(2):264–270, 1972.

[371] A. R. Zentner and A. P. Hearin. Asymmetric dark matter may alter the evolution of very low-mass stars and brown dwarfs. Phys. Rev. D, 84(10):101302, Nov. 2011.

[372] S. Zha, M.-C. Chu, S.-C. Leung, and L.-M. Lin. Accretion-induced collapse of dark matter admixed white dwarfs. II. rotation and gravitational-wave signals. *The Astrophysical Journal*, 883(1):13, sep 2019.

[373] S. Zha, M.-C. Chu, S.-C. Leung, and L.-M. Lin. Accretion-induced Collapse of Dark Matter Admixed White Dwarfs. II. Rotation and Gravitational-wave Signals. ApJ, 883(1):13, Sept. 2019.

[374] S. Zha, S.-C. Leung, T. Suzuki, and K. Nomoto. Evolution of ONeMg Core in Super-AGB Stars toward Electron-capture Supernovae: Effects of Updated Electron-capture Rate. ApJ, 886(1):22, Nov. 2019.

[375] K. Zhang, G.-Z. Huang, and F.-L. Lin. Gw170817 and gw190425 as hybrid stars of dark and nuclear matters, 2020.

[376] K. Zhang and F.-L. Lin. Constraint on hybrid stars with gravitational wave events. *Universe*, 6(12):231, Dec 2020.

[377] W. Zhao and L. Santos. Model-independent measurement of the absolute magnitude of type ia supernovae with gravitational-wave sources. *Journal of Cosmology and Astroparticle Physics*, 2019(11):009–009, Nov 2019.